Fall 1994

Local stress factors of pipe-nozzle under internal pressure

Jih-Lian Jack Ha
New Jersey Institute of Technology

Order Number 9514443

Local stress factors of pipe-nozzle under internal pressure

Ha, Jih-Lian Jack, Ph.D.

New Jersey Institute of Technology, 1994

U·M·I
300 N. Zeeb Rd.
Ann Arbor, MI 48106

ABSTRACT

LOCAL STRESS FACTORS OF PIPE-NOZZLE UNDER INTERNAL PRESSURE

by
Jih-Lian Jack Ha

This thesis presents a comprehensive study of local stresses around a pipe-nozzle due to internal pressure. The finite element method (FEM) was employed to provide a numerical solution which will furnish a database for stress analysts to compute local stresses of pipe-nozzle due to internal pressure. The local pressure stresses for both the pipe and the nozzle around the pipe-nozzle juncture are first normalized into pressure stress factors which are then plotted as functions of geometrical parameters, beta, β, (nozzle mean radius / pipe mean radius) and gamma γ, (pipe mean radius / pipe thickness). These local pressure stresses at each point on the shell have both the longitudinal and circumferential directional components with respect to the orientation of the nozzle and the pipe, respectively. These stress components are again subdivided into membrane and bending in character. All together, sixteen (16) different stress factor plots are provided in this thesis which allows pressure vessel engineers to compute local stresses on both the outside and inside shell of the pipe, as well as the nozzle, at locations where the longitudinal and circumferential symmetric plane intersect the pipe-nozzle geometry.

The ranges of these stress factors cover the beta, β, varies from 0.1 to 1.0 in an increment of one-tenth, and the gamma, γ, varies from 10 to 300 in nine randomly selected intervals.

To ensure accuracy of the numerical results from the finite element method, the plate / shell elements are used with 96 nodes around the pipe-nozzle juncture. The pipe length is modeled with a parameter alphap, α_p, (pipe length / pipe mean radius) of a value of 8.0.

The nozzle length is modeled with a parameter alphan, α_n, (nozzle length /nozzle mean radius) of a value of 4.0. As a result, the optimized full pipe-nozzle model has 5268 nodes and 3245 elements, when β=0.5.

The local stress due to pressure may be used in conjunction with the stress computation table of the Welding Research Council Bulletin 107, which computes the local stress around the pipe-nozzle due to other external nozzle loads. Therefore, the stress computation table of WRC 107 is revised in this thesis to accommodate the local pressure stress effects.

LOCAL STRESS FACTORS OF PIPE-NOZZLE UNDER INTERNAL PRESSURE

by
Jih-Lian Jack Ha

A Dissertation
Submitted to the Faculty of
New Jersey Institute of Technology
In Partial Fulfillment of the Requirements for the Degree of
Doctor of Philosophy

Department of Mechanical and Industrial Engineering

October 1994

APPROVAL PAGE

LOCAL STRESS FACTORS OF PIPE-NOZZLE UNDER INTERNAL PRESSURE

Jih-Lian Jack Ha

Dr. Benedict C. Sun, Dissertation Advisor — Date
Associate Professor of Engineering Technology, NJIT

Dr. Rong-Yaw Chen, Committee Chair — Date
Professor of Mechanical Engineering
and Associate Chairperson and Graduate Advisor
of Mechanical Engineering, NJIT

Dr. Bernard Koplik, Committee Member — Date
Professor of Mechanical Engineering and Chairperson
of the Department of Mechanical and Industrial Engineering, NJIT

Dr. Ernest S. Geskin, Committee Member — Date
Professor of Mechanical Engineering, NJIT

Dr. C.T. Thomas Hsu, Committee Member — Date
Professor of Civil and Environmental Engineering, NJIT

BIOGRAPHICAL SKETCH

Author: Jih-Lian Jack Ha

Degree: Doctor of Philosophy in Mechanical Engineering

Date: October, 1994

Undergraduate and Graduate Education

- Doctor of Philosophy in Mechanical Engineering,
  New Jersey Institute of Technology,
  Newark, New Jersey, 1994.

- Master of Science in Mechanical Engineering,
  New Jersey Institute of Technology,
  Newark, New Jersey, 1986.

- Bachelor of Science in Mechanical Engineering
  National Chung-Hsing University,
  Taichung, Taiwan, 1979.

Major: Mechanical Engineering

Presentations and Publications:

Ha, "On Vibration Frequency of the HVAC Duct," Master Thesis, NJIT, Newark, NJ, 1986

Awards:

Research Assistantship - New Jersey Institue of Technology, Newark, New Jersey.
Teaching Assistantship - New Jersey Institue of Technology, Newark, New Jersey.

This dissertation is dedicated to
my parents

ACKNOWLEDGMENT

The author wishes to express his sincere appreciation to his dissertation advisor, Dr. Benedict C. Sun, for his guidance, friendship, and moral support throughout this research.

Special thanks to Dr. Rong-Yaw Chen, Dr. Bernard Koplik, Dr. Ernest S. Geskin, and Dr. C.T. Thomas Hsu for serving as members of the committee and their kindly suggestions and support.

Also, the author would like to express his gratitude to his wife, Lilin, who with her love and patience, supported the writing of this dissertation.

TABLE OF CONTENTS

LIST OF TABLES

LIST OF FIGURES

Figure		Page

Figure		Page

Figure		Page

NOMENCLATURES

α_p = pipe length / pipe mean radius

α_n = nozzle length / nozzle mean radius

β = r / R

γ = R / T

$\varepsilon_{\theta 1}$, $\varepsilon_{\theta 2}$ = circumferential strains

ψ_1 = tee or hole curvature parameter for the pipe

ψ_2 = tee or hole curvature parameter for the nozzle

ζ_1 , ξ_2 = see equation (31)

ν = Poison' ratio

σ_{a1}, σ_{a2} = meridianal membrane stresses

σ_{b1}, σ_{b2} = meridianal bending stresses

σ_{c1}, σ_{c2} = circumferential membrane stresses

a = midsurface radius of a cylindrical shell in general

d = inside diameter of nozzle or hole

d_1 , d_2 = lengths of shell

D_1 , D_2 = flexural rigidity of pipe and nozzle, respectively. see equation (32)

E = Young's modules

h = thickness of a cylindrical shell in general

Lp = length of pipe

Ln = length of nozzle

M_{x1}, M_{x2} = shell bending moments

$M_x, M_\phi, M_{x\phi}$, = shell moment resultants

$N_{\theta 1}$, $N_{\theta 2}$ = circumferential direct stress resultants

N_{x1}, N_{x2} = meridianal direct stress resultants

$N_x, N_\phi, N_{x\phi}$, = shell force resultants p = internal pressure

Q_{x1}, Q_{x2} = transverse shear stress resultants

Q_x, Q_ϕ, = shearing force resultants

R = pipe mean radius

r = nozzle mean radius

S, s = nominal stresses see equation (31)

T = pipe thickness

t = nozzle thickness

u = displacement in x direction

v = displacement in ϕ direction

w = displacement in r direction

$\partial w_1 / \partial x_1, \partial w_2 / \partial x_2$ = rotations

x_1, x_2 = coordinates along shell meridians for pipe and nozzle respectively.

ρ = r / $\sqrt{RT}$

Subscripts

1, M = pipe, main shell

2, B = nozzle, branch

CHAPTER 1

INTRODUCTION

Local stresses around the pipe-nozzle under internal pressure, temperature and other external loads has attracted much attention in the past two decades due to the safety requirements of nuclear reactor.

Different from the related axisymmetric problem of a pressurized spherical shell containing a radial circular nozzle, the problem of local stress around the pipe-nozzle under internal pressure involves tremendous mathematical difficulties due to the absence of axial symmetry. Especially due to the fact that the intersection of the midsurfaces at the pipe-nozzle juncture is not a geodesic curve on either the pipe or the nozzle, this restricts the approximate solution to small values of pipe-nozzle geometrical parameters. Based on the elastic thin-shell theory, Lind, [13] viewed this problem as a boundary value problem and developed an overall equilibrium equation at the crotch of a pipe-nozzle connection for limited geometry configurations. Several other researchers achieved different approximate solutions at certain locations on the intersection of special geometry configuration by various assumptions. The linear distribution of nominal bending stresses through the thickness of the pipe-nozzle intersection, and continuity conditions of axial membrane stress, circumferential strain, and the rotation of bending moment at the intersection of pipe-nozzle connection, are common assumptions in most of the theoretical approximate solutions. Therefore, the results from these previous studies can only be used as references.

To date, several researchers have studied some special cases of the local pressure stress at the pipe-nozzle by using the finite element method. Due to computational restrictions, a quarter model of the pipe-nozzle with appropriate boundary conditions were used. However, the purposes of their studies were for certain specific pipe-nozzle size to evaluate or justify their designs. Therefore, these results are not sufficient to be used as a design guide. There is a need for a comprehensive parametric study of these local stresses at the pipe-nozzle connection under internal pressure. The numerical results of such a study may be used in conjunction with Welding Research Council Bulletin 107 [38], which computes local stresses due to external loadings.

This thesis presents a comprehensive study of such local pressure stresses around the pipe-nozzle by using a full pipe-nozzle model. After a comparative study of the existing mathematical models from other authors, a mathematical model with certain modified assumptions is then presented in this thesis. The approximate solution from this proposed new model will be used to compare with the numerical solution of the finite element results from this thesis. To ensure a proper asymptotic of the numerical results, a comprehensive study on the number of nodes around the pipe-nozzle juncture was made. For optimum accuracy within the framework of the software, the finite element model of plate/shell element with 96 nodes on the pipe-nozzle juncture are adopted. The plate/shell elements, which are skewed to the global coordinate system (typical of shell model), have all six degrees of freedom active. The asymptotic studies also adopt a value of 8.0 for the parameter $alpha_p$, α_p, (pipe length / pipe mean radius) and a value of 4.0 for the parameter $alpha_n$, α_n, (nozzle length / nozzle mean radius). These values would ensure that the boundary conditions at the ends of the pipe and the nozzle will not affect the accuracy of numerical results. The nozzle thickness is assumed to be proportional to the pipe thickness by the value of beta, i.e. $t=\beta T$.

To present a comprehensive range of local pressure stress results, the geometrical parameter beta, β, (nozzle mean radius / pipe mean radius) range is selected from 0.1 to 1.0 with an increment of 0.1 and the gamma, γ, (pipe mean radius / pipe thickness) range is selected from 10 to 300 in nine randomly selected intervals (see the typical configuration of pipe with a nozzle attachment subjected to internal pressure in Figure 1).

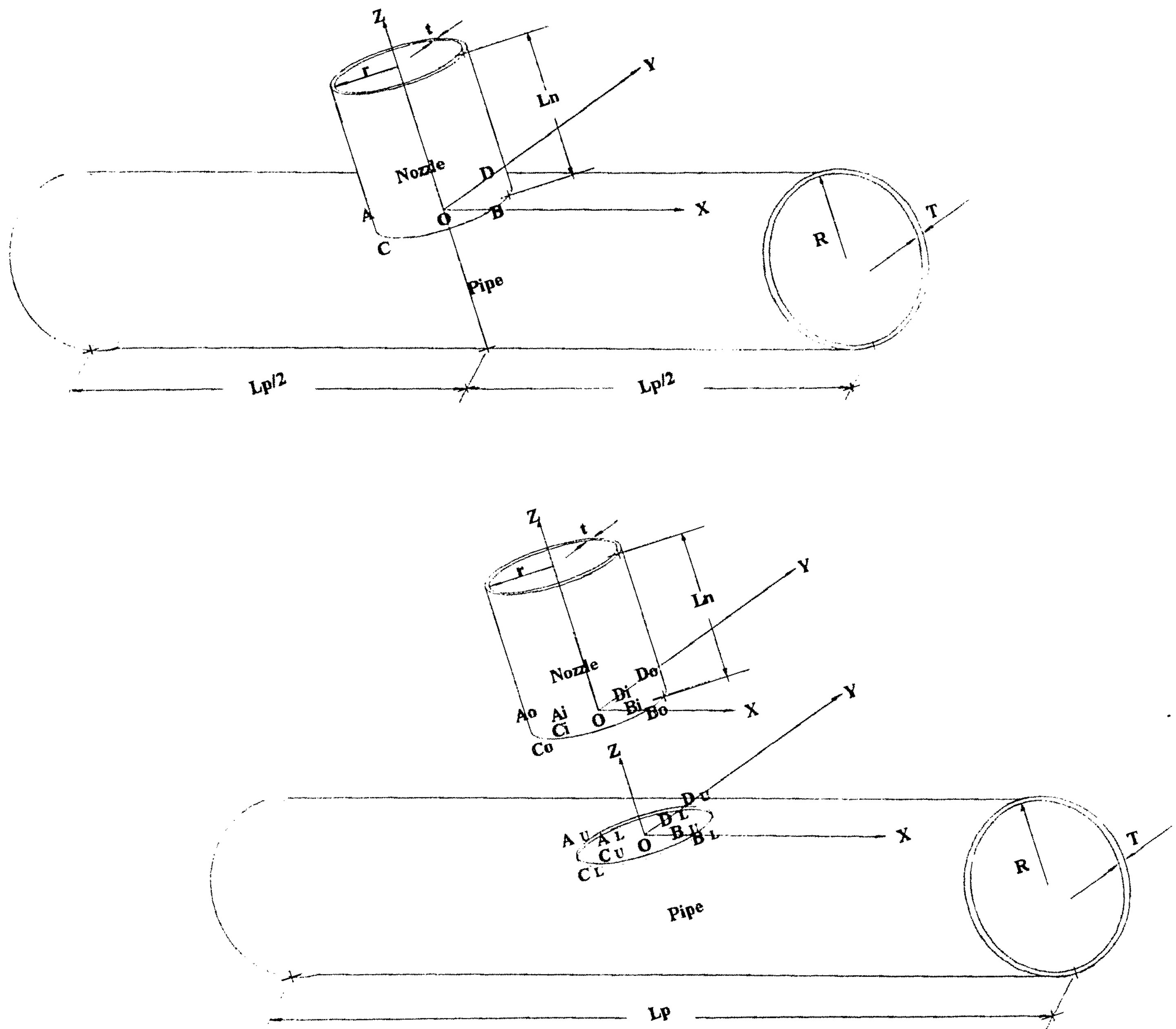

$$\alpha_n = \frac{L_n}{r}, \quad \alpha_p = \frac{L_p}{R}, \quad \beta = \frac{r}{R}, \quad \gamma = \frac{R}{T} = \frac{r}{t}, \quad t = T\beta$$

Figure 1 Typical configuration of pipe with a nozzle attachment subjected to internal pressure

The local stresses in circumferential and longitudinal directions of the pipe, as well as the nozzle, on both the inside and outside of the shells at the intersections of the pipe-nozzle symmetric plans (longitudinal and transverse) are investigated. The numerical stress results are further normalized by the pressure value used in the computation into a pressure stress factors. As a result, a series of sixteen (16) pressure stress factor plots are presented in this thesis. They are functions of beta, β (nozzle mean radius / pipe mean radius) and gamma, γ (piping mean radius / pipe thickness).

Comparisons of data from available literature show that the finite element results from this thesis provide a significant improvement over all the previous studies.

CHAPTER 2

LITERATURE SURVEY

A review of literature indicates that a considerable amount of work on local pressure stresses on pipe-nozzle have been performed in the past.

2.1 Theoretical analysis

The theoretical analysis of pipe-nozzle local stresses involve tremendous mathematical difficulties due to the absence of axial symmetry. Instead of an ordinary differential equation for the stress field, partial differential equations with various non-symmetric terms are needed for the pipe-nozzle geometry which led to difficulties in obtaining exact kinematics or force (and moment) equilibrium at the juncture of the pipe-nozzle. The approximate solutions to date are restricted to fairly small ranges of the intersecting curvatures, since the midsurfaces of the pipe-nozzle intersection is generally not a geodesic curve. Several researchers achieved different approximate solutions for certain specific locations on the intersection of special geometry configuration by assuming a linear distribution of nominal bending stress through the thickness of the pipe-nozzle intersection, and the continuity conditions of axial membrane stress, circumferential strain, rotation of normal, bending moment at the intersection of pipe-nozzle connection. Usually the elastic deformation, change of geometry effects and strain hardening are ignored in those approximate solutions. Some of these approximations can be very inaccurate in certain cases. The first lower-bound approximate results was attempted by Goodall [9] who performed the limit analysis by using the limited interaction yield surface of approximate Tresca two-moment method. His method, employing the shallow shell equations for the main vessel, was restricted to the case of very small diameter nozzles. It was not possible to achieve equilibrium of forces and moments at the intersection due to the simple stress field assumed.

An estimate of the limit pressure for cylindrical nozzle on cylindrical shell was derived from an upper bound analysis for the two-moment surface by Cloud and Rodabaugh [4]. They provided a simplified formula for pressure stress calculation. However, because of the neglect of several terms in the boring differential equations and some approximations made, this method is restricted to nozzle / shell diameter ratios of 0.5 or less, and can be regarded as a rough estimate.

Schroeder's and Rangarajan's [23] upper bound to plastic limit pressure of branch-pipe tee connections is based on an Ilyushin approximation to the Von Mises yield surface. It is limited to beta, β, (r/R) larger than 0.4 and gamma, γ, (R/T) greater than 20. The assumption has some degree of freedom so that it is possible to gradually lower the upper bounds, which is based on an approximate rigid, perfectly plastic analysis. By using nonlinear programming method, the bounds allowed a more general case and could be further improved.

Very recently, Biron [2] attempted a lower bound formulation by using the same yield surface as defined by Von Mises [23] and by dividing the configuration into limited number of zones and simple expressions for stresses. Because of the small number of these zones, the results obtained are not satisfactory in that all equilibrium requirements can not be satisfied outside of a given tolerance, and the lower bound dependency on this tolerance was not negligible. Within such zones, the stress resultants are approximated by a finite series, then the coefficients of which are optimized. In his research the appropriate continuity conditions must be satisfied across the boundaries, and the equilibrium at the intersection must be satisfied to a specified tolerance.

2.2 Experimental method

Many experimental results with parameters have been provided by different researchers. J. Schroeder and P. Rangarajan [23] set up an experimental model with tee machined from an annealed plate of forged 1020C mild steel (ANSI specification). The yield strength obtained from the annealed specimens was almost identical to the yield strength exhibited by unannealed material cut from branch and pipe where elastic deformations had occurred. Measuring devices were attached to pivots glued to the branch or pipe to avoid shifting of contact points of dial gauges. Both tees indicated pronounced yield points. It should be pointed out that the experimental results are subjected to a great deal of uncertainty for many reasons: (1) the effect of anisotropy and strain hardening of the material used and the difficulty in defining yield stress, (2) the differing amounts of weld at the intersection of the pipe-nozzle, and (3) local defects due to geometry inaccuracies or inhomogeneities. In addition to these, there is a major uncertainty in the definition of limit pressure from experimental results. The experimental data also depends on the strain gage locations and the dial gauge readings.

For the cases of beta, β, (nozzle mean radius /pipe mean radius) up to 0.7 and gamma, γ, (pipe mean radius / pipe thickness) equal to 12.5, J. Schroeder, J. Gartenburg, and K. R. Srinivasaiah [28] performed an experimental analysis with specimens machined from forging process and have fillet but no welds. Also the effect of external reinforcement in the form of fillets is investigated. It was assumed that the prestraining during assembly had a negligible effect on the limit load since a redistribution of strain occurs when limit conditions are approached.

2.3 Numerical analysis

Goodell, R. A. [10] analyzed the stress distribution across the pipe-nozzle intersection numerically for the case of gamma, γ, (R/T), of 3.7, beta, β, (r/R), of 0.65, and (r/t), of 1.6. An axisymmetric geometric assumption combined with the use of asymmetric loading conditions and finite plate method was employed by Brown, S. J. [3] for pipe-nozzle connection of small beta cases, ($r/R < 0.5$). Shortly afterwards, Truitt, J. B. and Raju, P. P. [35] presented a comparative study between a three-dimensional and an axisymmetric finite-element analysis of reactor pressure-vessel inlet nozzle subject to internal pressure. A quarter-symmetric section of the nozzle was modeled with a three-dimensional quadratic isoparametric finite element. This comparative study proved that the axisymmetric analysis is unconservative if based upon common axisymmetric modeling techniques.

A parametric survey of lower-bound limit pressures at the pipe-nozzle connection was then conducted by Robinson, M. [20]. Because of uncertainty and ambiguity in interpreting the experimental data and an inadequate number of good upper-bound results, there is still a need for further work to be done. A better solution would require a three-dimensional elastic-plastic finite element analysis taking account of change of geometry effects.

Based on the boundary-point-least-squares (BPLS) technique, Redekop, D. and Schroeder, J. [18] formulated an approximate method to predict elastic hoop stresses in the longitudinal plane of an unreinforced pressurized tee, using axisymmetric solutions from plate-cylindrical shell intersections. Correspondence of values is such that the present method may be preferred to a full-scale finite element analysis for some cases. A comparison is also made between the hoop stresses in the transverse plan of tees and those in sphere-cylinder intersections.

Since ASME Boiler and Pressure code is limited and does not include some components which are presently being used in plant fabrication, Sadd, M. H. and Avent, R. R. [21] employed a finite element package, Georgia Tech ICES STRUDL, using a quadrilateral element with six degree of freedom at each of the four corner nodes was used, to analyze the pipe trunnion under internal pressure and combined with various end loadings as well. The $alpha_p$ value (pipe length / pipe mean radius) was taken as 8.0 for their model. Several computer runs were made for those cases $R/2 < r < R$ and a gamma, γ, (pipe mean radius / pipe thickness) range from 5 to 20 only, and empirical formulas were developed to express the stress indices as a function of certain dimensionless ratios.

Maximum stress intensities for an equal diameter unreinforced cylinder/cylinder pipe intersection of mean diameter / thickness ratio, 24.7(2 x γ), under internal pressure and six individual moment loadings, were then studied by Moffat, D. G. and Mistry, J. [17]. The significant of the results are: 1) for multiple combined moment loadings, design code may underestimate the resulting maximum stress intensity and 2) for many of the interacting load combinations considered, the circular interaction used by design codes appears to be satisfactory. In some cases, it is significantly conservative due to the reinforcing effect of one load upon another. However, in other cases, in particular for run pipe in-plan and out-of-plan moment combinations, linear interaction has been shown to be more relevant.

Tabone, C. J. and Mallett, R. H. [32] established a finite element model of a nozzle in a cylindrical shell subjected to internal pressure, out-of-plan moment, and a combination of pressure plus out-of-plan moment for one special case of alpha, L/R = 2.83, beta, β, r/R = 0.649, and gamma, γ, R/T =29.95 by using ANSYS finite element package. Three-dimensional finite element model of a nozzle in a cylindrical shell was used and load versus displacement behavior was given. The analysis considered inelastic behavior at small displacements. Two elements along thickness direction of the nozzle and vessel were employed in this geometrical model. The purpose of this paper is to obtain an estimation of limit loads based on extrapolation of the load-versus-inverse-displacement curves. A conclusion was given for the effect of the combined loading, for a case in which the internal pressure reduces the moment capability of the nozzle by 35 percent.

In 1990 and 1991, comprehensive results on local pipe stresses were published by Sun, Sun, and Herman, using finite element method solutions. These papers reported a series of bending and membrane stress factors for local circumferential and longitudinal stresses on the pipe region of the pipe-nozzle juncture due to external loading components. The stress factors due to radial load and overturning moments were reported in Ref. [29], and those for torsional moment and shear forces were reported in Ref. [30]. Both papers adopted the fundamental assumption that the thickness ratio of nozzle to pipe is unified. A related study of the local stresses on the nozzle region of the pipe-nozzle juncture was published by Lin, J., Sun, B. C. and Koplik, B. [12] to complement the pressure vessel design database. Additional data on local stress due to external radial load was presented by Lu, Sun, Koplik [14] with a new assumption that the thickness ratio of nozzle to pipe is equal to the radius ratio of nozzle to pipe. The local pressure stresses reported from this thesis may be used in conjunction either with external local stresses computation provided by the Welding Research Council Bulletin 107, or the above mentioned papers. One should note that the WRC 107 data was not taken into account the pipe-nozzle thickness ratio and the local stresses on the nozzle region.

For certain combinations of geometrical parameters, some researchers have studied the same topic by using the finite element method. However, the purposes of their studies were for verification of certain specific pipe-nozzle geometries. Their limited results are not sufficient to extend over a large range to cover most practical needs in analysis and design. There is a need for a comprehensive study of these local stresses of pipe-nozzle connection under internal pressure. Due to the difficulty in mathematical modelling, using the finite element approach is probably the best choice to pursue this subject. The existing literature in theoretical, experimental and numerical approach are tabulated in chronological order as shown in Figure 2.

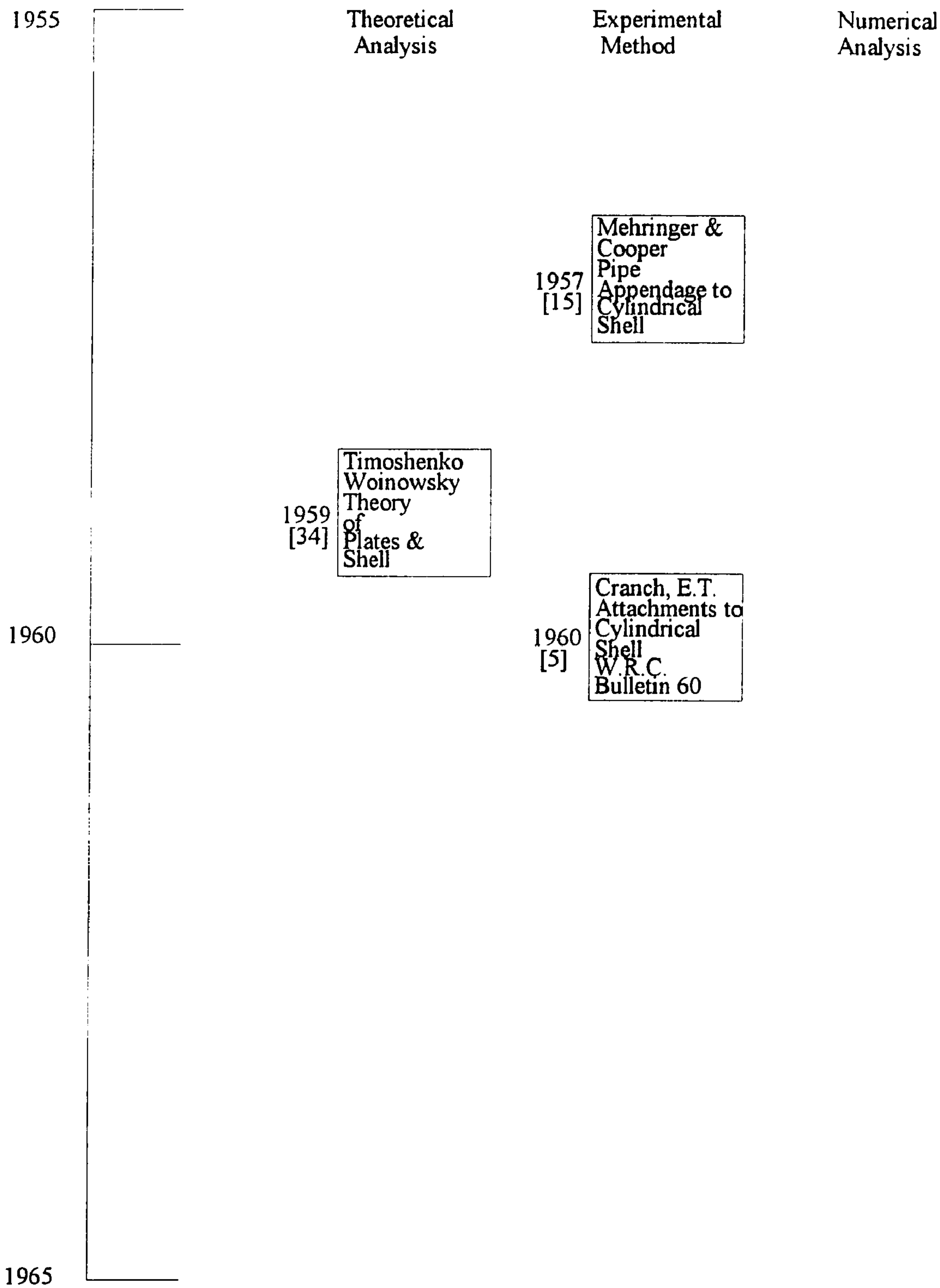

Figure 2 Literature survey table

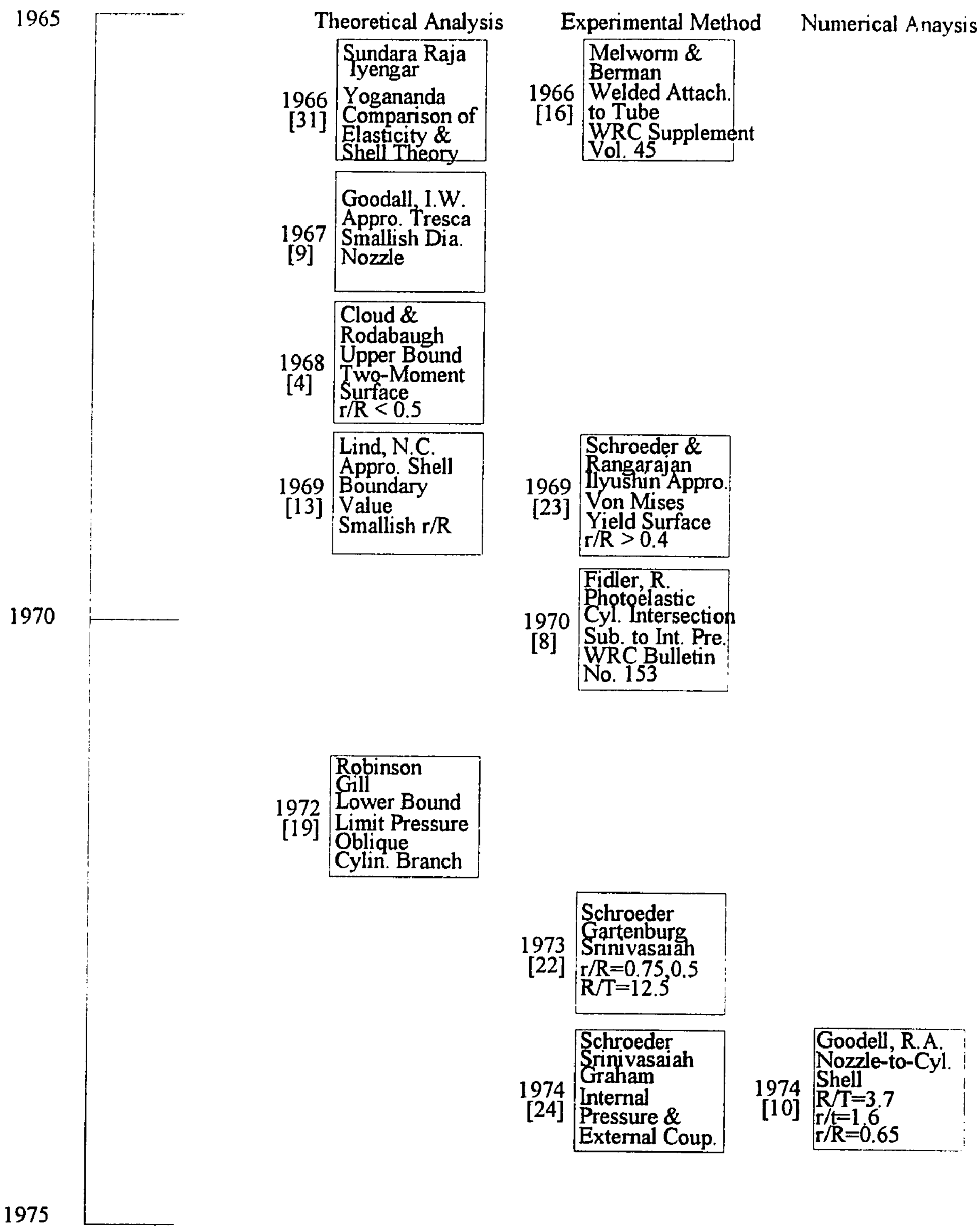

Figure 2 Literature survey table (continued)

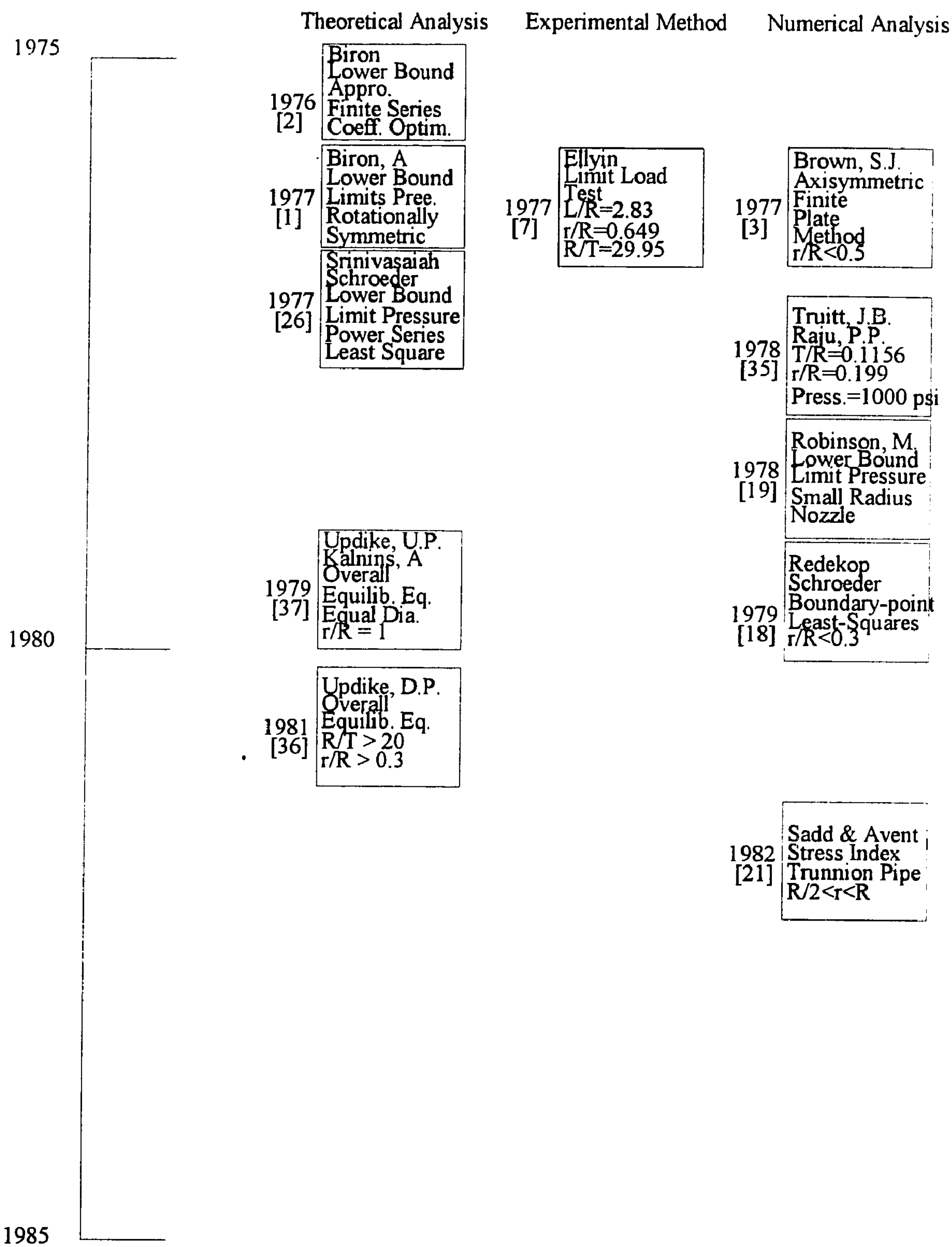

Figure 2 Literature survey table (continued)

Year	Theoretical Analysis	Experimental Method	Numerical Analysis
1985			
1986 [17]			Moffat & Mistry Equal Dia.r/R=1 External Moment with Inter. Pressure
1987 [32]			Tabone & Mallett L/R=2.83 r/R=0.649 R/T=29.95
1988 [25]			Simitses, G. Chen, Z Buckling of Delaminated Cyl. Panel External Press.
1989 [11]			Kishida & Sasaki T/R=.04 r/R=.125,.250 .375,.500
1990			
1990 [28]			Sun, H.C. Sun, B.C. Herman, H. Finite Element Spring Constant
1990 [29]			Sun, H.C. Sun, B.C. Herman, H. Finite Element Local Stresses
1991 [30]			Sun, H.C. Sun, B.C. Herman, H. Finite Element Shear Stress Torsion Moment
1991 [27]			Sun, H.C. Sun, B.C. Herman, H. Finite Element Local Stress Spring Constant
1995			

Figure 2 Literature survey table (continued)

CHAPTER 3

BASIC THEORY

The problem of local stress around the pipe-nozzle under internal pressure involves tremendous mathematical difficulties caused by the absence of axial symmetry. Several researchers achieved different approximate solutions for certain locations on the intersection of special geometry configuration with different assumptions. The linear distribution through the thickness of the pipe-nozzle intersection and continuity conditions of axial membrane stress, circumferential strain, rotation of normal, bending moment at the intersection of pipe-nozzle connection, are commonly assumed in most of the theoretical approximate solution. In comparison with the related axisymmetric problem of a pressurized spherical shell containing a radial circular nozzle, more serious difficulties arise from the circumstance that the intersection of the midsurfaces at the junction is not generally a geodesic curve on either the pipe or nozzle, which restricted the approximate solution to fairly small values of the intersection curvature parameter. Therefore, the results from these local stress studies are limited by the location and special geometry configuration and can also only be used carefully as a reference. Based on the elastic thin-shell theory, Lind [13] assumed this problem as a boundary value problem and developed an overall equilibrium equation at the crotch of a pipe-nozzle connection for limited pipe-nozzle geometry configuration. By employing conformal mapping, Thiel, Eringen and Naghdi [33] achieved solutions to the similar problems of a circular hole in a cylindrical shell (see Equation 1), restricting the solution to a very small values of the opening curvature parameter as reported in Welding Research Council Bulletin 102.

$$\psi = (d/4)(3-3\nu^2)^{\frac{1}{4}}(aT)^{-\frac{1}{2}} \tag{1}$$

The uniformly distributed traction over the edge of the hole acting in the direction of the nozzle axis and equal to the resultant pressure over the area of the hole was assumed in the special case analyzed in Welding Research Council Bulletin 102 [33]. In other words, the closed pressure vessel in which the hole is normally intersected by a closed membrane cylinder with the assumption that the axial stress in the membrane does not vary around the juncture. Actually, considerable variations of this stress exist even for thin walled nozzle through photoelastic experiment.

Most experimental data have shown that the region of highest stress in the pipe-nozzle connection under internal pressure exist at the vicinity of points "A" & "B" (see Figure 1), where large hoop stresses occur as a result of the removed material of the hole from the pipe. In all available experimental data, the highest stress have proven to occur at "A" & "B", and then become the governing stress for design.

In terms of the components of the displacement field and their partial derivatives, the equilibrium equation has been established by Timoshenko [34] and then modified by Lind [13]. Let the components of displacement be u, v, w respectively in the direction of x, ϕ, and r (see the cylindrical-shell coordinates, displacement components, and shell force components in Figure 3).

$$\partial^2(u)/\partial x^2 + \frac{1-\nu}{2}\partial^2(u)/\partial\phi^2 + \frac{1+\nu}{2}\partial^2(v)/\partial x\partial\phi + \nu\partial w/\partial x$$
$$+k[\frac{1-\nu}{2}\partial^2(u)/\partial\phi^2 - \partial^3(w)/\partial x^3 + \frac{1-\nu}{2}\partial^3(w)/\partial x\partial\phi^2] = 0$$

$$\frac{1+\nu}{2}\partial^2(u)/\partial x\partial\phi + \partial^2(v)/\partial\phi^2 + \frac{1-\nu}{2}\partial^2(v)/\partial x^2 + \partial w/\partial\phi$$
$$+k[\frac{3}{2}(1-\nu)\partial^2(v)/\partial x^2 - \frac{3-\nu}{2}\partial^2(w)/\partial x^2 = 0 \tag{2}$$

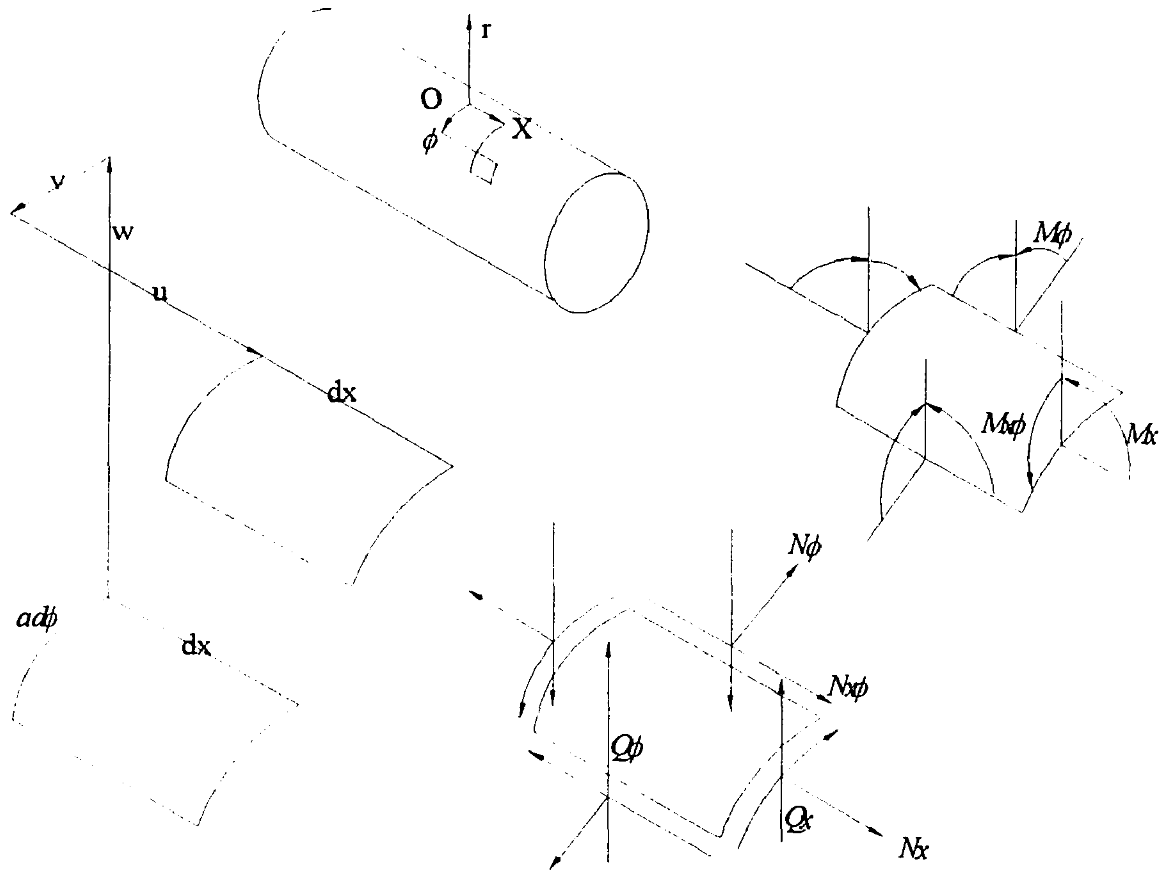

Figure 3 Cylindrical-shell coordinates, displacement components, and shell force components

$$\nu\partial u/\partial x+\partial v/\partial\phi+w+k[\frac{1-\nu}{2}\partial^3(u)/\partial x\partial\phi^2-\partial^3(u)/\partial x^3$$

$$-\frac{3-\nu}{2}\partial^3(v)/\partial^2x\partial\phi+\partial^4w/\partial x^4+2\partial^4(w)/\partial^2x\partial^2\phi$$

$$+\partial^4(w)/\partial\phi^4+2\partial^2(w)/\partial\phi^2+w]-\frac{pa^2}{D}=0$$

$D=Eh^3/[12(1-\nu^2)]$ (see page 29)

$k=h^2/(12a^2)$ (3)

The complementary solution to equation (2) may be written as

$$u = \sum C_m \omega m \quad u = \sum C_m$$

$$u = \sum_{m=0}^{m=\infty} C_m \omega_m \cos(m\phi) \exp(\lambda_m x / a)$$

$$v = \sum_{m=0}^{m=\infty} C_m \rho_m \sin(m\phi) \exp(\lambda_m x / a) \tag{4}$$

$$w = \sum_{m=0}^{m=\infty} C_m \cos(m\phi) \exp(\lambda_m x / a)$$

The complete complementary solution will be the summations of terms from m=0 to m=∞. One can assume that the series may be truncated after the term m=n when n is larger enough. In equation (4), $\lambda_m, \omega_m, \rho_m$, are to satisfy the conditions

$$[\lambda_m{}^2 - \frac{1-\nu}{2} m^2 (1+k)]\omega_m + [\frac{1+\nu}{2} \lambda_m m]\rho_m$$
$$= k(\lambda_m{}^3 + \frac{1-\nu}{2} \lambda_m m^2) - \nu\lambda_m$$

$$[\frac{1+\nu}{2} \lambda_m m]\omega_m + [-\frac{1-\nu}{2} \lambda_m{}^2 + m^2 - \frac{3}{2}(1-\nu)k\lambda_m{}^2]\rho_m$$
$$= \frac{3-\nu}{2} k\lambda_m{}^2 m - m \tag{5}$$

$$\lambda_m{}^8 - 2(2m^2 - \nu)\lambda_m{}^6 + [\frac{1-\nu^2}{k} + 6m^2(m^2 - 1)]\lambda_m{}^4$$
$$-2m^2[2m^4 - (4-\nu)m^2 + (2-\nu)]\lambda_m{}^2 + m^4(m^2 - 1)^2 = 0$$

The m-th terms in equation (4) for m≠0 contribute to the displacements with amplitude of wavelength $2\pi a/m$ in the ϕ direction. As previously assumed, there exists a sufficiently large value of n such that equation (4) may represent the complementary solution with prescribed tolerance.

If the pipe and nozzle is thin shell as assumed, the term $n^2 k^{1/2}$ is negligible in comparison with unity. Then, the condition on λ_m is satisfied independently of m by

$$\lambda_m = \lambda = (\pm)k_1 \pm i\mu_1 = (\pm)b \pm ib \tag{6}$$

where

$$b = [3(1-\nu^2)\frac{a^2}{h^2}]^{1/4} \tag{7}$$

the semi-infinite shell $x \geq 0$ is considered, the two solutions with positive, real part may be discarded in satisfaction of the conditions that solution be bounded for $x \to \infty$, Then ω_m, ρ_m, can be simplified for k negligible in comparison with unity, as follows

$$\omega_m = k\lambda - \nu / \lambda$$
$$\rho_m = -(3-\nu)km/(1-\nu) \tag{8}$$

for all m, the solution may be written as

$$\omega_m = \overline{\omega_1} \pm i\overline{\omega_2}$$
$$\rho_m = \overline{\rho_1} \pm i\overline{\rho_2} \tag{9}$$

where

$$\overline{\omega_1} = \nu / 2b - kb$$

$$\overline{\omega_2} = \nu / 2b + kb$$

$$\overline{\rho_1} = -\frac{3-\nu}{1-\mu} km$$

$$\overline{\rho_2} = 0 \tag{10}$$

The complementary displacements may now be determined from equation (4) and the membrane forces may be determined from the displacements. Of interest in this context are:

$$N_{\phi(\phi=0)} = \frac{D}{a}[(1-\nu^2)\sum C_{1m} - 2kb^2\nu\sum C_{2m}]x\exp(\frac{-bx}{a})\cos(\frac{bx}{a})$$

$$+\frac{D}{a}[(1-\nu^2)\sum C_{2m} + 2kb^2\nu\sum C_{1m}]\exp(\frac{-bx}{a})\sin(\frac{bx}{a}) \tag{11}$$

neglecting terms in $\sum m^2 C_{1m}$ which vanish, and

$$M_{\phi(x=0,\phi=0)} = kD(\sum C_{1m} - \sum m^2 C_{1m} - 2\nu b^2 \sum C_{2m}) \tag{12}$$

$$N_{x(x=0,\phi=0)} = -[(3-\nu)/(1-\nu)](D/a)(k\nu)\sum m^2 C_{1m} \tag{13}$$

$$M_{x(x=0,\phi=0)} = kD(\nu\sum C_{1m} - 2b^2\sum C_{2m} - \nu\sum m^2 C_{1m}) \tag{14}$$

where C_{1m} and $C_{2m}$are constants; all summations, range from m=0 to m=n, (N_ϕ , N_x) are normal force components, and (M_ϕ , M_x) are moment components in the complementary solution, shown in Fig. 2.

When the origin of the shell coordinate, both for the pipe and nozzle, is mapped onto the midpoint of the juncture with the X axis pointing away from the juncture, one boundary condition is obtained by setting N_x = 0 at the origin for both pipe and nozzle.

Thus, the following equation (15) is given

$$\sum m^2 C_{1m}{}^M = 0 \tag{15}$$

$$\sum m^2 C_{1m}{}^B = 0 \tag{16}$$

where, as in the following, superscripts M and B indicate pipe and nozzle, respectively; it is understood that the summations range from m=0 to m=n^M or m=n^B as applicable.

Overall equilibrium of quarter of the pipe-nozzle configuration requires necessarily

$$p(a^M - T/2)(a^B - t/2) = \int_0^\infty N_{\phi(\phi=0)} dx^M + \int_0^\infty N_{\phi(\phi=0)} dx^B + \int_0^\infty Q_{\phi(\phi=\frac{\pi}{2})} dx^M \tag{17}$$

For thin shells, the analysis is significantly simplified by a release of Q_ϕ along ϕ^M = $\pm\pi/2$. Then, the last integral in equation vanishes. Inserting N_ϕ from equation (11) into equation (17) and integrating gives, with equation (15) and (16)

$$\left\{\left(\frac{D}{2b}\right)(1-\nu^2)\left(\sum C_{1m} + \sum C_{2m}\right)\right\}^M + \{\ \}^B = p(a^M - T/2)(a^B - t/2) \tag{18}$$

By equation (15), (16), and (14)

$$\sum C_{2m} = \frac{\nu}{2b^2}\sum C_{1m} - \frac{M_{x(x=0,\phi=0)}}{2b^2 kD} \tag{19}$$

with this, and specializing equation (11) for x=0 and inserting the result into equation (18), one gets

$$\left\{\frac{ah}{2b}\left[\frac{N_{\phi(x=0,\phi=0)}}{h} + \frac{1-\upsilon^2}{2b^2 akh} M_{x(x=0,\phi=0)}\right]\right\}^M + \{\ \}^B = p(a^M - T/2)(a^B - t/2) \tag{20}$$

if the term with M_x, $\nu / 2b^2$ and k is kept in equation (20). Here, the terms containing M_x are identified as the bending stresses in the X directions at the juncture, at a point located approximately halfway between the midsurface and the internal surface. Assume that the curvature parameter is small and the longitudinally normal stress is linearly distributed across through the pipe thickness at the juncture of pipe-nozzle connection. The longitudinally normal stresses for pipe and nozzle then be inserted into equation (20) at this point. Then, by equation (20)

$$\left\{\frac{ah}{2b}\sigma_c + \frac{1-\upsilon^2}{2b^2 akh}\frac{2h}{a}\right\}^M + \left\{\frac{ah}{2b}\sigma_c + \frac{1-\upsilon^2}{2b^2 akh}\frac{2h}{a}\right\}^B$$

$$= p(a^M - T/2)(a^B - t/2) \tag{21}$$

Finally, continuity of hoop strain together with the conditions $N_x{}^B = N_x{}^M = 0$ at the juncture gives the result that the hoop stress, $\sigma_c + pa/h$, is continuous at the juncture:

$$\left(\sigma_c + p\frac{a}{h}\right)^M = \left(\sigma_c + p\frac{a}{h}\right)^B \tag{22}$$

Equation (21), (22) give the solution for the hoop stress at the juncture:

$$\sigma_c + \frac{pa}{h} = \frac{2a^M a^B + (a^2/b)^M + (a^2/b)^B}{(ah/b)^M + (ah/b)^B} p - p\left[\frac{4b^2 ak}{1-\upsilon^2}\cdot\frac{1}{h}\right]^M - p\left[\frac{4b^2 ak}{1-\upsilon^2}\cdot\frac{1}{h}\right]^B \tag{23}$$

where terms in the order of h/a have been neglected in comparison with unity. With respect to the nominal stress

$$\sigma_N{}^M = p(a/h)^M \tag{24}$$

the stress in equation (23) can be expressed in terms of the stress concentration factor:

$$K = \frac{2a^B h^M + (ah/b)^M + (a^2/b)^B/(a/h)^M}{(ah/b)^M + (ah/b)^B} - \left[\frac{4b^2 ak}{(1-\upsilon)^2 h}\right]^M - \left[\frac{4b^2 ak}{(1-\upsilon)^2 h}\right]^B \tag{25}$$

The pressure stress factors from the above model is to be compared with the results from the finite element analysis in this thesis and the results from other literature.

Based on the shell theory, Updike, D.P. and Kalnins, A. [37] treat an approximate analysis of the stresses in the vicinity of the crotch of a tee branch connection of cylindrical shell of equal diameter and thickness subjected to internal pressure loading. Updike, D. P. uses an overall equilibrium equation for a tee branch connection developed by Lind [13] to extend the simplified method of Updike, D.P. and Kalnins, A. [37] to include tees connecting cylindrical shells of unequal diameter and thickness. The material of the structure is treated as isotropic and linearly elastic.

In the simple axisymmetric model presented in [37], the crotch portion of the tee is modeled as the junction of two cylindrical panels such as ABML and AGNI of Figure 4. The analysis subjects these panels to continuity conditions at point A and the circumferential stresses on the cut GAB to an overall equilibrium condition. It was determined in [37] that the stresses in the cylindrical panels may be determined with reasonable accuracy by neglecting derivatives in the circumferential direction in comparison with those in the meridianal direction.

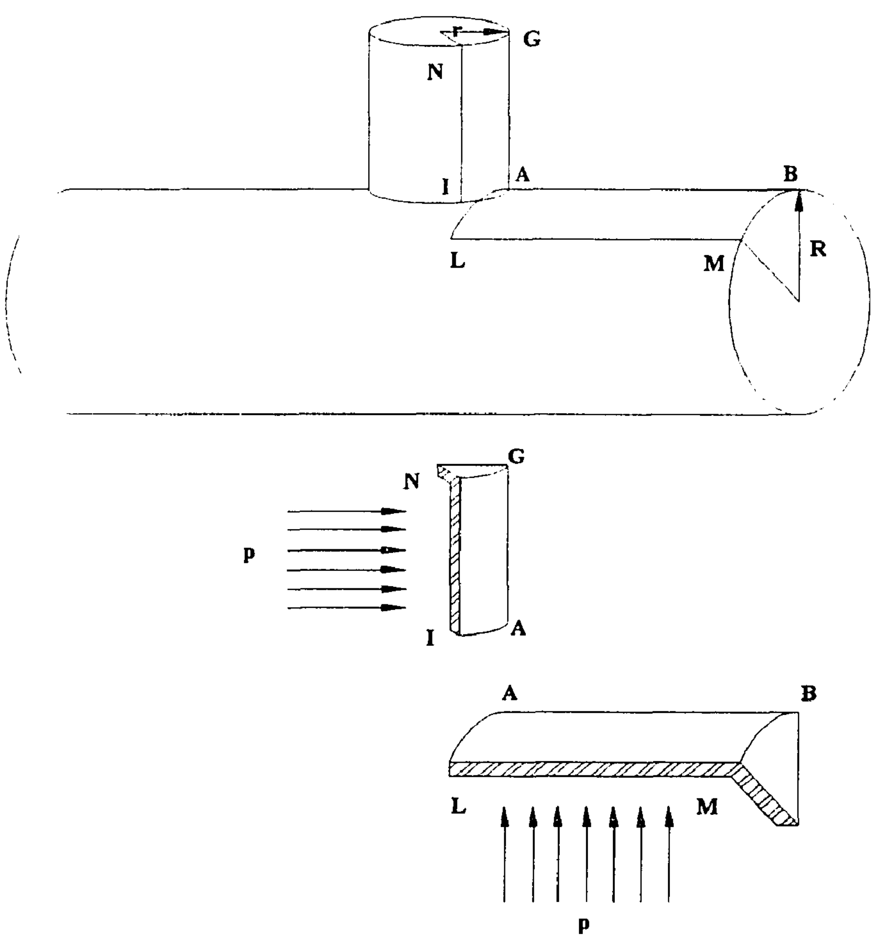

Figure 4 Pipe-nozzle connection

Updike neglected the derivatives in the circumferential direction and the approximation requires that application be limited to rather thin shells for which $\sqrt{RT}$ and $\sqrt{rt}$ are much larger than unity. As a practical working limit the restrictions

R / T > 20 (gamma)

r / t > 20

$$\frac{r}{t} = \frac{\frac{r}{R}}{\frac{t}{R}} = \frac{\beta}{\frac{1}{\gamma}} = \beta\gamma$$

r / R > 0.3

may be used.

The overall equilibrium equation for a tee branch connection developed by Lind [13] represents a balance of forces across the midplane of the structure. Referring to Figure 5 the tensile forces on the cross section HGABCJK of the structure are set equal to the resultant force of the pressure acting on area HGABCJK. If it is assumed that both the main shell and the branch are long and that the stress along KJ is the nominal loop stress, then the pressure times area ECJK is balanced by the tensile force along CJK.

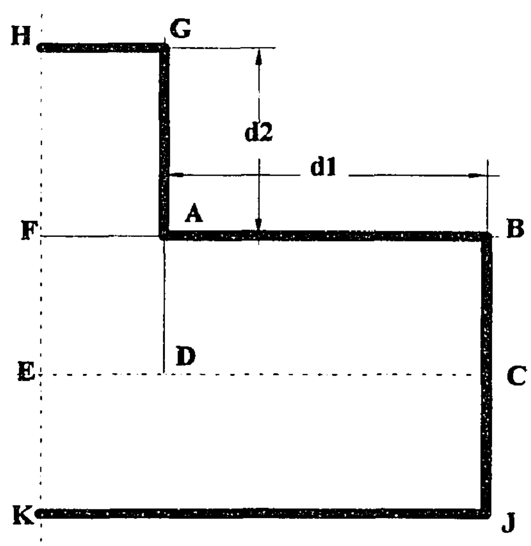

Figure 5 The cross section of Pipe-nozzle connection

This then requires that the tensile force on HGABC balance the pressure times area HGABCE (see Figure 5). The force balance equation then becomes

$$\int_{HGABC} N_\theta dx - pRd_1 - prd_2 = pRr \tag{26}$$

Expressions for the edge shearing forces Q_{x1} and Q_{x2} acting on the cylindrical panels ABML and AGNI at the junction point A (Figure 4) are derived in [37] to be

$$Q_{x1}R = \int_{ABC} N_\theta dx - pRd_1 \tag{27a}$$

$$Q_{x2}r = \int_{AGH} N_\theta dx - prd_2 \tag{27b}$$

Summing equations (27a) and (27b) and invoking (26) results in

$$Q_{x1}R + Q_{x2}r = pRr \tag{28}$$

The edge rotation and circumferential strain (refer to Figure 6) at point A (see Figure 4) of the cylindrical panels joined at A may be expressed in terms of edge moments and shearing forces [34] as

$$dw_1 / dx_1 = M_{x1} / (\beta_1 D_1) - Q_{x1} / (2\beta_1^2 D_1) \tag{29a}$$

$$dw_2 / dx_2 = M_{x2} / (\beta_2 D_2) - Q_{x2} / (2\beta_2^2 D_2) \tag{29b}$$

$$\varepsilon_{\theta 1} = Q_{x1} / (2\beta_1^3 D_1 R) - M_{x1} / (2\beta_1)$$

$$\varepsilon_{\theta 1} = Q_{x1} / (2\beta_1^3 D_1 R) - M_{x1} / (2\beta_1^2 D_1 R) + (pR)/(ET) - (\nu N_{x1})/(ET) \tag{30a}$$

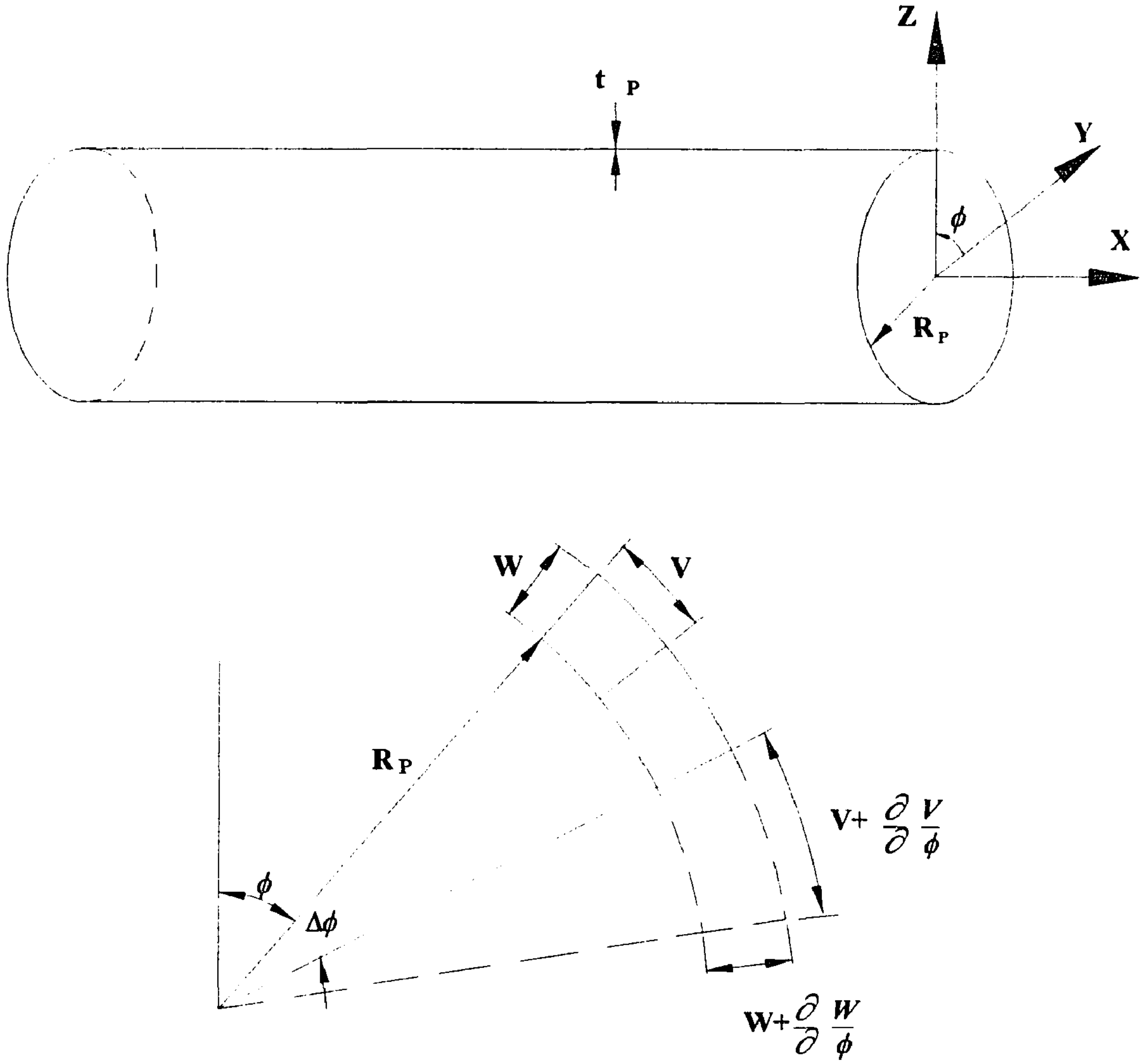

Figure 6 Cylindrical coordinate applied to a cylindrical pipe with displacement u, v, and w in X, Y, Z direction respectively

$$\varepsilon_{\theta 2} = Q_{x2} / (2\beta_2{}^3 D_2 r) - M_{x2} / (2\beta_2{}^2 D_2 r) + (pr)/(Et) - (\nu N_{x2})/(Et) \tag{30b}$$

where

$$\xi_1{}^4 = 3(1-\nu^2)/(R^2T^2) \tag{31a}$$

$$\xi_2{}^4 = 3(1-\nu^2)/(r^2t^2) \tag{31b}$$

and

$$D_1 = ET^3 / [12(1-\nu^2)] \text{ (see page 17)} \tag{32a}$$

$$D_2 = Et^3 / [12(1-\nu^2)] \tag{32b}$$

The stress resultants $M_{x1}, Q_{x1}, N_{x1}, M_{x2}, Q_{x2}$, and N_{x2} at point A are now determined using the equilibrium equation (28) and five continuity conditions at A. The continuity conditions are

$$\varepsilon_{\theta 2} = \varepsilon_{\theta 1} \tag{33}$$

for the circumferential strain,

$$dw_2 / dx_2 = -dw_1 / dx_1 \tag{34}$$

for the rotation of normal,

$$M_{x2} = M_{x1} \tag{35}$$

for the bending moments,

A satisfactory approximation away from the intersection for the axial membrane stresses are

$$N_{x1} = pR / 2 \tag{36a}$$

$$N_{x2} = pr / 2 \tag{36b}$$

Equations (28)-(36) are a system of algebraic equations for the stress couples M_{x1} and M_{x2} and the hoop strains $\varepsilon_{\theta 1}$ and $\varepsilon_{\theta 2}$.

Once the stress resultants N_{x1}, N_{x2}, M_{x1}, and M_{x2} and the circumferential strains $\varepsilon_{\theta 1}$ and $\varepsilon_{\theta 2}$ have been found, stresses at point A may be calculated based on assumed distributions through the thickness. Direct stresses and nominal bending stresses are obtained by assuming a linear distribution. The meridianal direct stresses in the two shells where they attach at point A are given by

$$\sigma_{a1} = N_{x1} / T \qquad (37a)$$

$$\sigma_{a2} = N_{x2} / t \qquad (37b)$$

while the nominal meridianal bending stresses are

$$\sigma_{b1} = 6M_{x1} / T^2 \qquad (38a)$$

$$\sigma_{b2} = 6M_{x2} / t^2 \qquad (38b)$$

The circumferential direct stresses are obtained from Hook's law as

$$\sigma_{c1} = E\varepsilon_{\theta} + \nu N_{x1} / T \qquad (39a)$$

$$\sigma_{c2} = E\varepsilon_{\theta} + \nu N_{x2} / t \qquad (39b)$$

The above equations give the stress components according to shell theory, which assumes that stresses vary linearly through the wall thickness. Right at the crotch section, this stress distribution does not apply; therefore, the manner in which these calculations are applied in the design of pressure vessels depends on the type of loading present and the kind of failure anticipated. The local pressure stress from the above equations is to be compared with the results from the finite element analysis in this thesis. All the normalized stress factors may be inserted into the computation and sign notation sheet for local stress of pipe-nozzle model as shown in Table 1 and Figure 7, which are the standard computation sheet from WRC 107.

Table 1 Modified stress computation table of WRC 107 including local pressure stresses

From Fig.	Read curves for	Compute absolute value of stress and enter result	A_U	A_L	B_U	B_L	C_U	C_L	D_U	D_L
3C(1)	$\frac{N_\phi}{P/R_m}=$	$K_n(\frac{N_\phi}{P/R_m})\frac{P}{R_m T}=$	-	-	-	-	-	-	-	-
1C(1)	$\frac{M_\phi}{P}=$	$K_b(\frac{M_\phi}{P})\frac{6P}{T^2}=$	-	+	-	+	-	+	-	+
3A(1)	$\frac{N_\phi}{M_c/R_m^2\beta}=$	$K_n(\frac{N_\phi}{M_c/R_m^2\beta})\frac{M_c}{R_m^2\beta T}=$					-	-	+	+
1A(1)	$\frac{M_\phi}{M_c/R_m\beta}=$	$K_b(\frac{M_\phi}{M_c/R_m\beta})\frac{6M_c}{R_m\beta T^2}=$					-	+	+	-
3B(1)	$\frac{N_\phi}{M_L/R_m^2\beta}=$	$K_n(\frac{N_\phi}{M_L R_m^2\beta})\frac{M_L}{R_m^2\beta T}=$	-	-	+	+				
1B(1) or 1B-1(1)	$\frac{M_\phi}{M_L/R_m\beta}=$	$K_b(\frac{M_\phi}{M_L R_m\beta})\frac{6M_L}{R_m\beta T^2}=$	-	+	+	-				
5P Thru 8P	Pressure stress factor	Pressure stress factor x P =	+	+	+	+	-	-	-	-
Add algebraically for summation of circumferential stresses, σ_ϕ =										
4C(1)	$\frac{N_\phi}{P/R_m}=$	$K_n(\frac{N_\phi}{P/R_m})\frac{P}{R_m T}=$	-	-	-	-	-	-	-	-
2C(1)	$\frac{M_\phi}{P}=$	$K_b(\frac{M_\phi}{P})\frac{6P}{T^2}=$	-	+	-	+	-	+	-	+
4A(1)	$\frac{N_\phi}{M_c/R_m^2\beta}=$	$K_n(\frac{N_\phi}{M_c/R_m^2\beta})\frac{M_c}{R_m^2\beta T}=$					-	-	+	+
2A(1)	$\frac{M_\phi}{M_c/R_m\beta}=$	$K_b(\frac{M_\phi}{M_c/R_m\beta})\frac{6M_c}{R_m\beta T^2}=$					-	+	+	-
4B(1)	$\frac{N_\phi}{M_L/R_m^2\beta}=$	$K_n(\frac{N_\phi}{M_L R_m^2\beta})\frac{M_L}{R_m^2\beta T}=$	-	-	+	+				
2B(1) or 2B-1(1)	$\frac{M_\phi}{M_L/R_m\beta}=$	$K_b(\frac{M_\phi}{M_L R_m\beta})\frac{6M_L}{R_m\beta T^2}=$	-	+	+	-				
1P Thru 4P	Pressure stress factor	Pressure stress factor x P =	+	-	+	-	-	+	-	+
Add algebraically for summation of longitudinal stresses, σ_x										
Shear stress due to Torsion, M_T		$\tau_{\phi x}=\tau_{x\phi}=\frac{M_T}{2\pi r_o^2 T}$	+	+	+	+	-	-	-	-
Shear stress due to load, V_C		$\tau_{x\phi}=\frac{V_C}{\pi r_o T}$	+	+	-	-				
Shear stress due to load, V_L		$\tau_{x\phi}=\frac{V_L}{\pi r_o T}$					-	-	+	+
Add algebraically for summation of shear stresses, τ=										
COMBINED STRESS INTENSITY, S										

(Note 1. Refer to figure in WRC 107 [38])

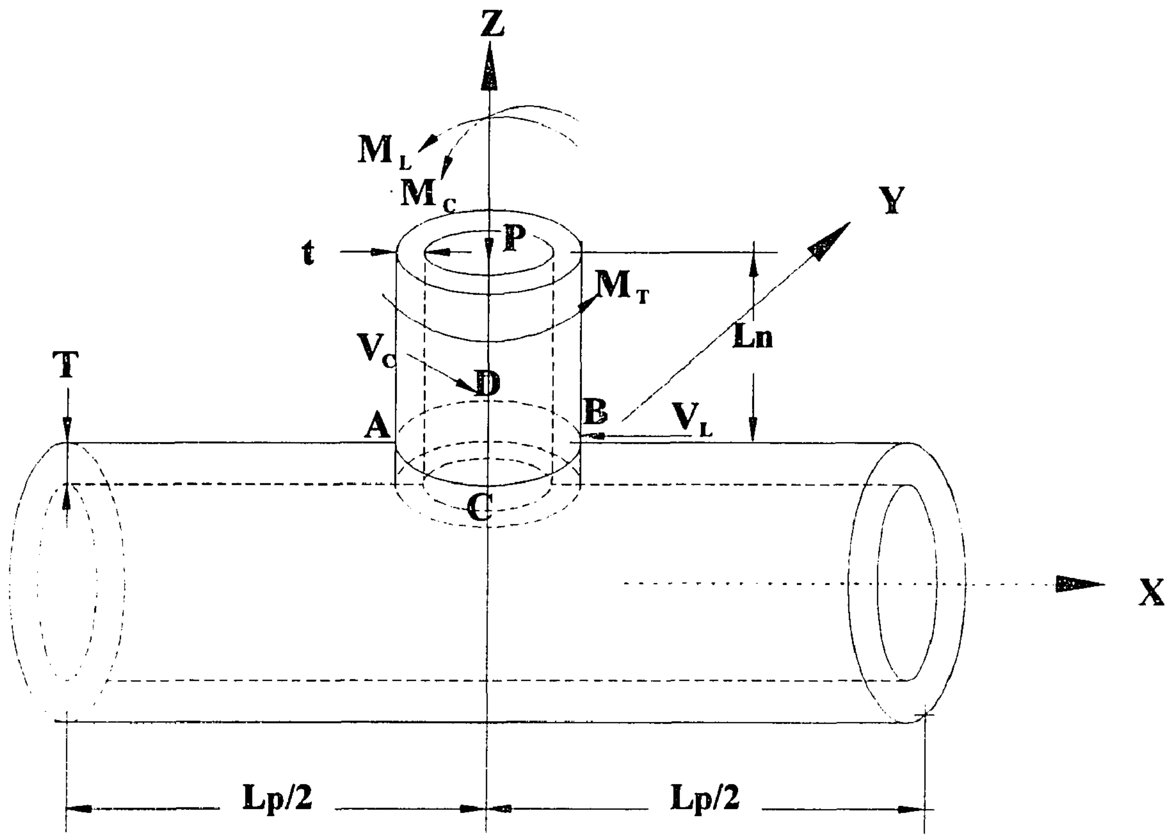

P = Radial Load	T = Pipe Thickness
M_c = Circumferential Moment	t = Nozzle Thickness
M_L = Longitudinal Moment	β = Nozzle Mean Radius / Pipe Mean Radius
M_T = Torsion Moment	= Nozzle Thickness / Pipe Thickness
V_C = Circumferential shear Load	γ = Pipe Mean Radius / Pipe Thickness
V_L = Longitudinal shear Load	α_p = Pipe Length / Pipe Mean Radius
p = Internal Pressure	α_n = Nozzle Length / Nozzle Mean Radius
Lp= Pipe length	Ln= Nozzle length

Figure 7 Typical loads applied on pipe-nozzle connection
(refer to Table-1, Modified stress computation table of WRC 107)

CHAPTER 4

THREE DIMENSIONAL FINITE ELEMENT ANALYSIS

4.1 General

The finite element model of the pipe-nozzle in this thesis uses plate/shell elements which are either three or four nodes formulated in three dimensional space. The normal rotation to the plane of the plate is not defined. Three translations and two rotations which produce out-of-plane bending are defined for these elements (see Figure 8 & 9). Plate/shell elements which are skewed to the global coordinate system (typical of shell models) must have all six degrees of freedom active. At these nodes, where surrounding elements are nearly coplanar but not globally aligned. In this thesis isotropic material is used for all the model. The material property data must produce a positive definite stress-strain matrix. Stress output includes in-plane membrane and out-of-plan bending stress.

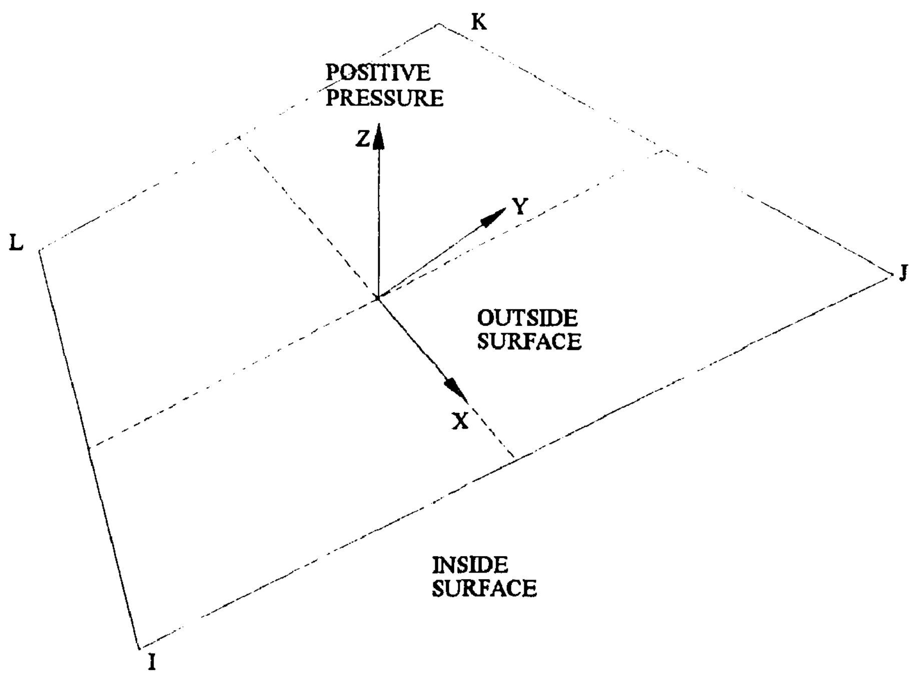

Figure 8 Plate/shell element positive pressure direction (quadrilateral)

In this thesis, by using plate/shell elements with six degrees of freedom, the pipe-nozzle full model is created by quadrilateral and triangle thin shell elements for a wide range of beta and gamma which cover most of the needs in pipe-nozzle stress analysis. Due to the absence of axial symmetry, it is required to develop large number of elements and generate sufficient meshes to provide the asymptotic of stress results.

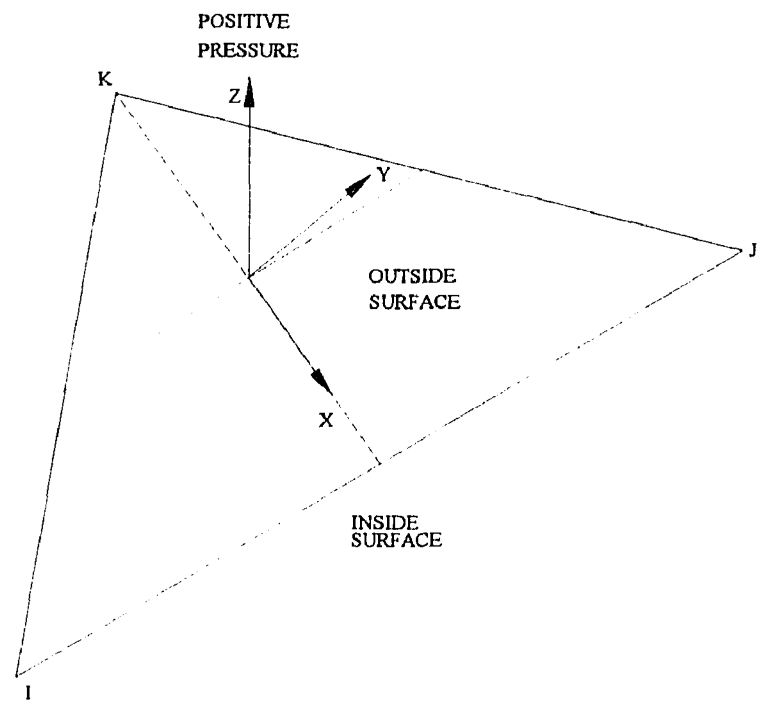

Figure 9 Plate/shell element positive pressure direction (triangle)

4.2 Improved technique

From the pipe-nozzle geometry, elastic properties, and support conditions, one can easily see that it is symmetric with respect to the X-Y or Y-Z planes. Therefore, some quarter models presented in the past need to be very careful about the boundary conditions assigned to each cut-off plane and the expression of the results. Also the quarter model are not suitable for the pipe-nozzle configuration with large beta values. Since the point C (see Figure 1) at the pipe-nozzle juncture will lose the support from the pipe-nozzle configuration. In lieu of the above difficulties, this thesis employs the full finite element model which quadruple the model points and the quarter model analysis.

The stiffness of the triangle element is different with the quadrilateral element. In order to minimize the effect caused by different elements, it is necessary to assign the triangle element away from the pipe-nozzle juncture as much as possible. The positive pressure direction for quadrilateral element and triangle element are shown on Figure 4 and Figure 5. It is very important to make sure all the elements in the pipe-nozzle model, having the positive pressure, are directed to the outgoing normal of the shell surface.

Due to the requirement of accuracy, one would like to use smaller elements around the pipe-nozzle juncture. The ratio of the size of the largest element to the size of the smallest element is restricted to a certain value in the finite element package. For the reason of keeping all the elements not having too much difference in their size, the total number of the elements is limited to a certain number to compromise the element size ratio.

There are approximately five thousand node points and three thousand elements in each of the above models. The actuarial numbers of node and thus element vary with the beta, β, value of the model as tabulated in Table 2. Ten different full model of pipe-nozzle configurations have been created for each beta value, respectively, in this thesis. All these models require about 10,000 seconds of CPU time and 300 Megabytes hard disk memory to run a single case. The results need to be compressed and saved onto a floppy disk right after each run for future reference. All the computation were performed on a DX-66, 486 CPU, personal computer with 8 Megabytes of RAM. A computer graphics representation for the full model finite element results is presented as shown in the Appendix D.

Table 2 The number of node and element for each model with different beta value, β

beta, β	number of node	number of element
0.1	5011	3009
0.2	4965	2982
0.3	5021	3020
0.4	5174	3113
0.5	5268	3245
0.6	4862	2963
0.7	4989	2991
0.8	5118	3018
0.9	5002	3001
1.0	5131	3089

4.3 Assumptions

The typical configuration and basic nomenclature of the pipe-nozzle connection is defined as shown in Figure 1. The following assumptions are used:

1. The homogeneous and isotropic material is assumed in this analysis, and Hook's law is applied. The resulting stresses and strains are within the proportional limit of the material.
2. The influence of self-weight and temperature are neglected.
3. In the pipe-nozzle connection model, all the ends of the pipe and nozzle are assumed to be either fixed or "built-in". The length of the pipe and nozzle are sufficiently long so that the boundary conditions at the ends of the pipe, as well as the nozzle, will not effect the stress results.
4. There are no reinforcing, fillets, or transitions at the pipe-nozzle juncture.

4.4 Asymptotic study

To ensure the accuracy of the results, several models with different elements and node numbers have been studied. For optimum accuracy within the framework of the software and hardware, the finite element model of plate/shell element with 96 nodes on the juncture of pipe-nozzle connection is adopted, which is concluded from the asymptotic study as shown in Figures B-1 through B-16 of Appendix B. Figures C-1 through C-16 of Appendix C show the percentage of improvement with larger α_p to the previous α_p, and Figures C-17 through C-32 show the percentage of improvement with larger α_n to the previous α_n. As a result, the alpha$_p$, α_p, (pipe length/pipe mean radius) should be as large as 8.0 and the alpha$_n$, α_n, (nozzle length/nozzle mean radius) should be as large as 4.0. For all those pipe-nozzle configurations which satisfy the above requirements, the boundary at the pipe and nozzle ends can either be simply supported or fixed. In other words, once the pipe and nozzle lengths are long enough, the effects due to either fixed end or simply supported end, has no significant effect to the stress results. In this thesis, fixed end boundary conditions are used for the pipe and nozzle ends.

4.5 Normalization studies

A normalization study was performed to ensure the validity of using β, (nozzle mean radius / pipe mean radius) and γ, (pipe mean radius / pipe thickness) as the pipe-nozzle geometric parameters. Three models are discussed as follows:

In model 1, two physical pipe-nozzle models of different sizes are run with identical parameters of α_p =8, α_n =4, β = 0.4, and γ = 75 and under the same internal pressure. Table D-1 through D-4 of Appendix D show that the local stresses from both runs are identical. This verifies the validity of using α, β, and γ as geometric parameters for the study.

In model 2, two more models of pipe-nozzle with the same parameters, α_p =8, α_n =4, β = 0.5, and γ = 50 are used. Again, the results from Tables D-5 through D-8 of Appendix D prove that the geometric parameters α, β, and γ are valid for the finite element analysis.

In model 3, two models with the same geometric configurations but under different internal pressures are run. The local pressure stresses results are listed in Tables D-9 through D-12 of Appendix D. Again, they have shown that the normalization of pressure stress factor by a randomly selected applied internal pressure is valid.

CHAPTER 5

COMPARISON OF DATA

The pressure stress factors from this thesis for the cases of beta, $\beta = r/R = 0.500$, $t=\beta T$, and gamma, $\gamma = R/T = 150, 75, 25, 10$, respectively, are compared with previously published data from Updike, D.P. [36], which was derived from theoretical stress function approach, also comparisons are made from data provided by Dickey, J.R., and Krishnamurthy, N., [34] with numerical approach for the cases of beta, $\beta = r/R = 0.500$, gamma, $\gamma = R/T = 150, 75, 25, 10$, $t/T = 0.3$, and 0.6, respectively. The column (a) in Table 3-6 are the results of finite element analysis from this thesis with $t=\beta T$. The columns (b) and (d) are the results from Updike, D.P. [36], columns (c) and (e) are results for numerical analysis data from Dickey, J.R., and Krishnamurthy, N., [6] for the cases of $t/T = 0.3$, and 0.6, respectively. The last column (f) are the results calculated by the newly proposed mathematical model from this thesis. Although the percentage of differences are seemly large as listed in Table 3 through Table 6, since the thickness ratio are different and the lack of information on node points and boundary conditions from Ref. [36] and [6], therefore one may conclude that the stress factors from this thesis by finite element analysis and other mathematical models are in general agreement. Also, the stress factor results from the proposed mathematical model are closer to the finite element results presented in this thesis when γ is small. This implies that one may use the simplified results from the mathematical model presented in this thesis when the pipe-nozzle are relatively thick.

The following tables (3-6) demonstrate all details of the above discussions:

Case # 1

Table 3 Data comparison of stress factor for γ = 150

	(a)	(b)	(c)	(d)	(e)	(f)
$\alpha_p = L_p / R$	8	not reported	not reported	not reported	not reported	8
$\alpha_n = L_n / R$	4	not reported	not reported	not reported	not reported	4
number of node points at the juncture of pipe-nozzle connection	96	not reported	not reported	not reported	not reported	not used
β=r/R	0.5	0.5	0.5	0.5	0.5	0.5
γ=R/T	150	150	150	150	150	150
t/T	.5	.3	.3	.6	.6	.5
Pressure stress factor in the circumferential direction of the pipe at point A_L	1623	1902	1713	1432	1349	1857
Percentage of difference	0%	17%	5.5%	-11.8%	-16.9%	14%

(a) Stress factor from this thesis by finite element analysis, symbol " ■ " on Figure 10 through 13.

(b) Stress factor from Updike, D.P. [36], by theoretical approximation for t/T=0.3, symbol "Δ" on Figure 10 through 13.

(c) Stress factor from Dickey, J.R., Krishnamurthy, N, [6], by finite element for t/T=0.3, symbol "□ "on Figure 10 through 13.

(d) Stress factor from Updike, D.P. [36], by theoretical approximation for t/T=0.6, symbol "◊" on Figure 10 through 13.

(e) Stress factor from Dickey, J.R., Krishnamurthy, N, [6], by finite element for t/T=0.6, symbol "×" on Figure 10 through 13.

(f) Stress factor from the mathematical model in this thesis for t/T=β, Symbol "○" on Figure 10 through 13.

Case # 2

Table 4 Data comparison of stress factor for $\gamma = 75$

	(a)	(b)	(c)	(d)	(e)	(e)
$\alpha_p = L_P / R$	8	not reported	not reported	not reported	not reported	8
$\alpha_n = L_n / r$	4	not reported	not reported	not reported	not reported	4
number of node points at the juncture of pipe-nozzle connection	96	not reported	not reported	not reported	not reported	not used
β=r/R	0.5	0.5	0.5	0.5	0.5	0.5
γ=R/T	75	75	75	75	75	75
t/T	.5	.3	.3	.6	.6	.5
Pressure stress factor in the circumferential direction of the pipe at point A_L	563.2	694	737	526	578	638.4
Percentage of difference	0%	23.2%	30.8%	-6.6%	2.6%	13.2%

Case #3

Table 5 Data comparison of stress factor for γ = 25

	(a)	(b)	(c)	(d)	(e)	(e)
$\alpha_p = L_P / R$	8	not reported	not reported	not reported	not reported	8
$\alpha_n = L_n / r$	4	not reported	not reported	not reported	not reported	4
number of node points at the juncture of pipe-nozzle connection	96	not reported	not reported	not reported	not reported	not used
β=r/R	0.5	0.5	0.5	0.5	0.5	0.5
γ=R/T	25	25	25	25	25	25
t/T	.5	.3	.3	.6	.6	.5
Pressure stress factor in the circumferential direction of the pipe at point A_L	118.3	144.2	174.0	110.9	135.5	124.13
Percentage of difference	0%	21.9%	47.1%	-6.25%	14.5%	4.9%

Case #4

Table 6 Data comparison of stress factor for $\gamma = 10$

	(a)	(b)	(c)	(d)	(e)	(e)
$\alpha_p = L_p / R$	8	not reported	not reported	not reported	not reported	8
$\alpha_n = L_n / r$	4	not reported	not reported	not reported	not reported	4
number of node points at the juncture of pipe-nozzle connection	96	not reported	not reported	not reported	not reported	not used
β=r/R	0.5	0.5	0.5	0.5	0.5	0.5
γ=R/T	10	10	10	10	10	10
t/T	.5	.3	.3	.6	.6	.5
Pressure stress factor in the circumferential direction of the pipe at point A_L	37.71	40.2	44.2	31.4	33.2	37.50
Percentage of difference	0%	6.6%	5.5%	17.2%	-16.7%	0.56%

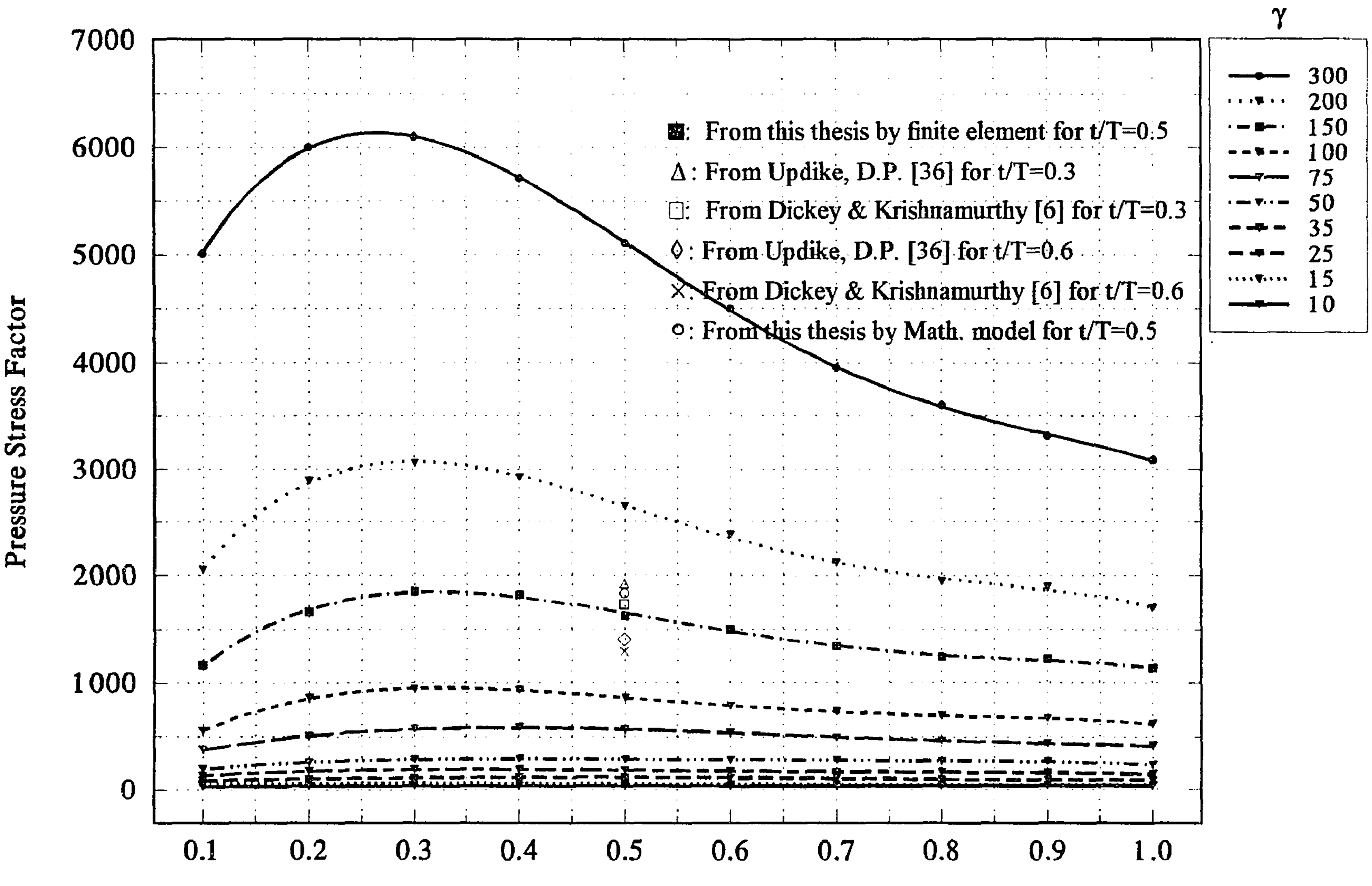

Figure 10 Data comparison of pressure stress factor in the circumferential direction of the pipe at point A_L for $\gamma = 150$, $\beta = 0.5$

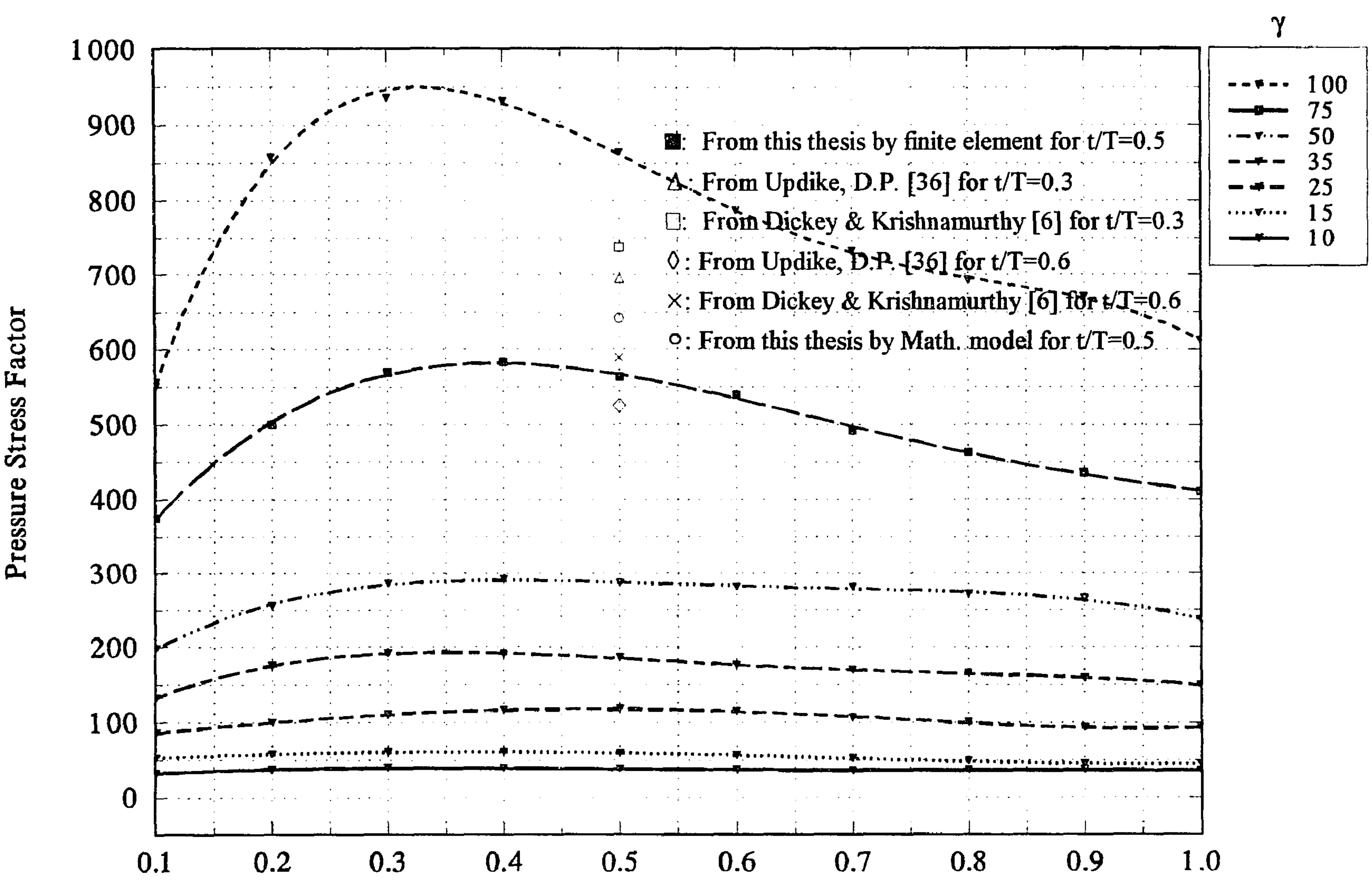

Figure 11 Data comparison of pressure stress factor in the circumferential direction of the pipe at point A_L for $\gamma = 75$, $\beta = 0.5$

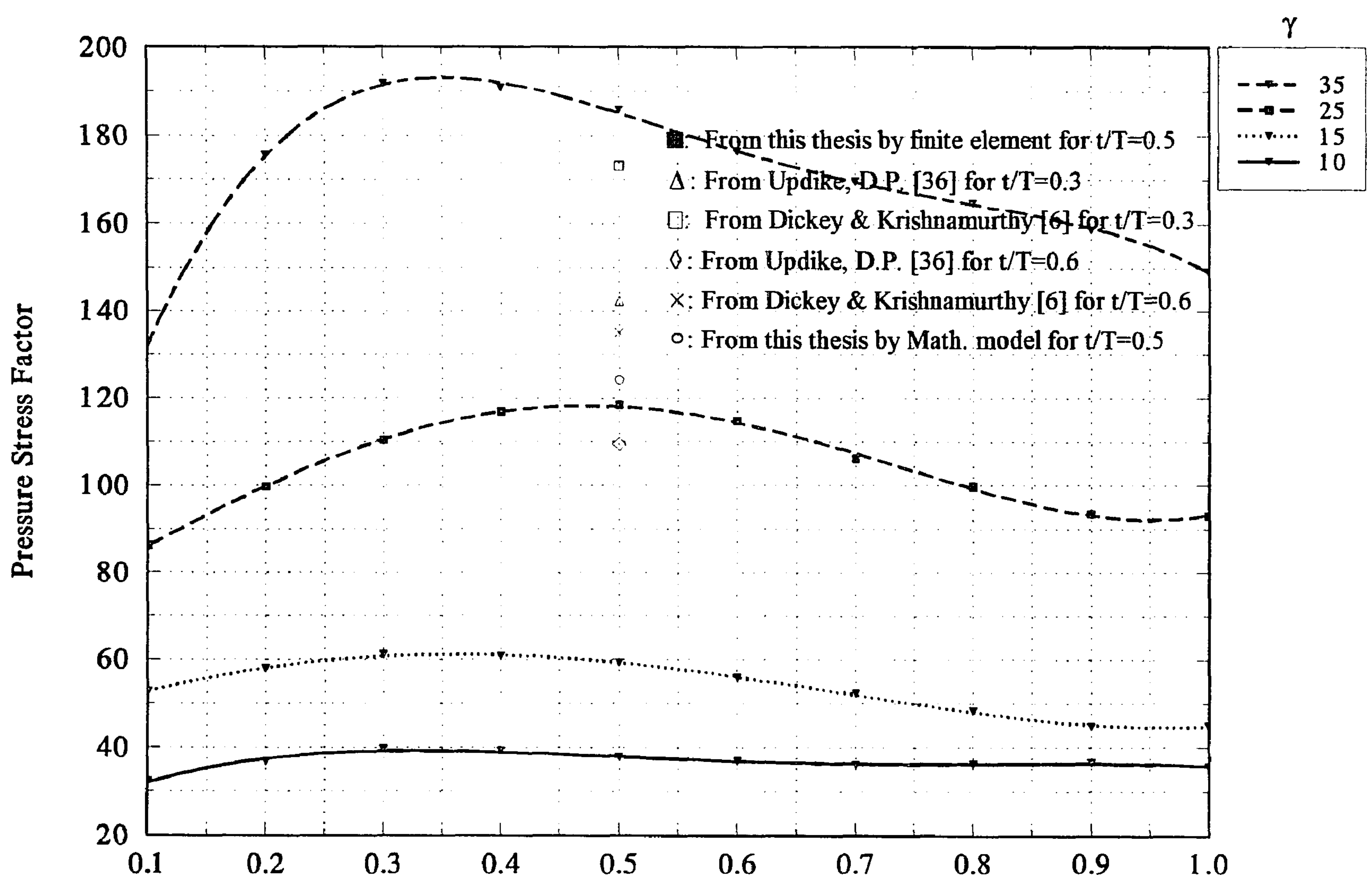

Figure 12 Data comparison of pressure stress factor in the circumferential direction of the pipe at point A_L for $\gamma = 25$, $\beta = 0.5$

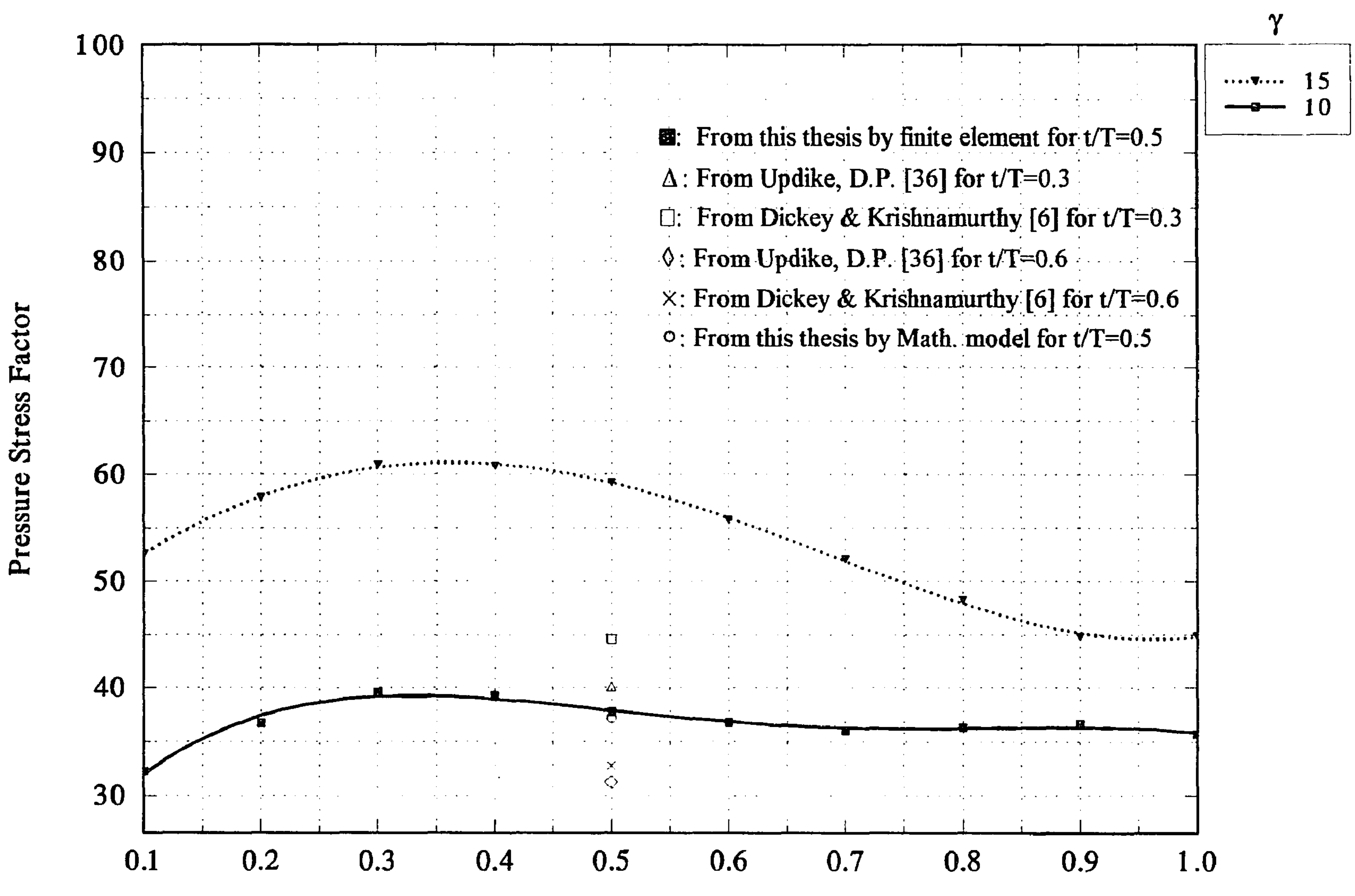

Figure 13 Data comparison of pressure stress factor in the circumferential direction of the pipe at point A_L for $\gamma = 10$, $\beta = 0.5$

CHAPTER 6

NUMERICAL EXAMPLES

The local pressure stress is then combined with other local stresses due to radial load, circumferential moment, longitudinal moment, and shear force to complement the computation and sign notation table for local stresses of pipe-nozzle model in WRC bulletin 107.

Example 1. A 12.75 in. O.D. pipe is intersected by a 5.325 in. nozzle with 0.375 in. thickness under internal pressure of 100 psi. In this model, mean radius of the pipe, R=6.1875 in., the pipe thickness, T=0.375 in., mean radius of nozzle, r=2.475, and the nozzle thickness, t=0.375. The detail information are listed in the following tables.

Table 7 Geometric parameters and dimensions of the illustrating pipe-nozzle model

α_p=Pipe length / Pipe mean radius	8
α_n=Nozzle length / Nozzle mean radius	4
β=Nozzle radius / Pipe mean radius	0.4
γ=Pipe radius / Pipe thickness	16.5
L_p=Pipe length	49.5 in
R=Pipe mean radius	6.1875 in
L_n=Nozzle length	9.9 in
r=Nozzle mean radius	2.475 in
T=Pipe thickness	0.375 in
t=Nozzle thickness	0.375 in

As a result: beta, (r/R), 2.475/6.1875=0.40 and gamma, (R/T), 6.1875/0.375=16.5. Assume alpha$_p$ (L_p/R) is 8.0 (i.e., a second nozzle, pipe bend, or trunnion is at least 49.5 inches away from the center line of the nozzle). Also, alpha$_n$ (L_n/r) is 4.0 (i.e., a second nozzle, pipe bend, or trunnion is at least 9.9 inches away from the juncture of the pipe-nozzle).

For the local pressure stress factors, one can get the following datum from the pressure stress factor plots in the appendix A from this thesis for t=βT.

Figure 1P gives pressure stress factor in the longitudinal direction at point A_U of the pipe = 77.20, then the local pressure stress = 7,720.00 psi.

Figure 2P gives pressure stress factor in the longitudinal direction at point A_L of the pipe = 37.80, then the local pressure stress = 3,780.00 psi.

Figure 3P gives pressure stress factor in the longitudinal direction at point C_U of the pipe = 19.40, then the local pressure stress = 1,940.00 psi.

Figure 4P gives pressure stress factor in the longitudinal direction at point C_L of the pipe = 5.20, then the local pressure stress = 520.00 psi.

Figure 5P gives pressure stress factor in the circumferential direction at point A_U of the pipe = 110.50, then the local pressure stress = 11,050.00 psi.

Figure 6P gives pressure stress factor in the circumferential direction at point A_L of the pipe = 61.80, then the local pressure stress = 6,180.00 psi.

Figure 7P gives pressure stress factor in the circumferential direction at point C_U of the pipe = 10.20, then the local pressure stress = 1,020.00 psi.

Figure 8P gives pressure stress factor in the circumferential direction at point C_L of the pipe = 17.40, then the local pressure stress = 1,740.00 psi.

For the local stresses due to radial load, circumferential moment, longitudinal moment, torsional moment, circumferential shear force, and longitudinal shear force, one can get all the local stress factors and local stresses from Welding Research Council Bulletin 107 [38]. Assuming that:

P (radial load) = 400 lb. (downward)

M_C = 500 lb.-in.

M_L = 500 lb.-in.

M_T = 500 lb.-in.

V_C = 300 lb.

V_L = -400 lb. (to the right) (see figure 7)

p (internal pressure) = 100 psi.

All the local stresses, summation, and combined stress intensity are calculated and listed in Table 8. In this table, the local stress factors from external loadings are taken from WRC 107 [38], and the local pressure stress factors, which are listed in Table 8a, are taken from Figures 1P to 8P of Appendix A.

This table also demonstrate the results of stress intensity from tri-axial state of stress by considering the third principal stress as -p/2.

Table 8 Computation sheet for local stresses of pipe-nozzle model on pipe region modified from WRC 107.

From Fig.	Read curves for	Compute absolute value of stress and enter result	A_U	A_L	B_U	B_L	C_U	C_L	D_U	D_L
* 3C	$\frac{N_\phi}{P/R_m} = 1.221$	$K_n(\frac{N_\phi}{P/R_m})\frac{P}{R_m T} =$	-210	-210	-210	-210	-210	-210	-210	-210
* 1C	$\frac{M_\phi}{P} = 0.0424$	$K_b(\frac{M_\phi}{P})\frac{6P}{T^2} =$	-723	723	-723	723	-723	723	-723	723
* 3A	$\frac{N_\phi}{M_c/R_m^2\beta} = 0.7059$	$K_n(\frac{N_\phi}{M_c/R_m^2\beta})\frac{M_c}{R_m^2\beta T} =$					-62	-62	62	62
* 1A	$\frac{M_\phi}{M_c/R_m\beta} = 0.0739$	$K_b(\frac{M_\phi}{M_c/R_m\beta})\frac{6M_c}{R_m\beta T^2} =$					-647	647	647	-647
* 3B	$\frac{N_\phi}{M_L/R_m^2\beta} = 1.4863$	$K_n(\frac{N_\phi}{M_L R_m^2\beta})\frac{M_L}{R_m^2\beta T} =$	-132	-132	132	132				
* 1B or 1B-1	$\frac{M_\phi}{M_L/R_m\beta} = 0.0180$	$K_b(\frac{M_\phi}{M_L R_m\beta})\frac{6M_L}{R_m\beta T^2} =$	-158	158	158	-158				
5P Thru 8P	Pressure stress factor, see Table 8a	Pressure stress factor x p =	11050	6180	11050	6180	-1020	-1740	-1020	-1740
Add algebraically for summation of circumferential stresses, σ_ϕ =			9827	6719	10407	6667	-2662	-642	-1244	-1812
* 4C	$\frac{N_\phi}{P/R_m} = 2.0280$	$K_n(\frac{N_\phi}{P/R_m})\frac{P}{R_m T} =$	-350	-350	-350	-350	-350	-350	-350	-350
* 2C	$\frac{M_\phi}{P} = 0.0227$	$K_b(\frac{M_\phi}{P})\frac{6P}{T^2} =$	-387	387	-387	387	-387	387	-387	387
* 4A	$\frac{N_\phi}{M_c/R_m^2\beta} = 1.6680$	$K_n(\frac{N_\phi}{M_c/R_m^2\beta})\frac{M_c}{R_m^2\beta T} =$					-148	-148	148	148
* 2A	$\frac{M_\phi}{M_c/R_m\beta} = 0.0349$	$K_b(\frac{M_\phi}{M_c/R_m\beta})\frac{6M_c}{R_m\beta T^2} =$					-306	306	306	-306
* 4B	$\frac{N_\phi}{M_L/R_m^2\beta} = 0.6817$	$K_n(\frac{N_\phi}{M_L R_m^2\beta})\frac{M_L}{R_m^2\beta T} =$	-60	-60	60	60				
* 2B or 2B-1	$\frac{M_\phi}{M_L/R_m\beta} = 0.0317$	$K_b(\frac{M_\phi}{M_L R_m\beta})\frac{6M_L}{R_m\beta T^2} =$	-278	278	278	-278				
1P Thru 4P	Pressure stress factor, see Table 8a	Pressure stress factor x p =	7720	-3780	7720	-3780	-1940	520	-1940	520
Add algebraically for summation of longitudinal stresses, σ_x			6645	-3525	7321	-3961	-3131	715	-2223	399
Shear stress due to Torsion, M_T		$\tau_{\phi x} = \tau_{x\phi} = \frac{M_T}{2\pi r_o^2 T}$	27	27	27	27	-27	-27	-27	-27
Shear stress due to load, V_C		$\tau_{x\phi} = \frac{V_C}{\pi r_o T}$	92	92	-92	-92				
Shear stress due to load, V_L		$\tau_{x\phi} = \frac{V_L}{\pi r_o T}$					-122	-122	122	122
Add algebraically for summation of shear stresses, τ=			119	119	-64	-64	-149	-149	95	95
COMBINED STRESS INTENSITY, S										
σ_1		$\frac{1}{2}[\sigma_\phi + \sigma_x + \sqrt{(\sigma_\phi - \sigma_x)^2 + 4\tau^2}]$	9832	6721	10409	6668	-2619	731	-1235	403
σ_2		$\frac{1}{2}[\sigma_\phi + \sigma_x - \sqrt{(\sigma_\phi - \sigma_x)^2 + 4\tau^2}]$	6641	-3527	7320	-3962	-3175	-658	-2232	-1816
σ_3		- p/2	-50.00	-50.00	-50.00	-50.00	-50.00	-50.00	-50.00	-50.00
Stress intensity			9882	10248	10459	10630	3125	1389	2182	2219
Maximum stress intensity						10630				

* See WRC 107 [38].

Table 8a For local pressure stress factors on pipe region.

From Fig.	Stress factor	A_U	A_L	B_U	B_L	C_U	C_L	D_U	D_L
5P	110.5	11050		11050					
6P	61.8		6180		6180				
7P	-10.2					-1020		-1020	
8P	-17.4						-1740		-1740
1P	77.2	7720		7720					
2P	-37.8		-3780		-3780				
3P	-19.4					-1940		-1940	
4P	5.2						520		520

In this example, one can see that the circumferential membrane stress under internal pressure away from the juncture of the pipe-nozzle is: $\frac{pR}{T} = \frac{100 \cdot 6.1875}{0.375} = 1650$ psi, which is approximately 6.7 times less than the maximum local circumferential pressure stress.

The longitudinal membrane stress under internal pressure away from the juncture of the pipe-nozzle is: $\frac{pR}{2T} = \frac{100 \cdot 6.1875}{2 \cdot 0.375} = 825$ psi, which is approximately 9.4 times less than the maximum local longitudinal pressure stress.

These indicate that the membrane pressure stresses can not be substituted as the local pressure stresses in pressure vessel design.

Another example is given for the local pressure stress of the nozzle, which is then combined with other local stresses due to radial load, circumferential moment, longitudinal moment, and shear forces to complement the stress computation table given by Lin, Sun, & Koplk [12].

Example 2. A 100.25 in. O.D. pipe with 0.25 in. thickness, is intersected by a 12.75 inches nozzle also with 0.25 in. thickness. The internal pressure is assumed as 100 psi. In this example, mean radius of the pipe, R=50 in., the mean radius of nozzle, r=6.25, the other external loadings are identical with example 1. As a result: beta, (r/R), 6.25/50=0.125 and gamma, (R/T), 50/0.25=200. Assume alphap (L_p/R) is 8.0 (i.e., a second nozzle, pipe bend, or trunnion is at least 400 inch away from the center line of the nozzle), alphan (L_n/r) is 4.0(i.e. the nozzle has a minimum length of 24.9 in.). The detail information are listed in the following tables.

Table 9 Geometric parameters and dimensions of the illustrating pipe-nozzle model

α_p=Pipe length / Pipe mean radius	8
α_n=Nozzle length / Nozzle mean radius	4
β=Nozzle radius / Pipe mean radius	0.125
γ=Pipe radius / Pipe thickness	200
L_p=Pipe length	400 in
R=Pipe mean radius	50 in
L_n=Nozzle length	24.9 in
r=Nozzle mean radius	6.25 in
T=Pipe thickness	0.25 in
t=Nozzle thickness	0.25 in

For the local pressure stress factors of the nozzle, one can get the following data from the pressure stress factor plots in the appendix A. One notes that the pressure stress factors listed in Table 10a, from Figures 9P to 16P of Appendix A, are for the case of t=β T, where as the local stress factors from Lin, Sun, & Koplik [12], are for the case of t=T.

Figure 9P gives pressure stress factor in the longitudinal direction at point A_o of the nozzle = 2514.00, then the local pressure stress = 251,400.00 psi.

Figure 10P gives pressure stress factor in the longitudinal direction at point A_i of the nozzle = 2125.00, then the local pressure stress = 212,500.00 psi.

Figure 11P gives pressure stress factor in the longitudinal direction at point C_o of the nozzle = 746.00, then the local pressure stress = 74,600.00 psi.

Figure 12P gives pressure stress factor in the longitudinal direction at point C_i of the nozzle = 567.90, then the local pressure stress = 56,790.00 psi.

Figure 13P gives pressure stress factor in the circumferential direction at point A_o of the nozzle = 3166.00, then the local pressure stress = 316,600.00 psi.

Figure 14P gives pressure stress factor in the circumferential direction at point A_i of the nozzle = 1639.00, then the local pressure stress = 163,900.00 psi.

Figure 15P gives pressure stress factor in the circumferential direction at point C_o of the nozzle = 594.20, then the local pressure stress = 59,420.00 psi.

Figure 16P gives pressure stress factor in the circumferential direction at point C_i of the nozzle = 163.20, then the local pressure stress = 16,320.00 psi.

All the local stresses, summation, and combined stress intensity are calculated and listed in Table 10.

Table 10 Computation sheet for local stresses of pipe-nozzle model on nozzle region modified from WRC 107.

From Fig.	Read curves for	Compute absolute value of stress and enter result	A_o	A_i	B_o	B_i	C_o	C_i	D_o	D_i
* Ref. [37] 11P, 15P	$\frac{N_\phi}{P/R_m}=0.6, 0.19$	$K_n(\frac{N_\phi}{P/R_m})\frac{P}{R_m T}=$	-154	-154	-154	-154	-49	-49	-49	-49
* Ref. [37] 9P, 13P	$\frac{M_\phi}{P}=0.012, 0.05$	$K_b(\frac{M_\phi}{P})\frac{6P}{T^2}=$	-461	461	-461	461	-1920	1920	-1920	1920
* Ref. [37] 7MC	$\frac{N_\phi}{M_c/R_m^2\beta}=0.05$	$K_n(\frac{N_\phi}{M_c/R_m^2\beta})\frac{M_c}{R_m^2\beta T}=$					-20	-20	20	20
* Ref. [37] 5MC	$\frac{M_\phi}{M_c/R_m\beta}=0.009$	$K_b(\frac{M_\phi}{M_c/R_m\beta})\frac{6M_c}{R_m\beta T^2}=$					-553	553	553	-553
* Ref. [37] 7ML	$\frac{N_\phi}{M_L/R_m^2\beta}=0.273$	$K_n(\frac{N_\phi}{M_L R_m^2\beta})\frac{M_L}{R_m^2\beta T}=$	-112	-112	112	112				
* Ref. [37] 5ML	$\frac{M_\phi}{M_L/R_m\beta}=0.0014$	$K_b(\frac{M_\phi}{M_L R_m\beta})\frac{6M_L}{R_m\beta T^2}=$	-86	86	86	-86				
13P Thru 16P	Pressure stress factor, see Table 10a	Pressure stress factor x p =	316600	163900	316600	163900	-59420	-16320	-59420	-16320
Add algebraically for summation of circumferential stresses, σ_ϕ =			315787	164181	316183	164233	-61962	-13916	-60816	-14982
* Ref. [37] 12P, 16P	$\frac{N_\phi}{P/R_m}=2.0280$	$K_n(\frac{N_\phi}{P/R_m})\frac{P}{R_m T}=$	-18	-18	-18	-18	-870	-870	-870	-870
* Ref. [37] 10P, 14P	$\frac{M_\phi}{P}=0.0227$	$K_b(\frac{M_\phi}{P})\frac{6P}{T^2}=$	-1306	1306	-1306	1306	-499	499	-499	499
* Ref. [37] 8MC	$\frac{N_\phi}{M_c/R_m^2\beta}=1.6680$	$K_n(\frac{N_\phi}{M_c/R_m^2\beta})\frac{M_c}{R_m^2\beta T}=$					-123	-123	123	123
* Ref. [37] 6MC	$\frac{M_\phi}{M_c/R_m\beta}=0.0349$	$K_b(\frac{M_\phi}{M_c/R_m\beta})\frac{6M_c}{R_m\beta T^2}=$					-184	184	184	-184
* Ref. [37] 8ML	$\frac{N_\phi}{M_L/R_m^2\beta}=0.6817$	$K_n(\frac{N_\phi}{M_L R_m^2\beta})\frac{M_L}{R_m^2\beta T}=$	-16	-16	16	16				
* Ref. [37] 6ML	$\frac{M_\phi}{M_L/R_m\beta}=0.0317$	$K_b(\frac{M_\phi}{M_L R_m\beta})\frac{6M_L}{R_m\beta T^2}=$	-258	258	258	-258				
9P Thru 12P	Pressure stress factor, see Table 10a	Pressure stress factor x p =	251400	-212500	251400	-212500	-74600	56790	-74600	56790
Add algebraically for summation of longitudinal stresses, σ_x			249802	-210970	250350	-211454	-76276	56480	-75662	56358
Shear stress due to Torsion, M_T		$\tau_{\phi x}=\tau_{x\phi}=\frac{M_T}{2\pi r_o^2 T}$	5	5	5	5	-5	-5	-5	-5
Shear stress due to load, V_C		$\tau_{x\phi}=\frac{V_C}{\pi r_o T}$	40	40	-40	-40				
Shear stress due to load, V_L		$\tau_{x\phi}=\frac{V_L}{\pi r_o T}$					20	20	-20	-20
Add algebraically for summation of shear stresses, $\tau=$			45	45	-35	-35	15	15	-25	-25
COMBINED STRESS INTENSITY, S										
σ_1		$\frac{1}{2}[\sigma_\phi+\sigma_x+\sqrt{(\sigma_\phi-\sigma_x)^2+4\tau^2}]$	315787	164181	316183	164233	-61962	-13916	-60816	-14982
σ_2		$\frac{1}{2}[\sigma_\phi+\sigma_x-\sqrt{(\sigma_\phi-\sigma_x)^2+4\tau^2}]$	249802	-210970	250350	-211454	-76276	56480	-75662	56358
σ_3		- p/2	-50	-50	-50	-50	-50	-50	-50	-50
Stress intensity			315837	375151	316233	375687	76226	70396	75612	71340
Maximum stress intensity						375687				

* See reference [12] by Lin, Sun, Koplik

Table 10a For local pressure stress factors on nozzle region.

From Fig.	Stress factor	A_o	A_i	B_o	B_i	C_o	C_i	D_o	D_i
13P	3166	316600		316600					
14P	1639		163900		163900				
15P	-594.2					-59420		-59420	
16P	-163.2						-16320		-16320
9P	2514	251400		251400					
10P	-2125		-212500		-212500				
11P	-746					-74600		-74600	
12P	567.9						56790		56790

In this example, one can see that the circumferential membrane stress under internal pressure away from the juncture of the pipe-nozzle is:

$\frac{pR}{T} = \frac{100 \cdot 100.25}{0.25} = 40100$ psi, which is 7.89 times less than the local pressure stress component.

The longitudinal membrane stress under internal pressure away from the juncture of the pipe-nozzle is:

$\frac{PR}{2T} = \frac{100 \cdot 100.25}{2 \cdot 0.25} = 20050$ psi, which is 12.5 times less than the local stress components.

CHAPTER 7

CONCLUSIONS

In this thesis, a comprehensive study by finite element stress analysis of the full pipe-nozzle model for an extended range of β value from 0.1 to 1.0 and γ value from 10 to 300 is presented. Also, a new mathematically approximate model for certain configuration is suggested. The pressure stress factors at the juncture of pipe-nozzle connection from this thesis may complement WRC 107 as a new component in conjunction with local stresses from other external loadings, such as radial load, moments, and shear forces.

From the local pressure stress factor plots, the following conclusions are made:

1. The increase of gamma, $\gamma = R/T$ (pipe mean radius/pipe thickness) generally makes the local pressure stress higher, which means, the thinner the shell the higher the local stresses.

2. The highest local pressure stress appears to be around 0.5 of β.

3. The local stress can be many times higher than the membrane stress away from the pipe-nozzle intersection due to internal pressure. Therefore, these results provide significant data base for pressure vessel design.

4. The node point C, at the transverse plane of the pipe-nozzle intersection, generally are under compression and have less stress value than the node point A, at the longitudinal plane of the pipe-nozzle intersection.

5. The modified mathematical approximation method suggested in this thesis (see equation 25) provide the results which are good for small curvature of pipe-nozzle configuration, such as, $\beta < 0.5$, $\gamma < 75$.

6. One notices that the maximum local pressure stresses do not always occur on the pipe portion of the juncture.

7. When the engineering modulus is different from 30×10^6 psi, the new local pressure stress factors may be obtained by multiplying the ratio of new modulus to 30×10^6 psi to the factors.

APPENDIX A

PRESSURE STRESS FACTOR PLOTS

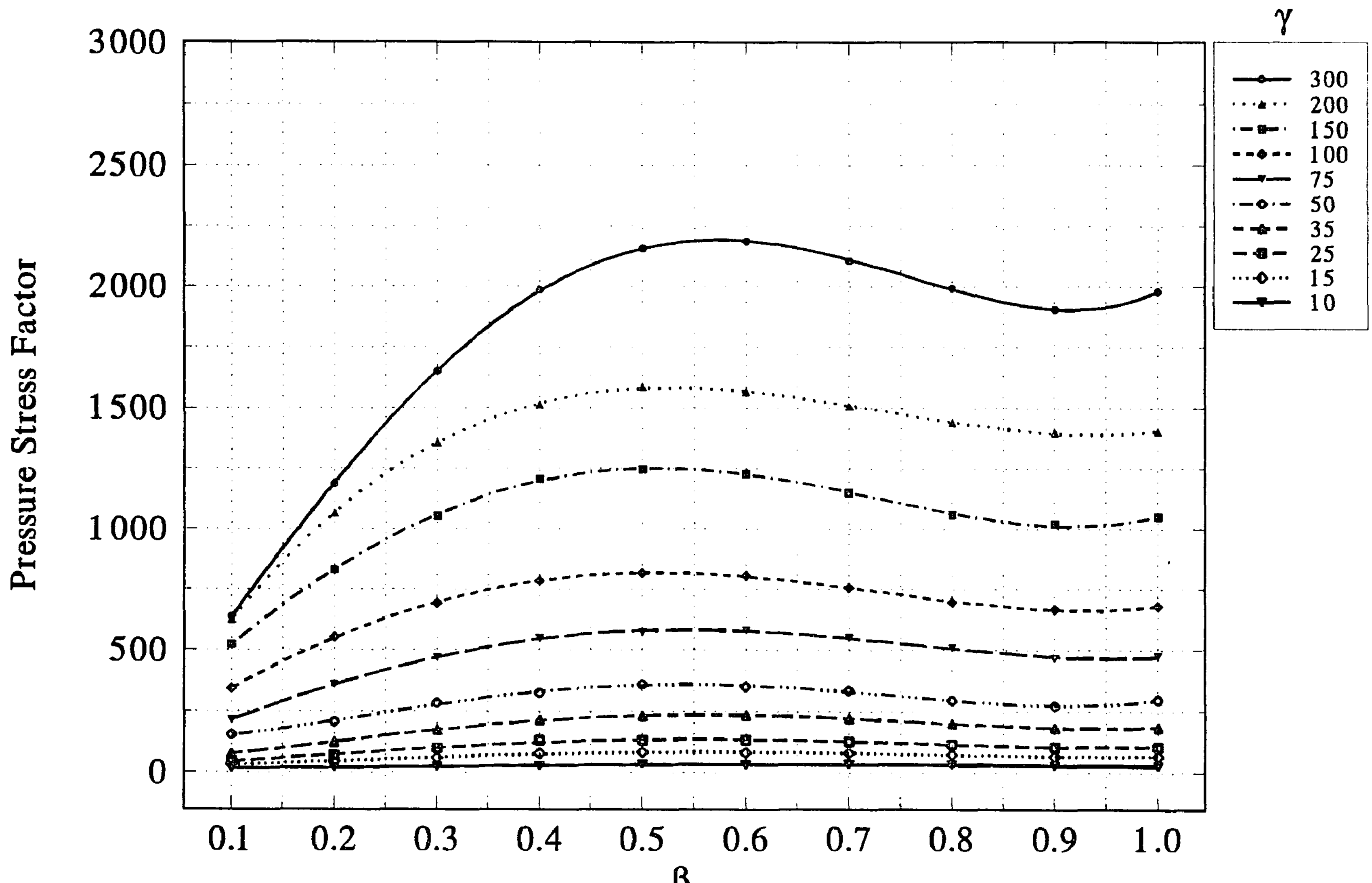

Figure 1P Pressure stress factor in the longitudinal direction of the pipe at point AU

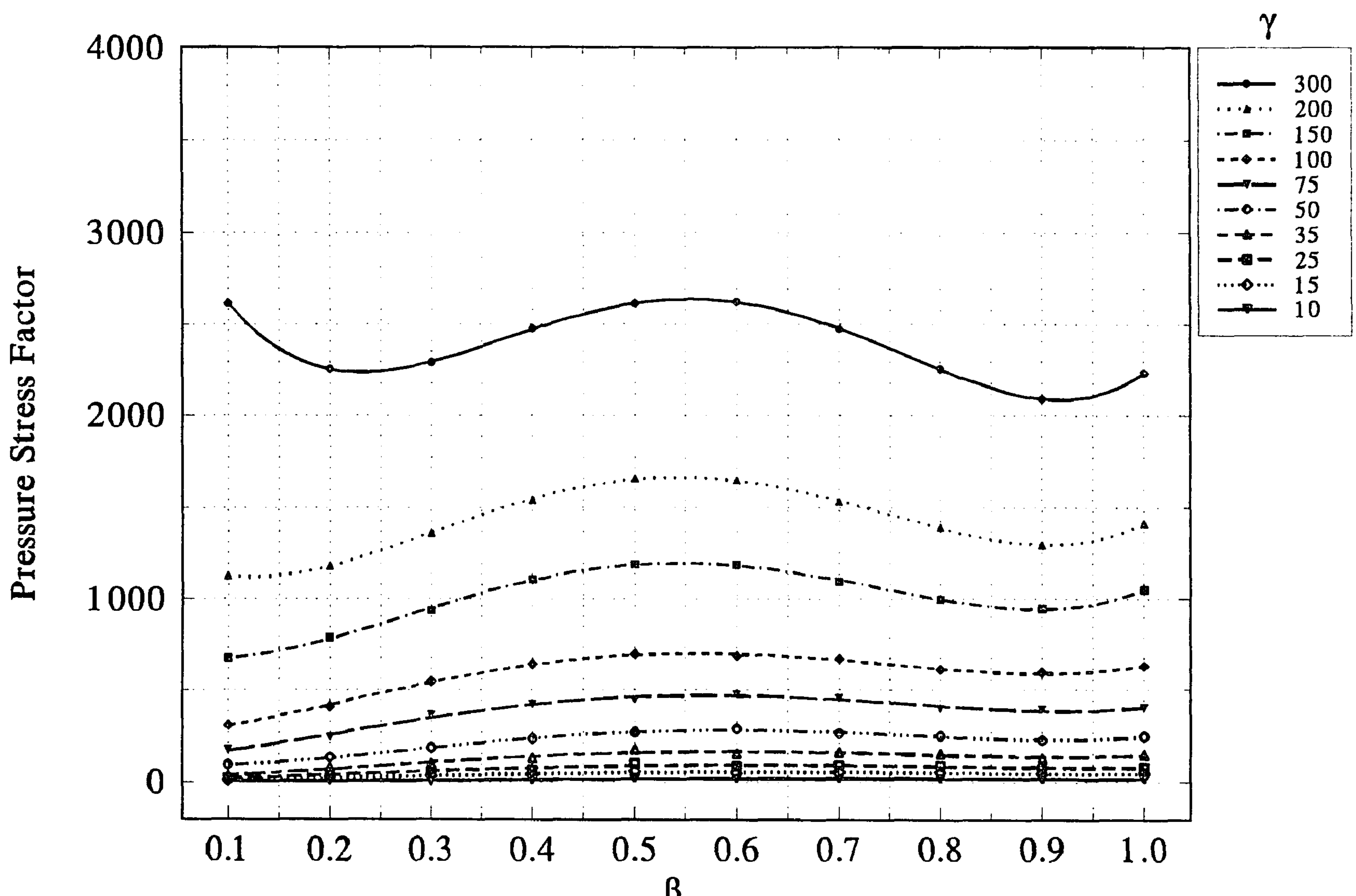

Figure 2P Pressure stress factor in the longitudinal direction of the pipe at point A_L

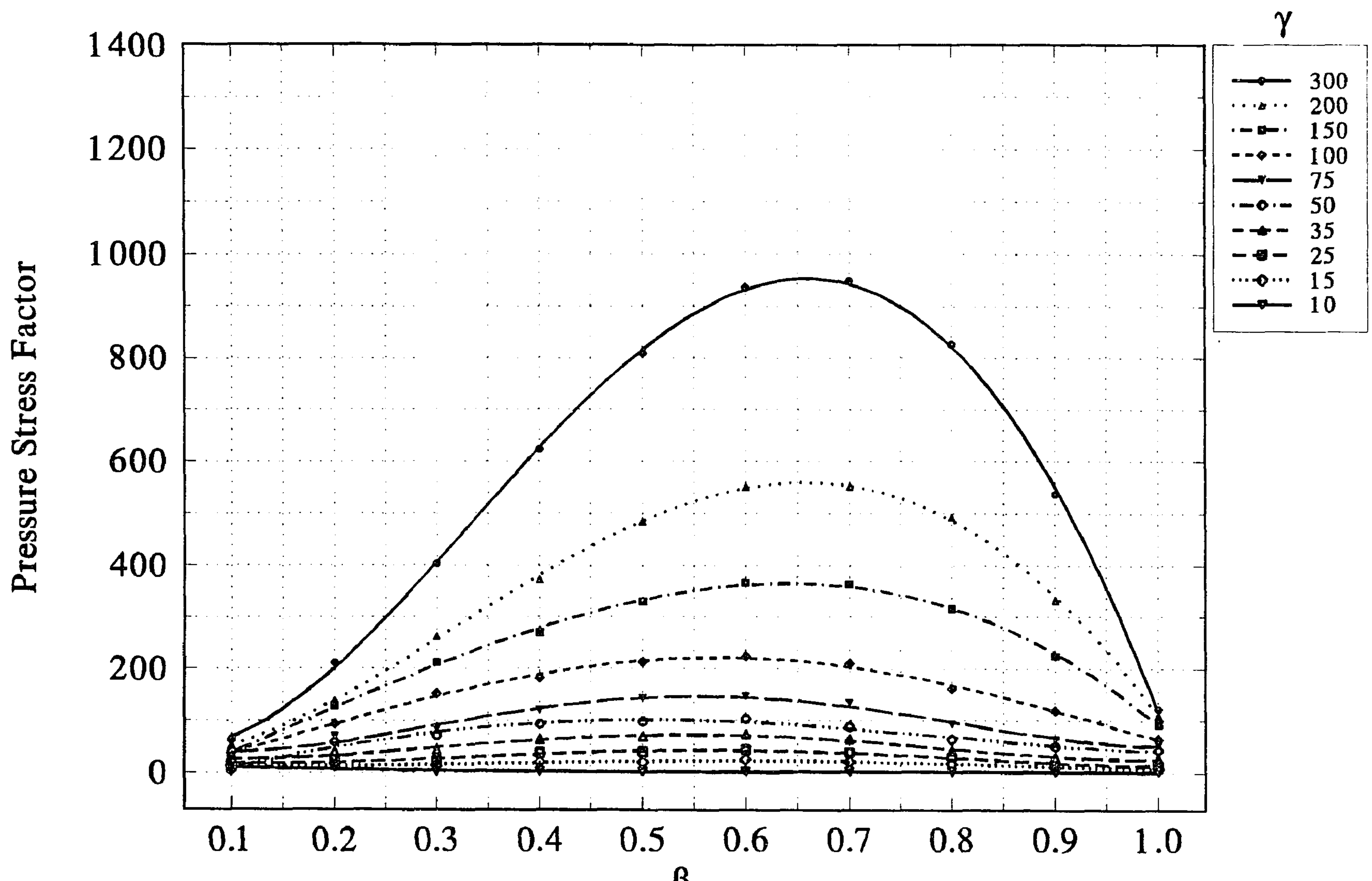

Figure 3P Pressure stress factor in the longitudinal direction of the pipe at point Cu

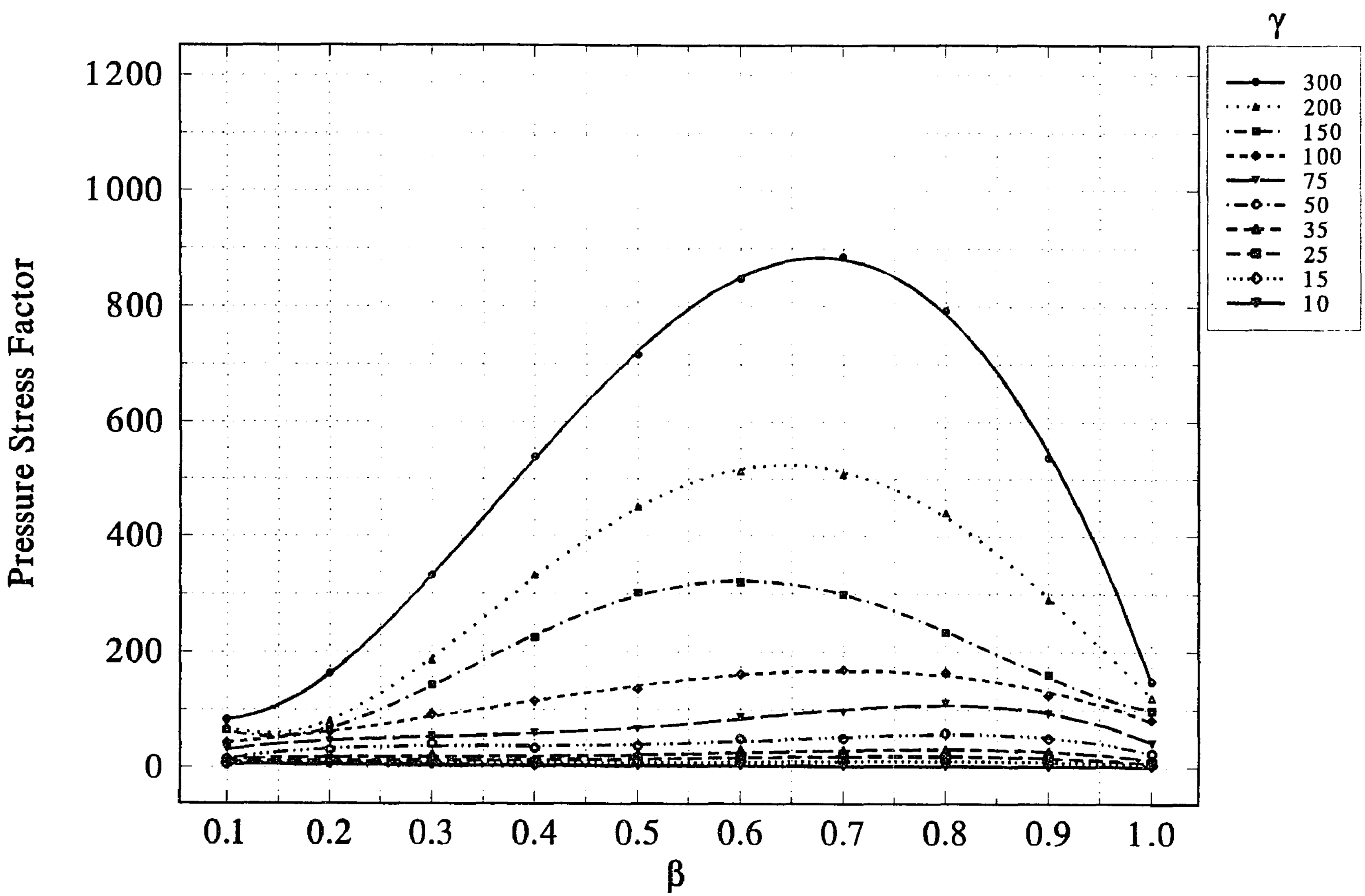

Figure 4P Pressure stress factor in the longitudinal direction of the pipe at point C_L

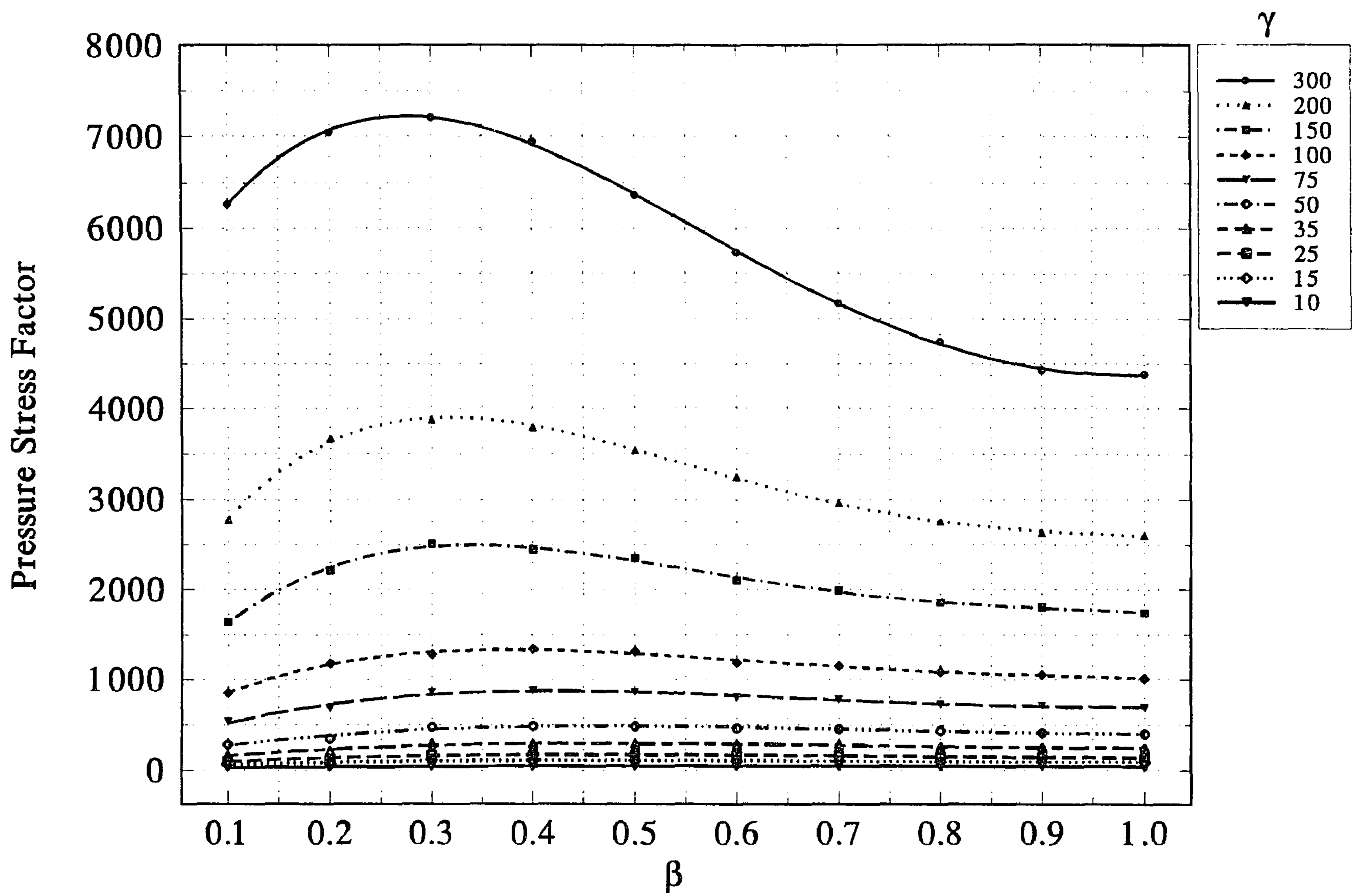

Figure 5P Pressure stress factor in the circumferential direction of the pipe at point Au

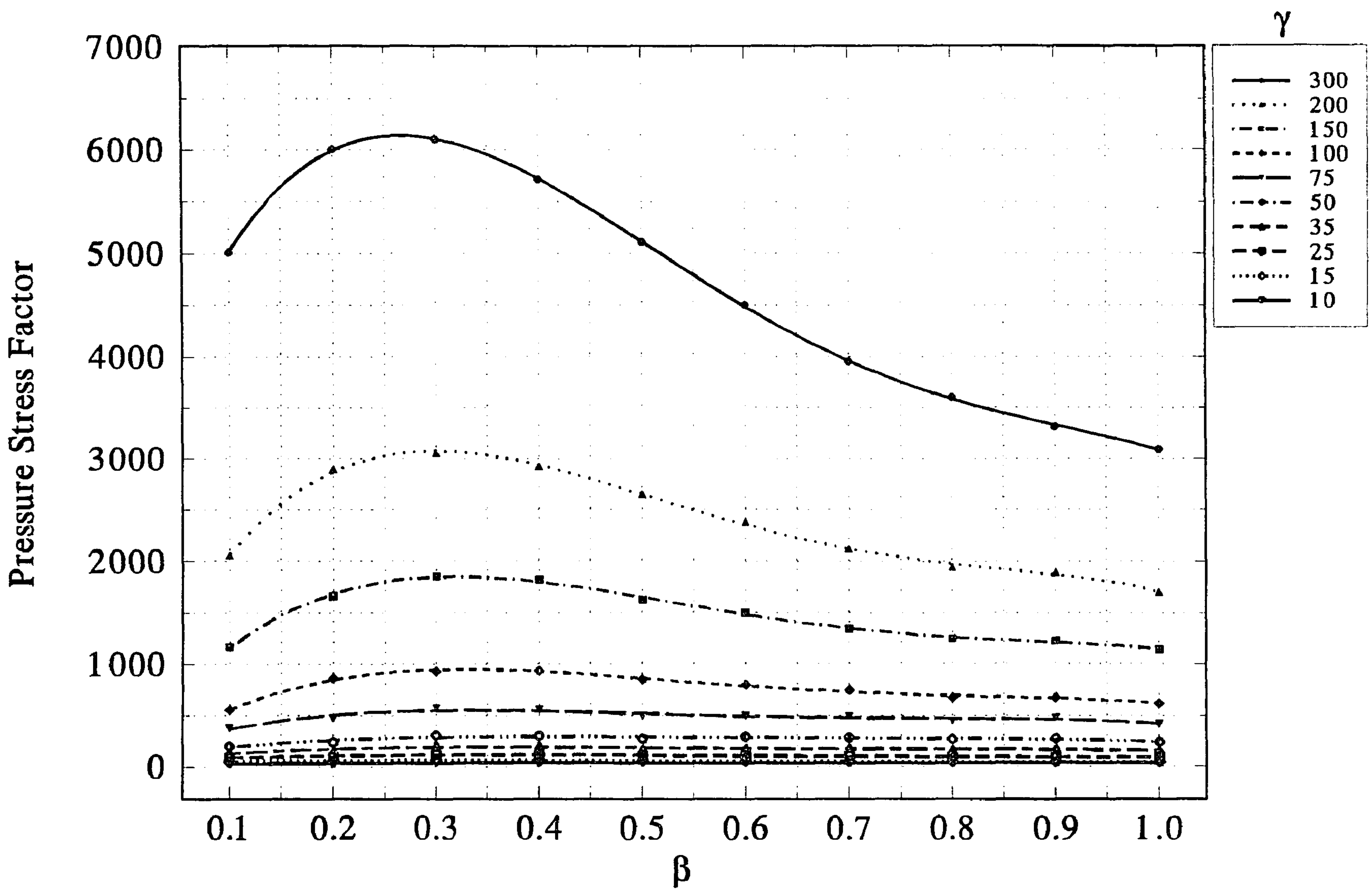

Figure 6P Pressure stress factor in the circumferential direction of the pipe at point A_L

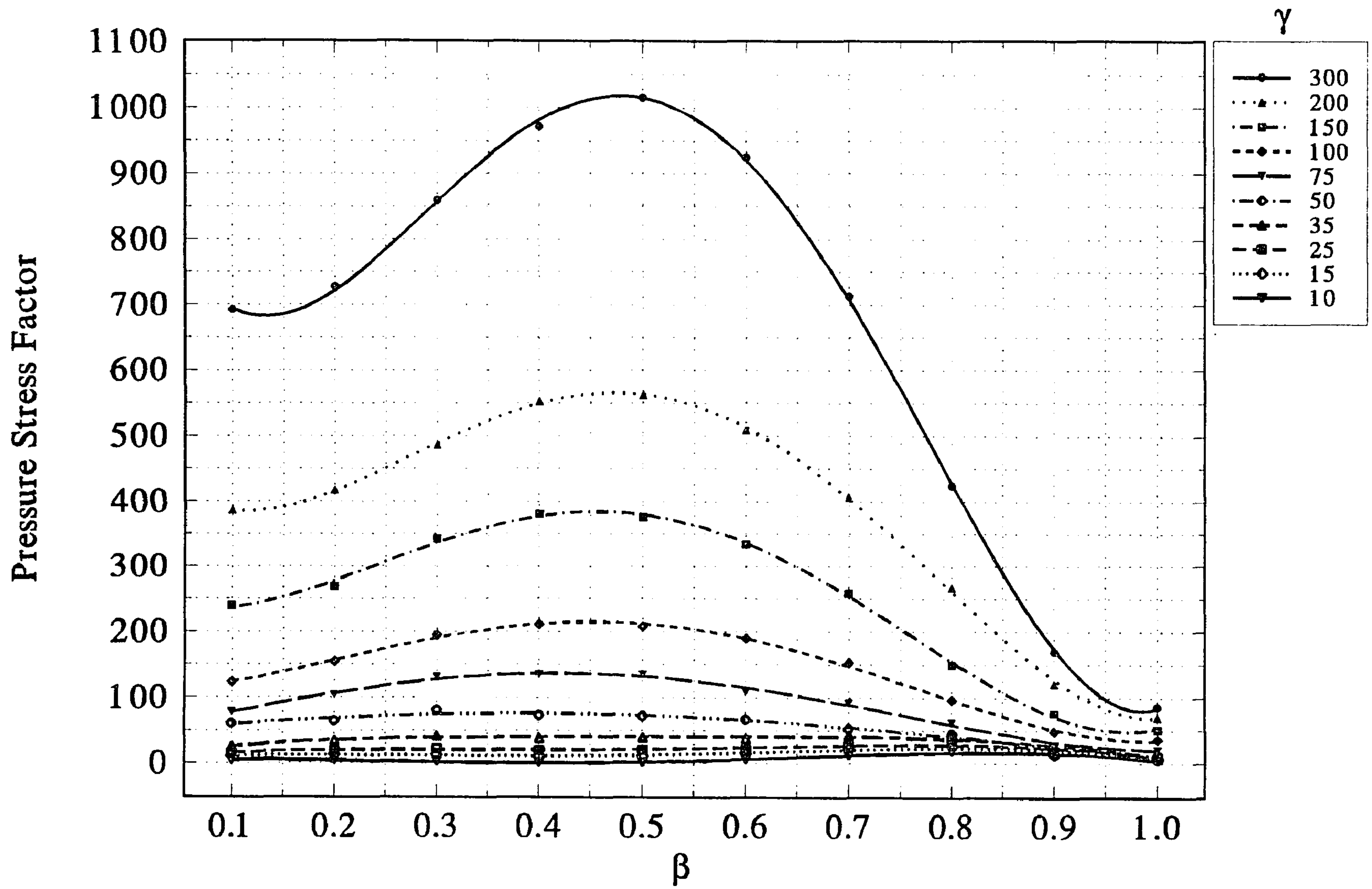

Figure 7P Pressure stress factor in the circumferential direction of the pipe at point CU

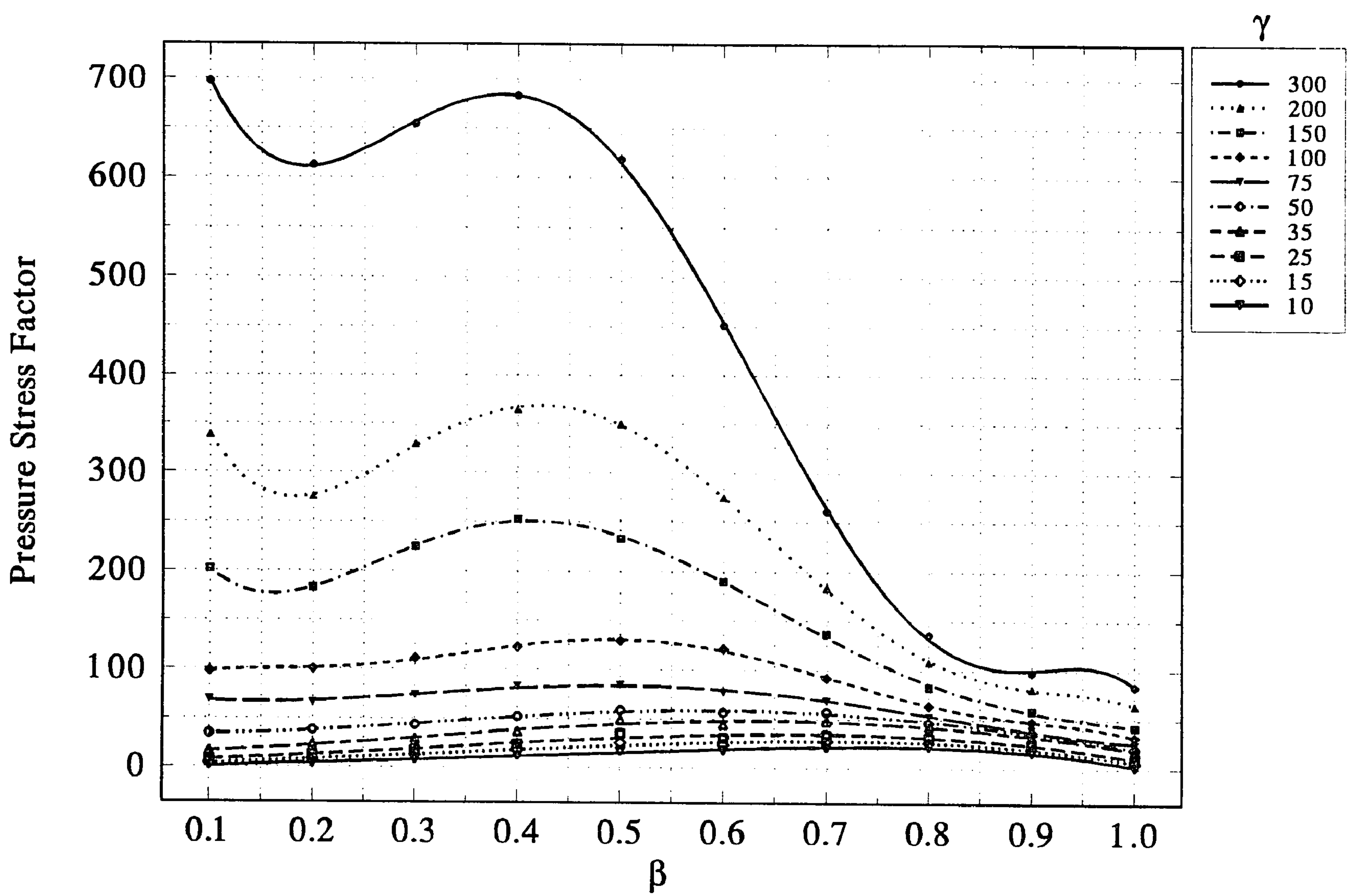

Figure 8P Pressure stress factor in the circumferential direction of the pipe at point C_L

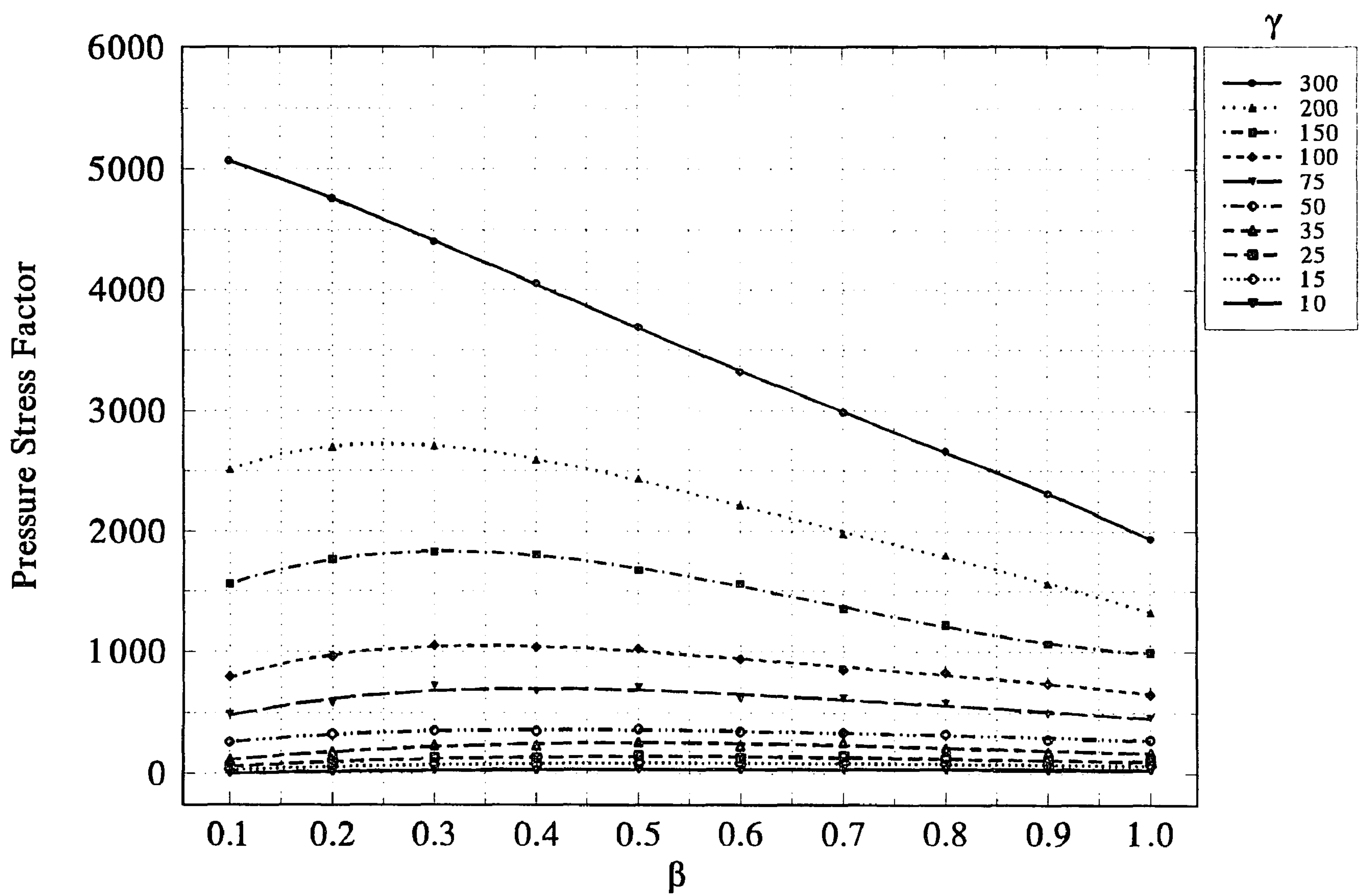

Figure 9P Pressure stress factor in the longitudinal direction of the nozzle at point A_o

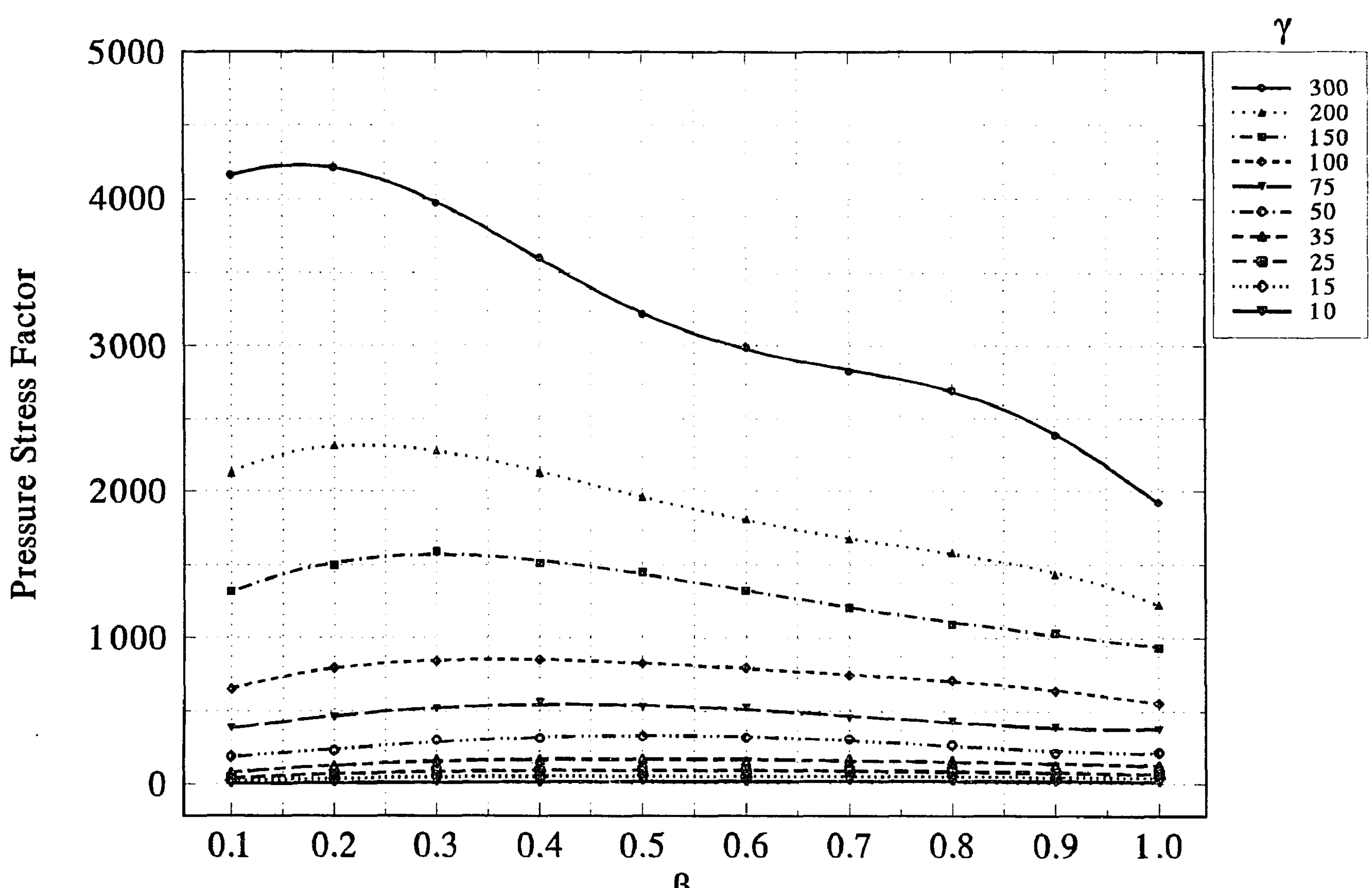

Figure 10P Pressure stress factor in the longitudinal direction of the nozzle at point A_i

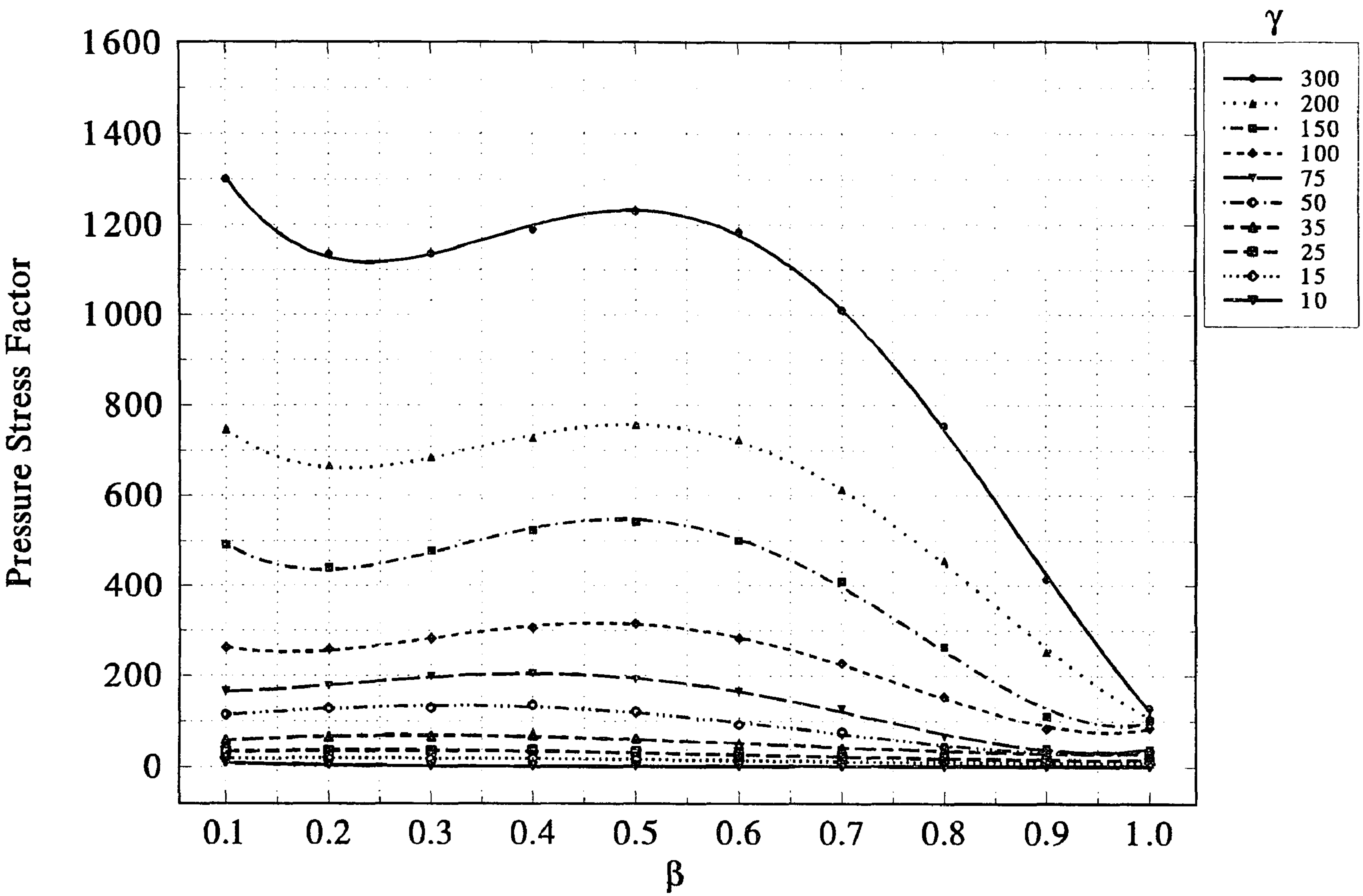

Figure 11P Pressure stress factor in the longitudinal direction of the nozzle at point C_o

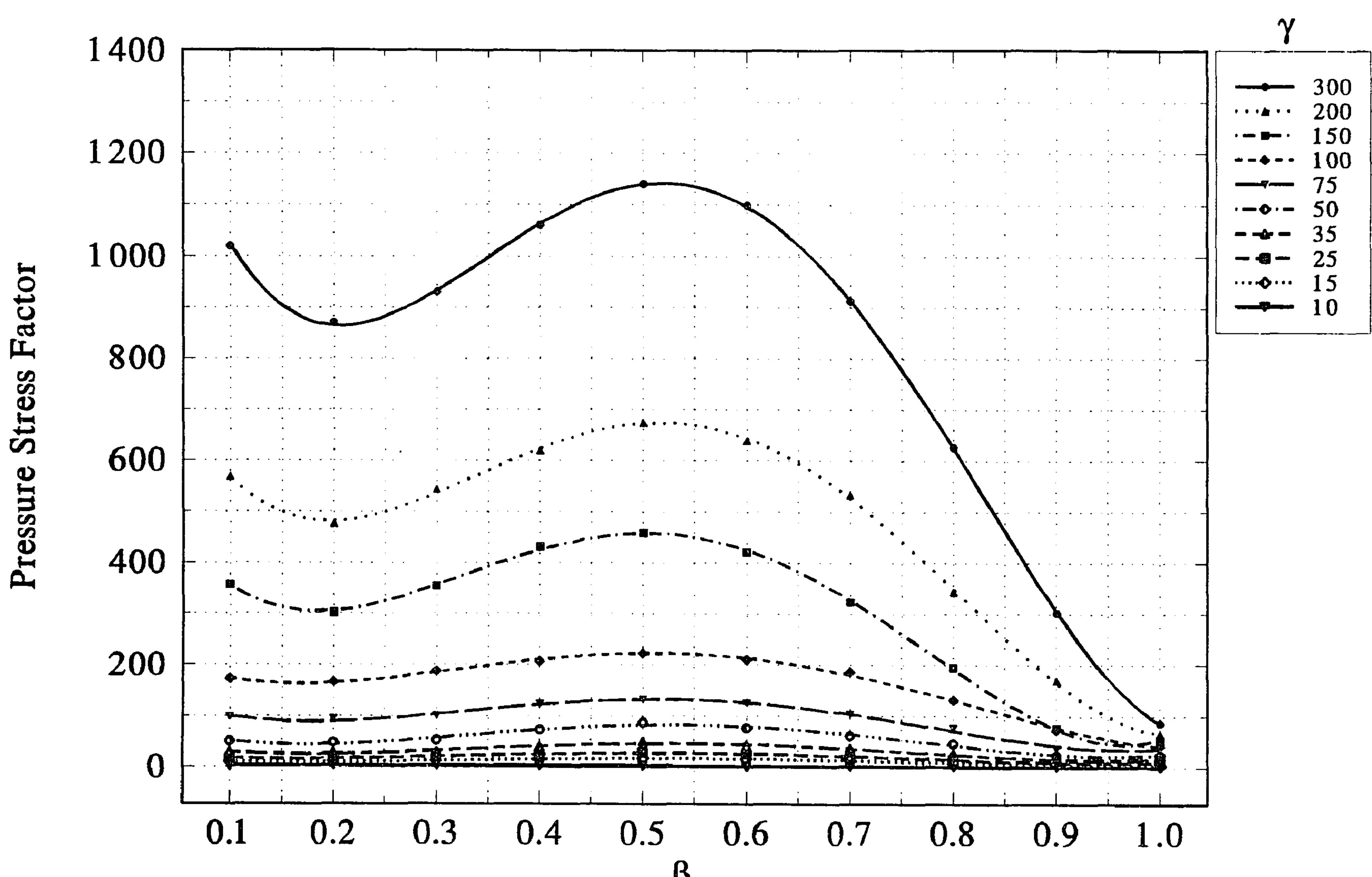

Figure 12P Pressure stress factor in the longitudinal direction of the nozzle at point C_i

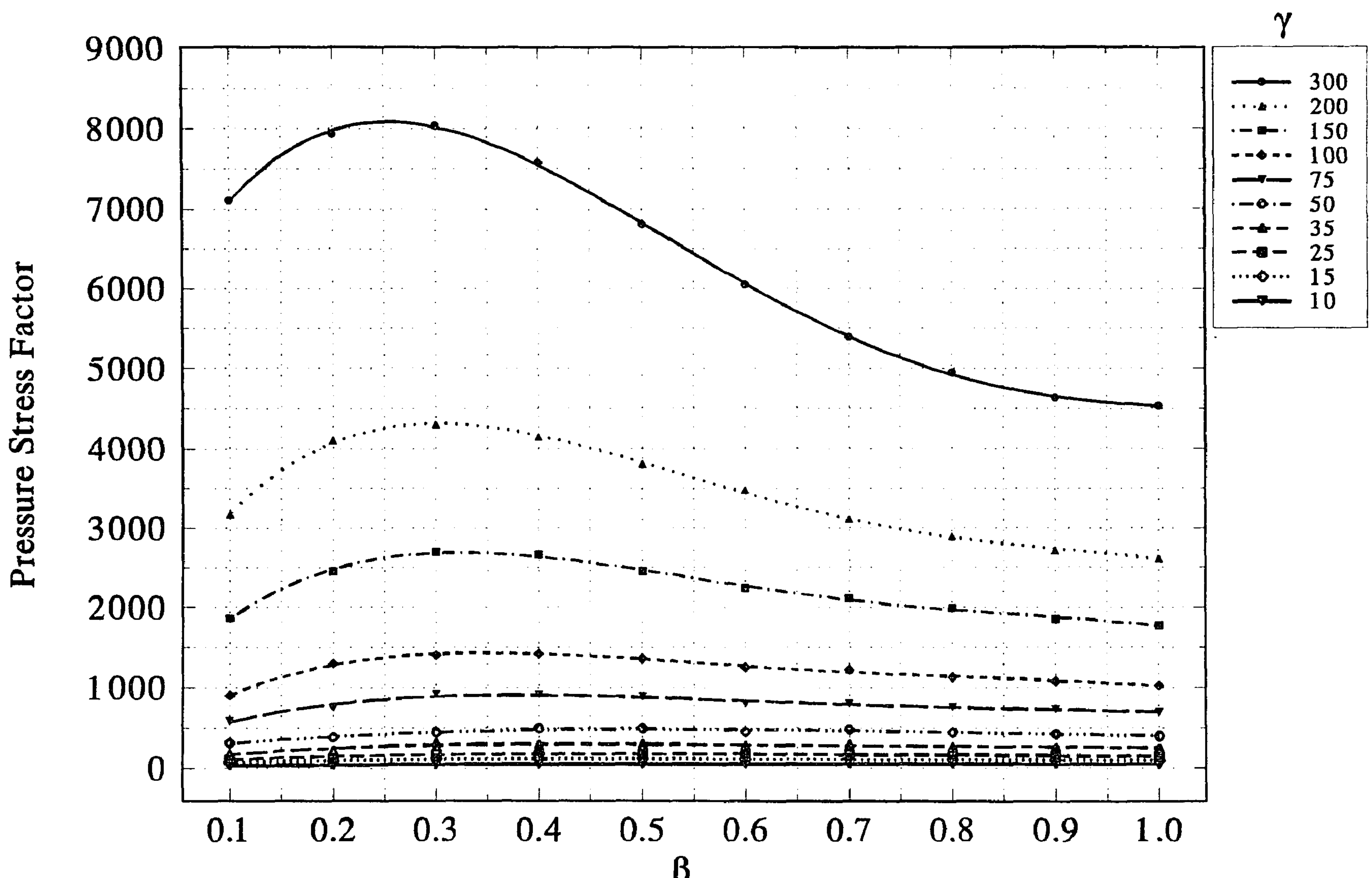

Figure 13P Pressure stress factor in the circumferential direction of the nozzle at point A_o

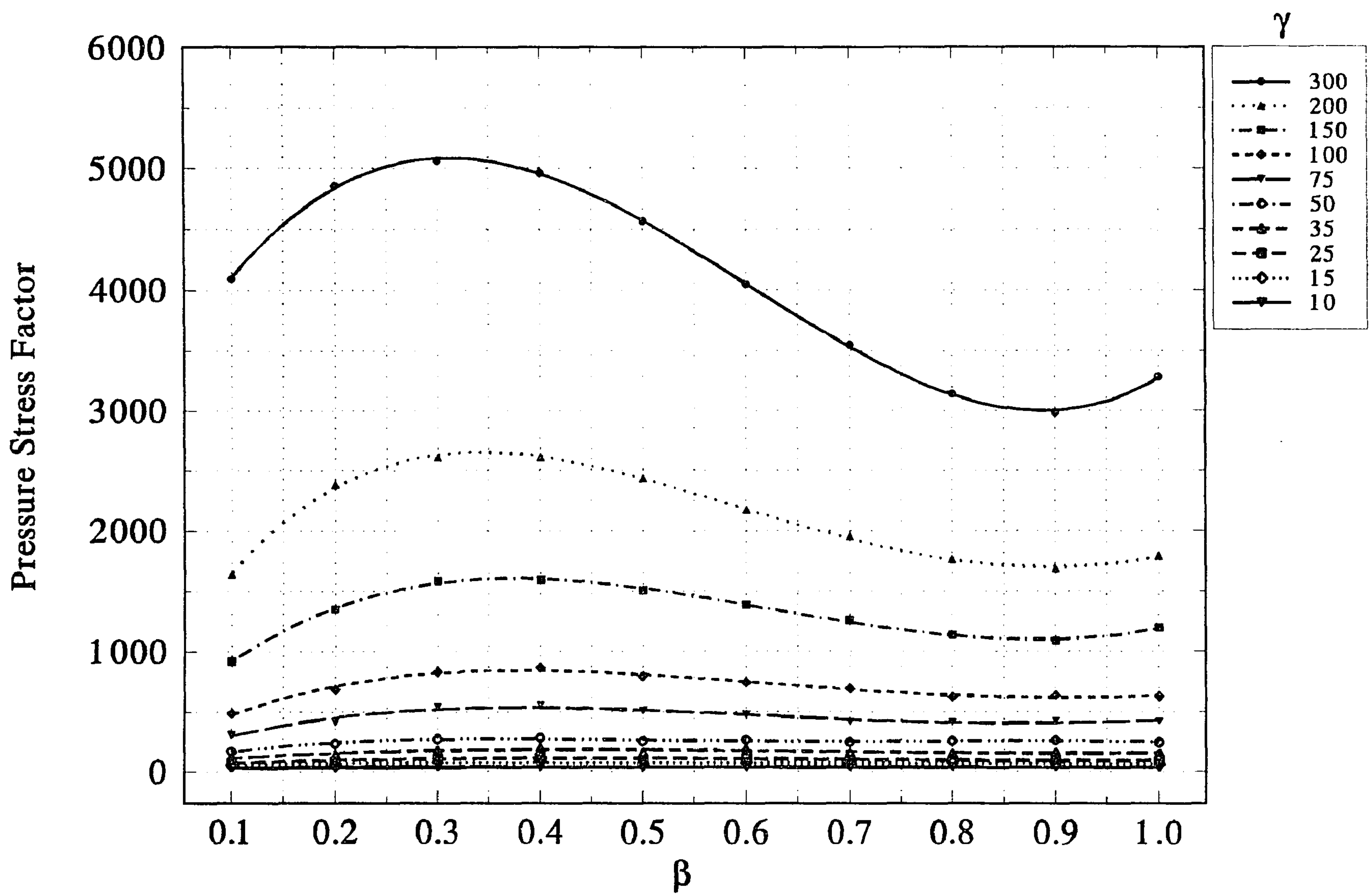

Figure 14P Pressure stress factor in the circumferential direction of the nozzle at point A_i

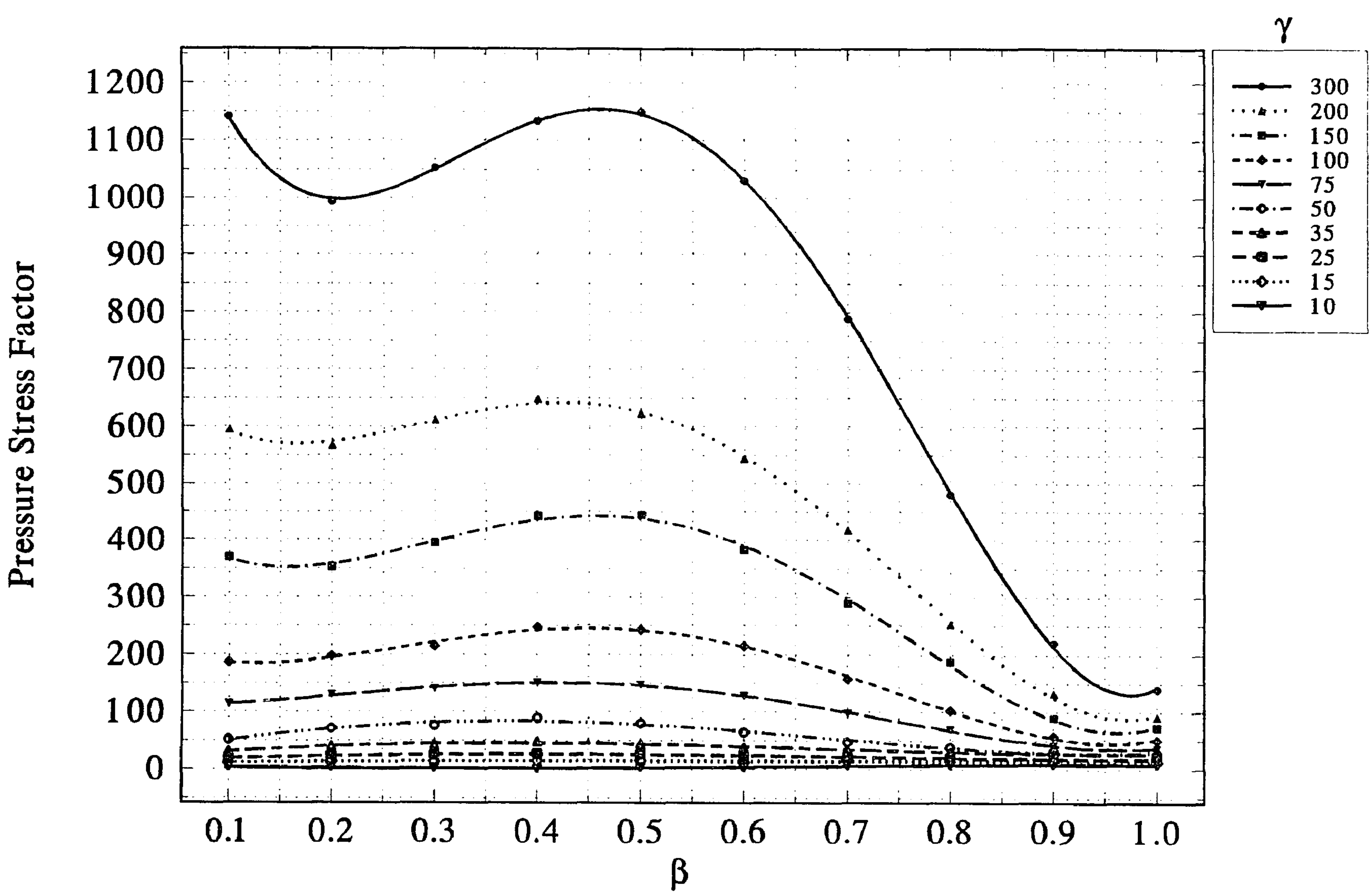

Figure 15P Pressure stress factor in the circumferential direction of the nozzle at point C_o

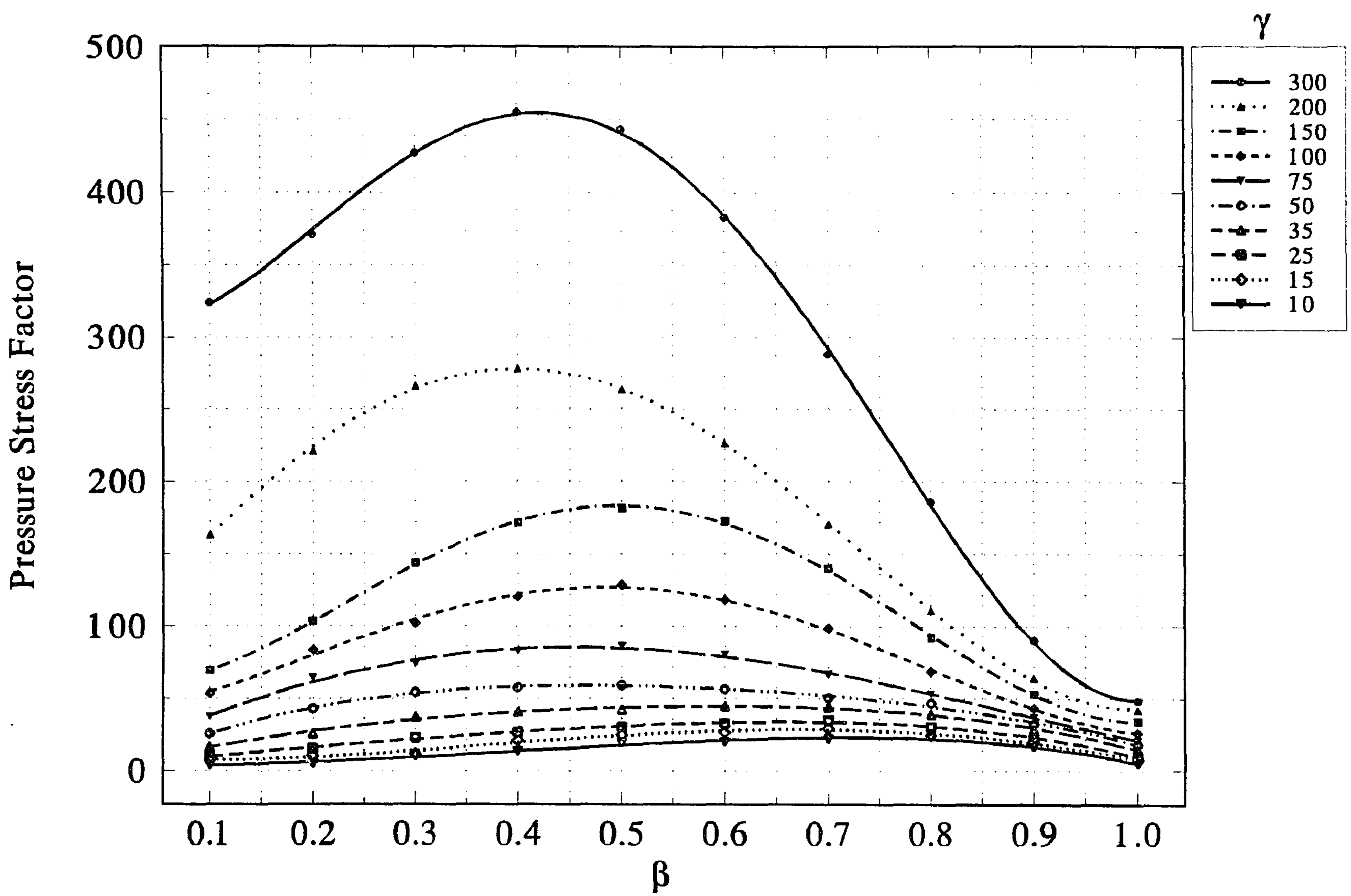

Figure 16P Pressure stress factor in the circumferential direction of the nozzle at point C_i

APPENDIX B

NODE POINT NUMBER ASYMPTOTIC STUDY

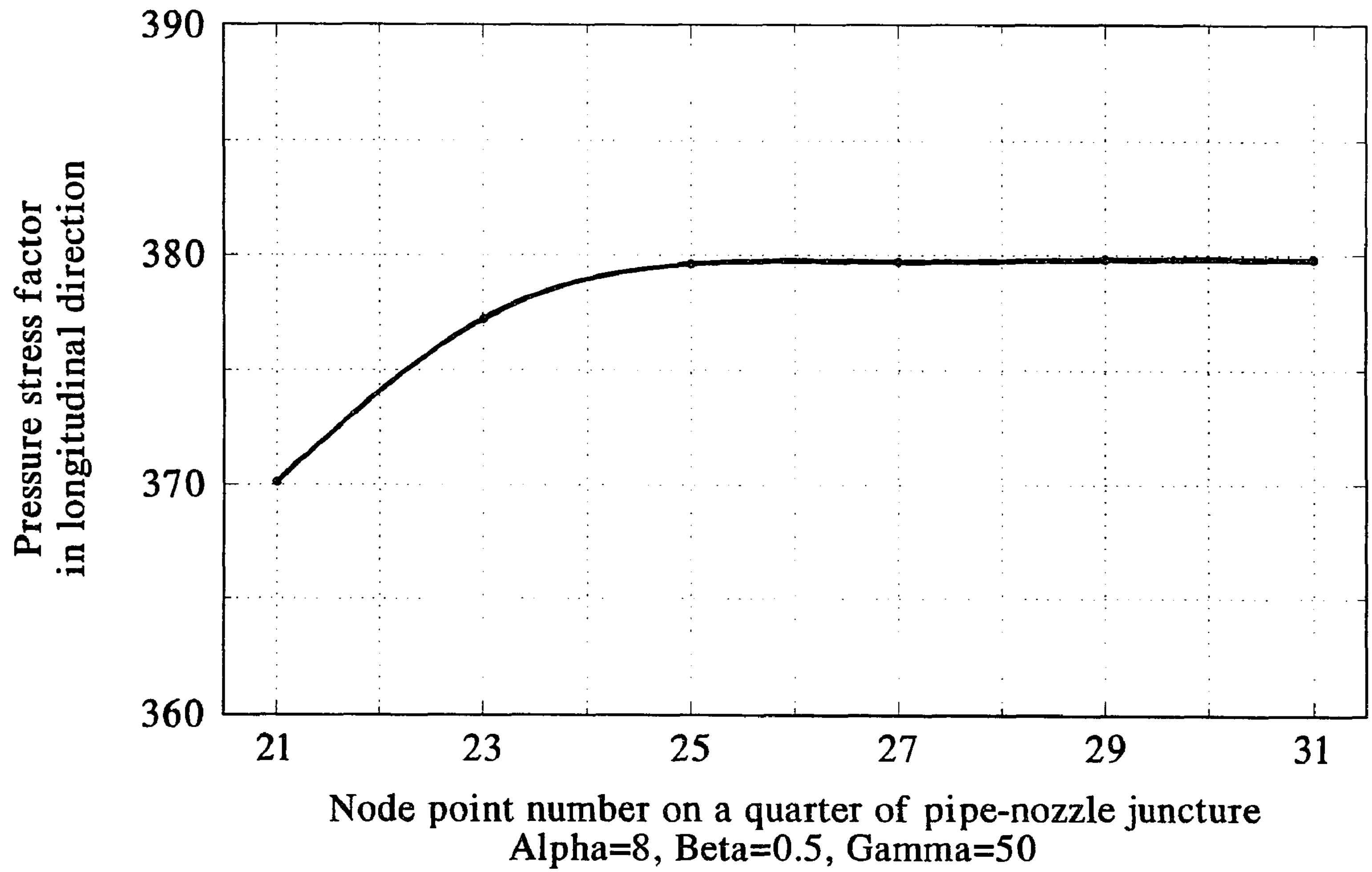

Figure B-1 Asymptotic study at point A_o of pipe

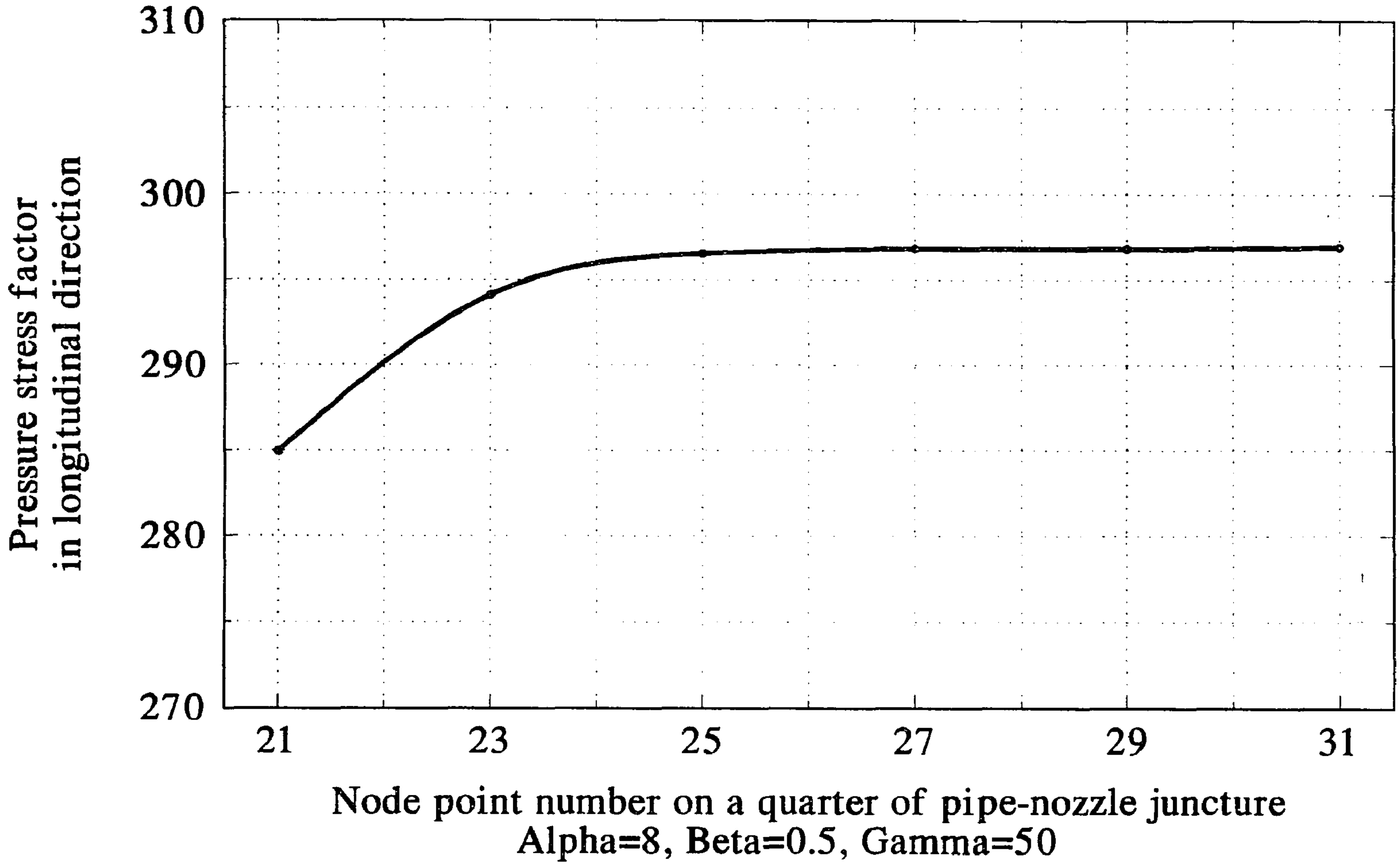

Figure B-2 Asymptotic study at point A_i of pipe

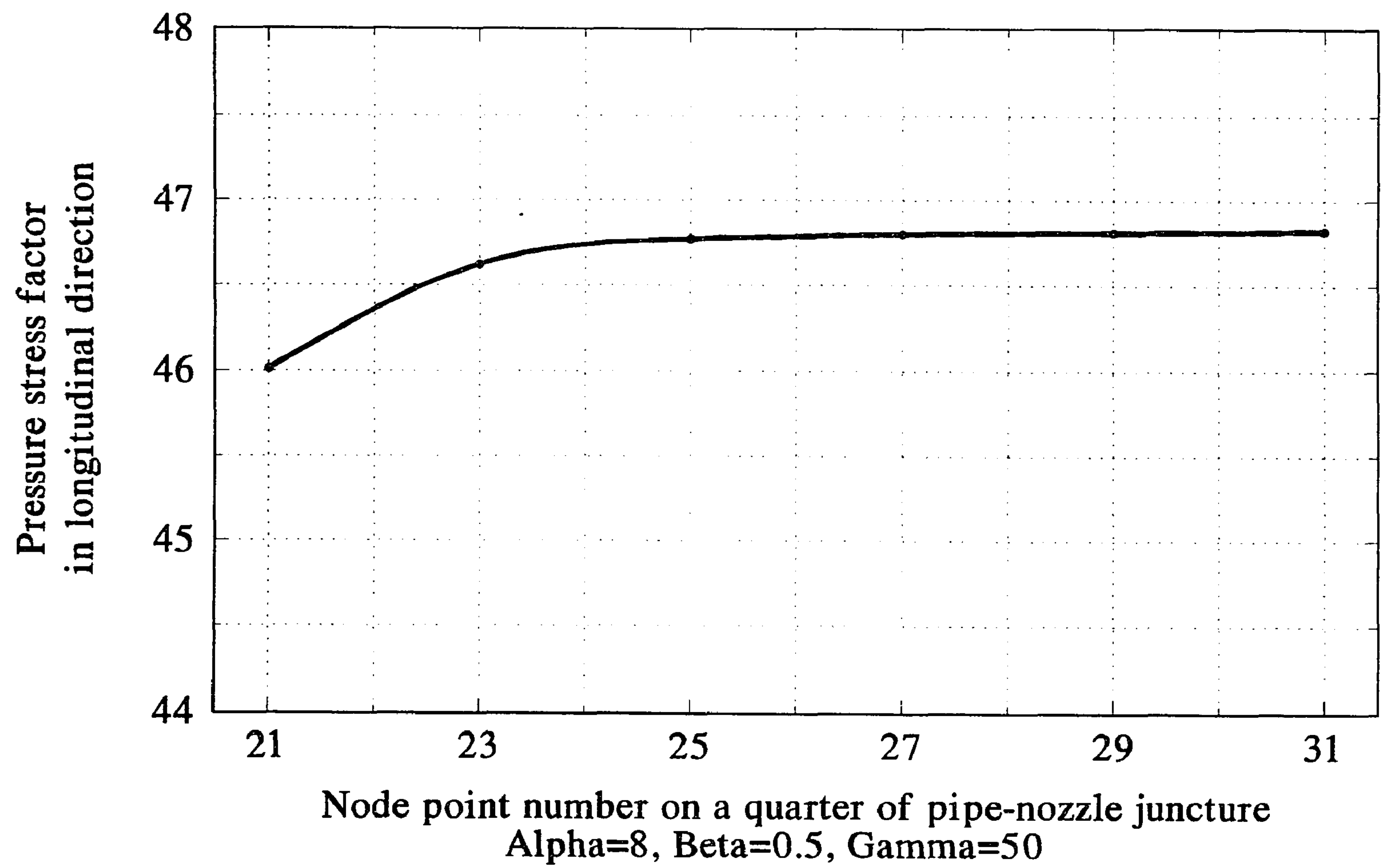

Figure B-3 Asymptotic study at point C_o of pipe

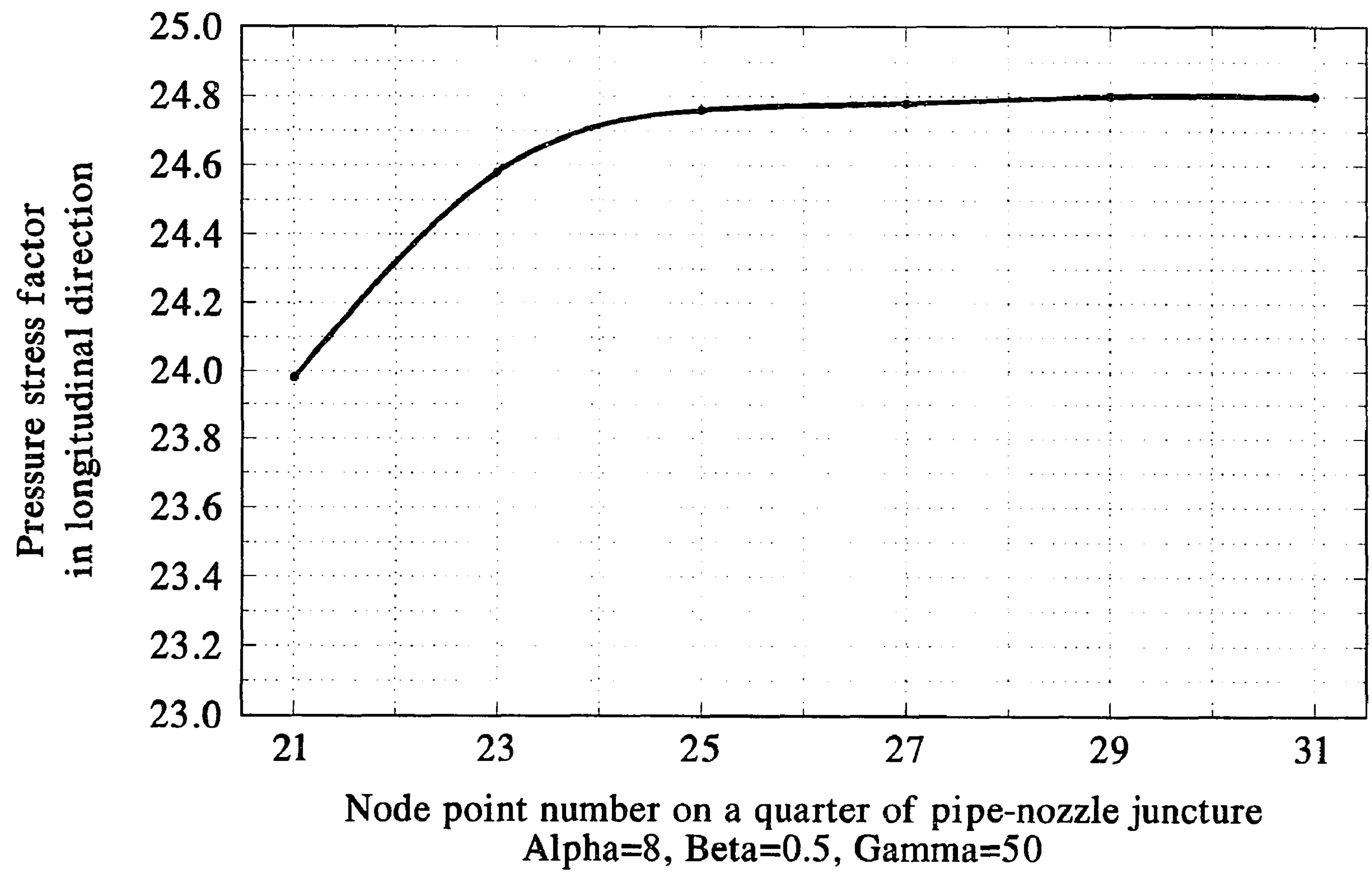

Figure B-4 Asymptotic study at point C_i of pipe

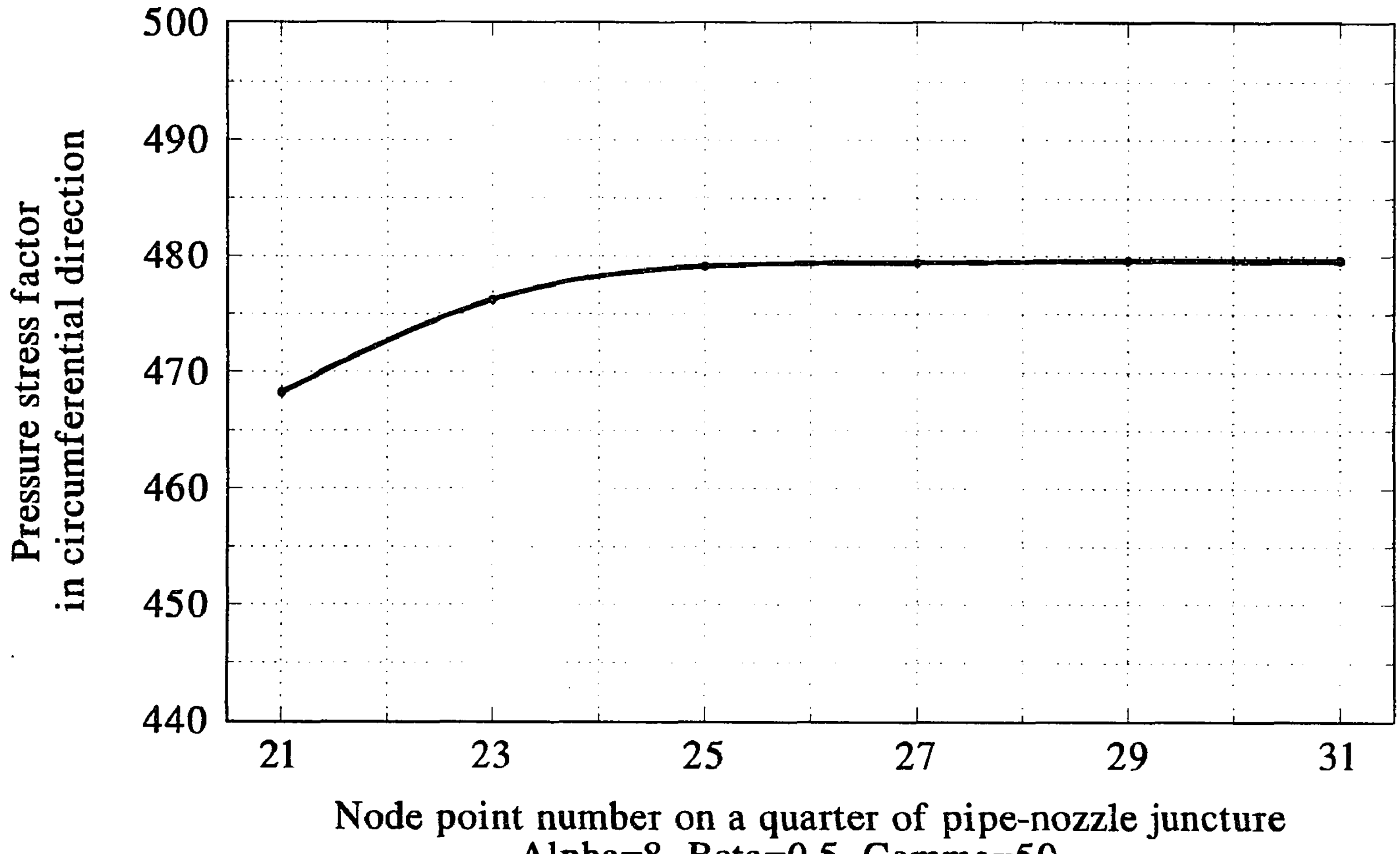

Figure B-5 Asymptotic study at point A_o of pipe

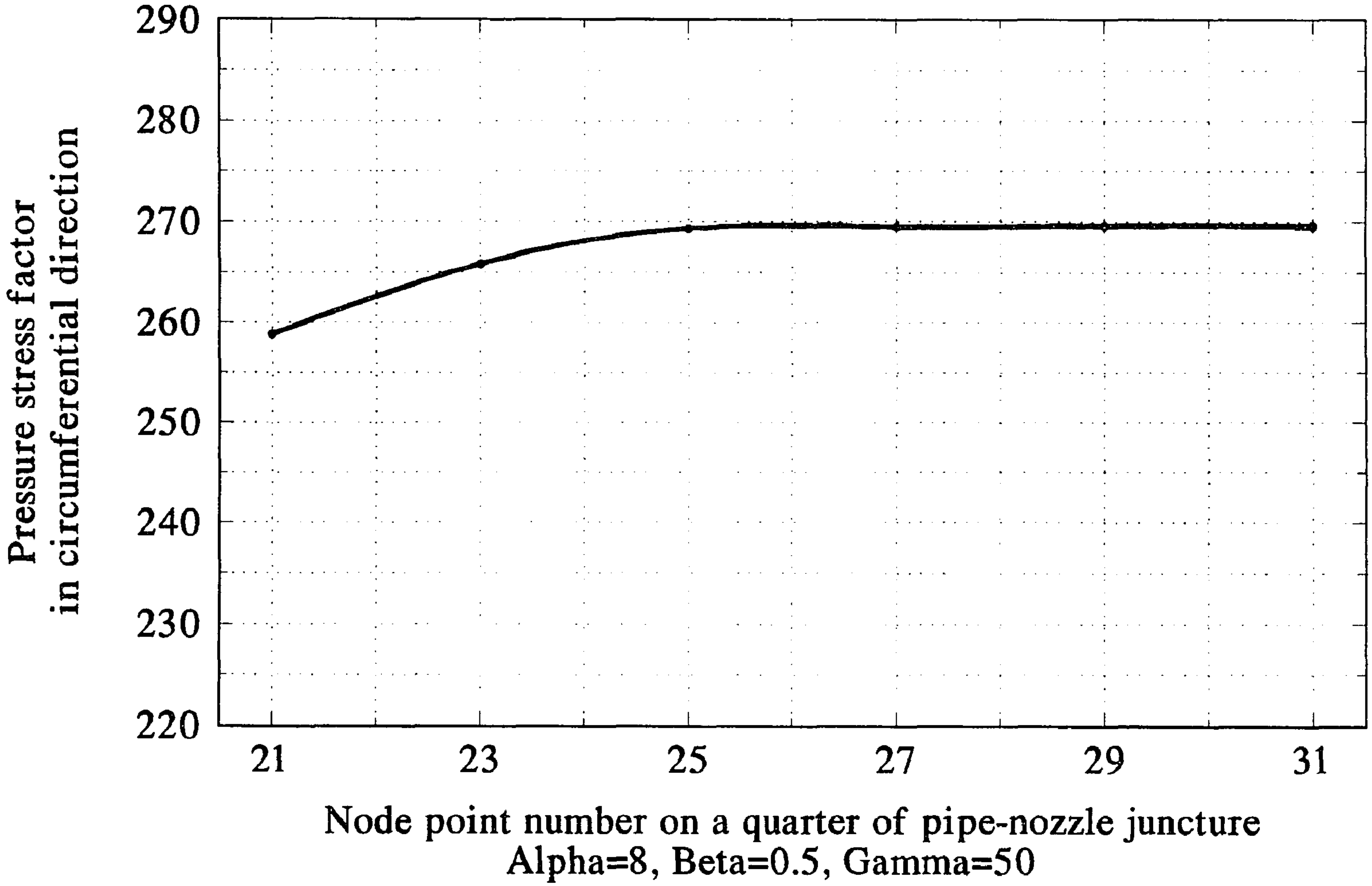

Figure B-6 Asymptotic study at point A_i of pipe

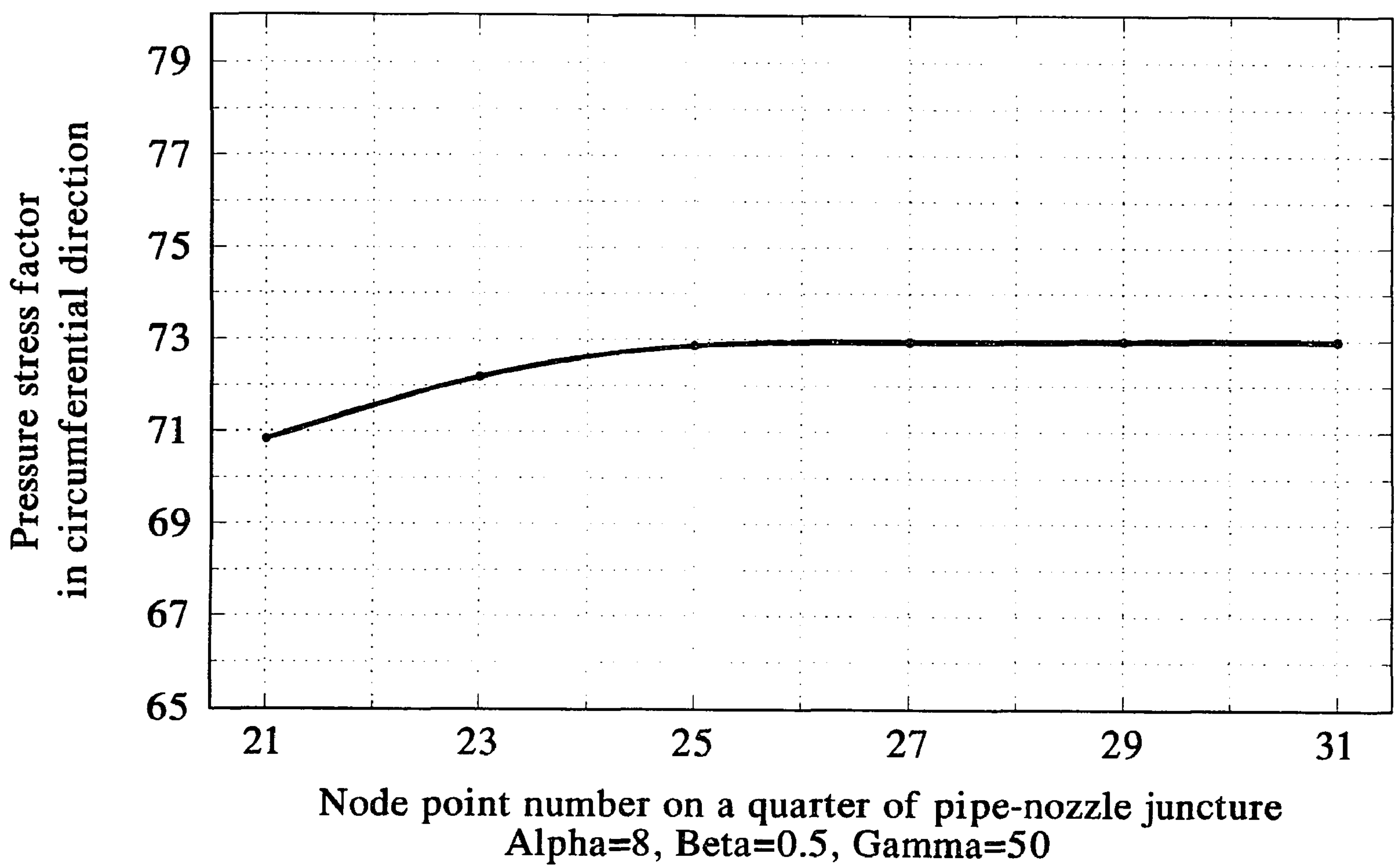

Figure B-7 Asymptotic study at point C_o of pipe

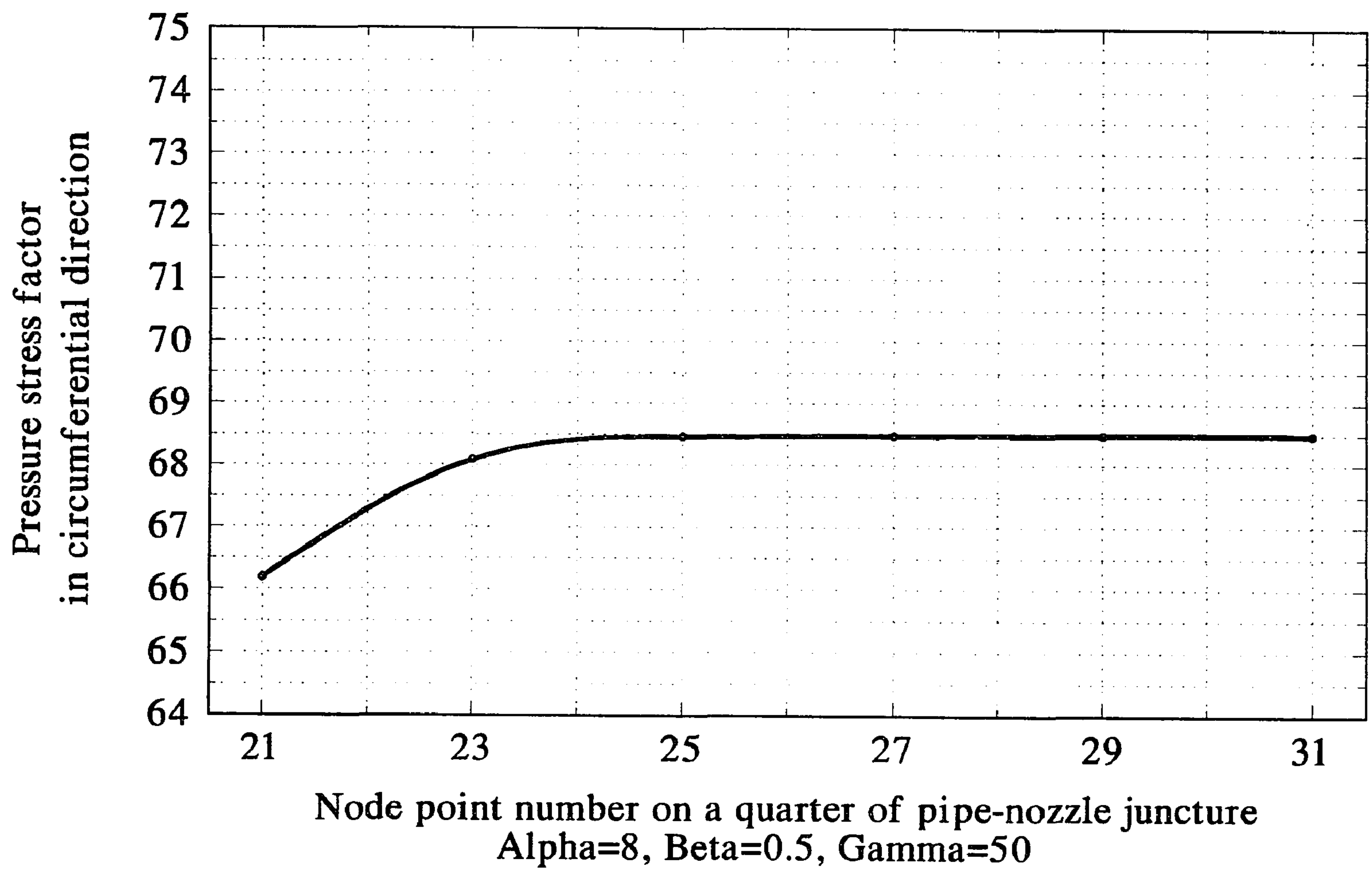

Figure B-8 Asymptotic study at point C_i of pipe

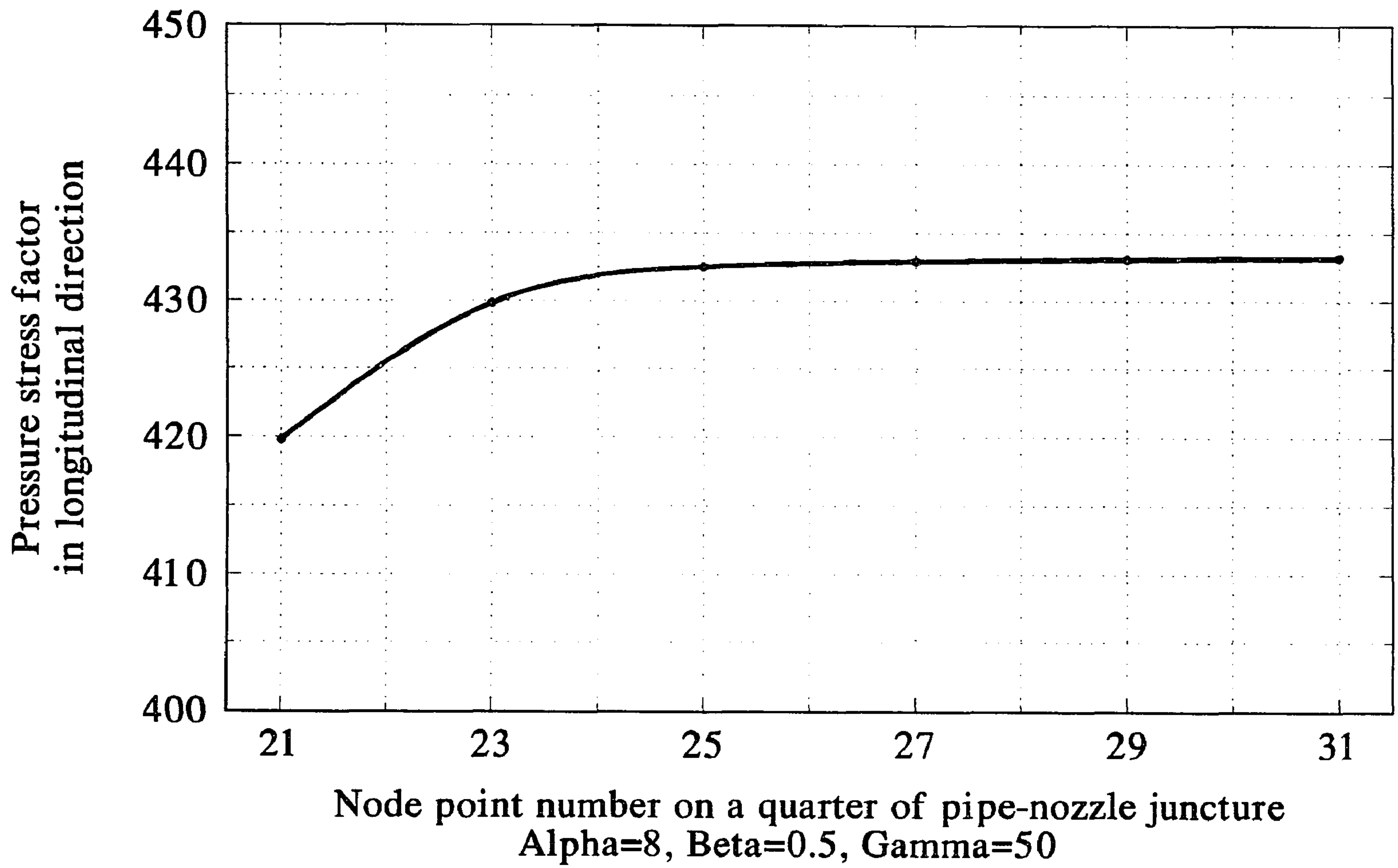

Figure B-9 Asymptotic study at point A_o of nozzle

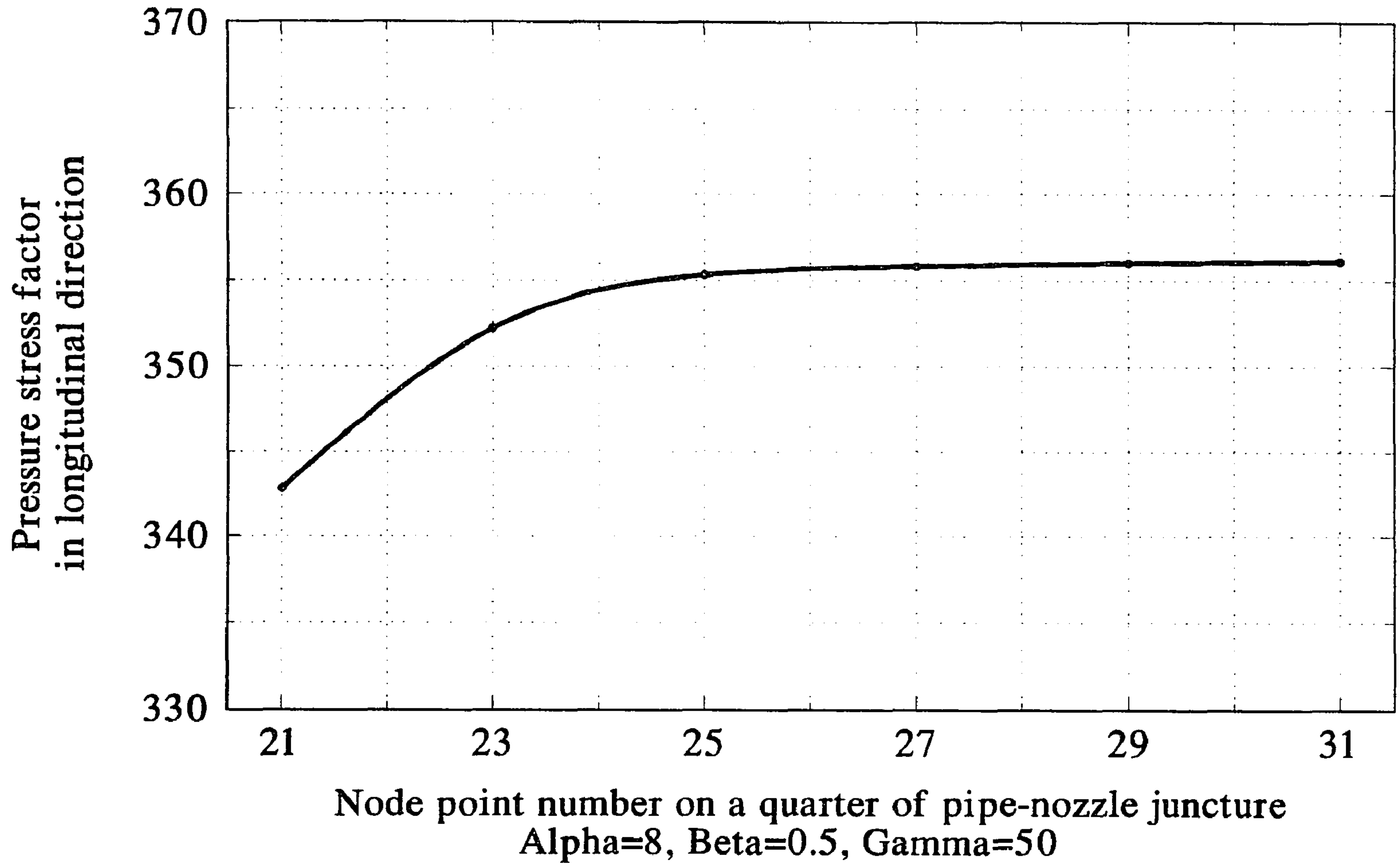

Figure B-10 Asymptotic study at point A_i of nozzle

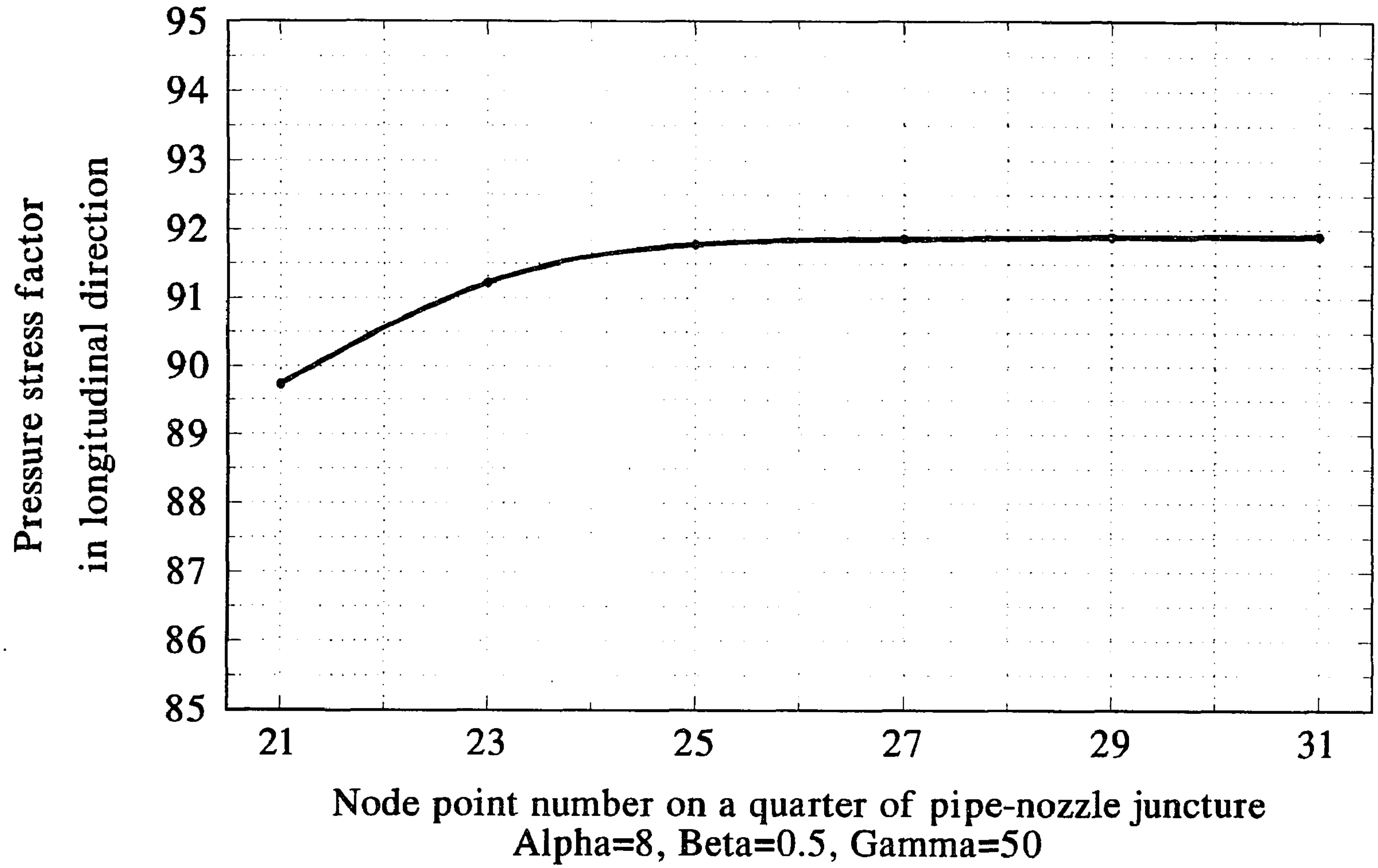

Figure B-11 Asymptotic study at point C_o of nozzle

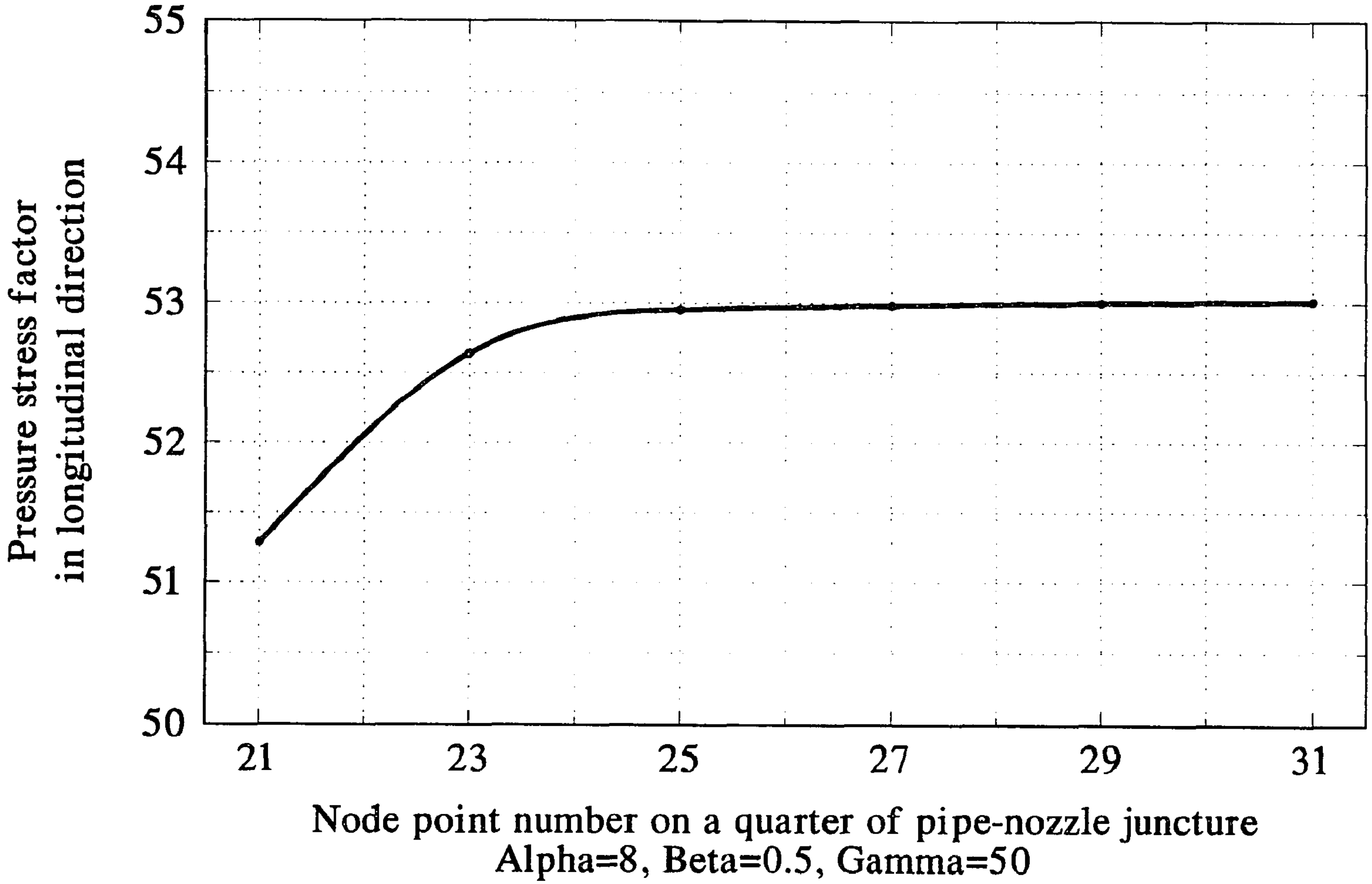

Figure B-12 Asymptotic study at point C_i of nozzle

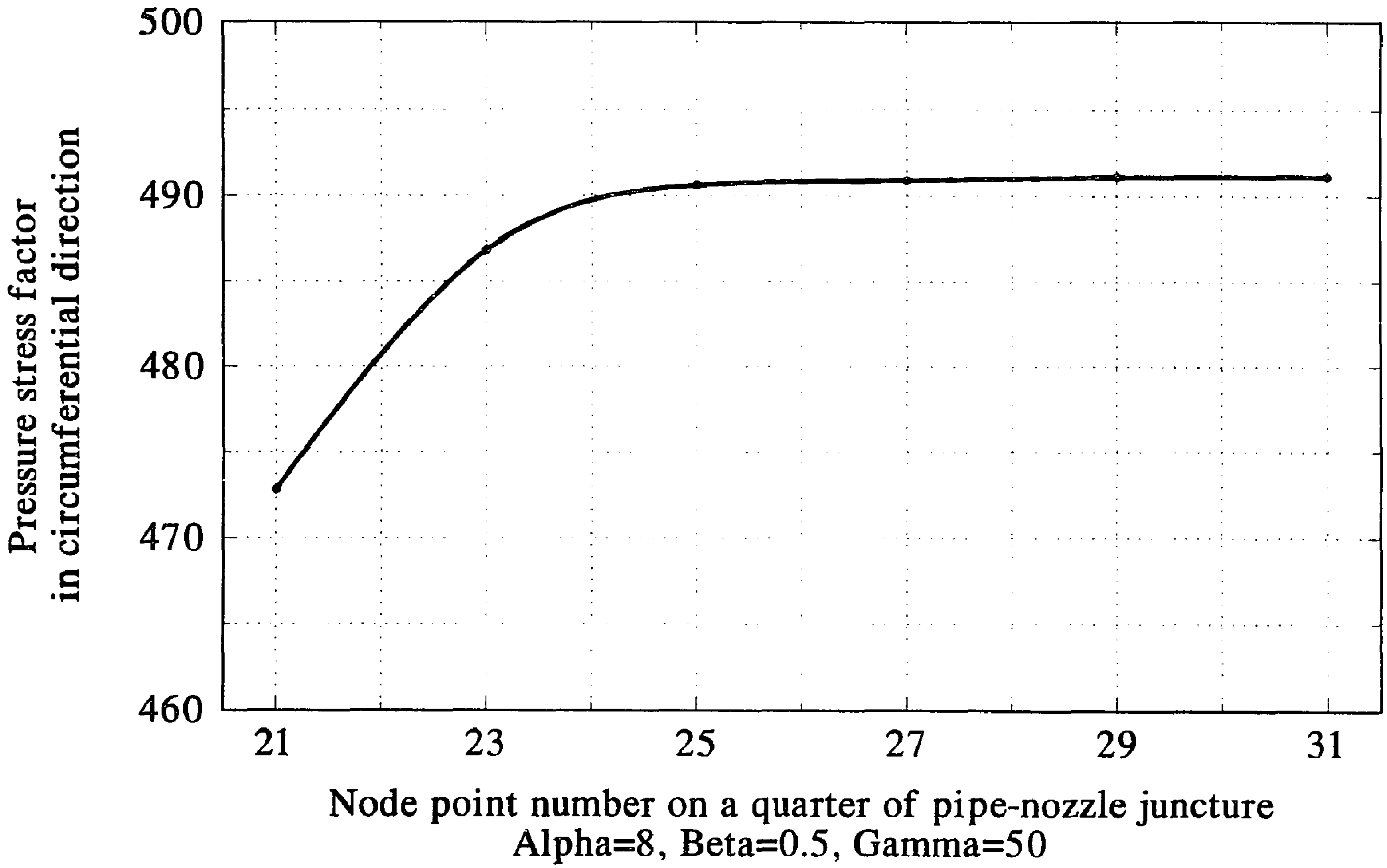

Figure B-13 Asymptotic study at point A_o of nozzle

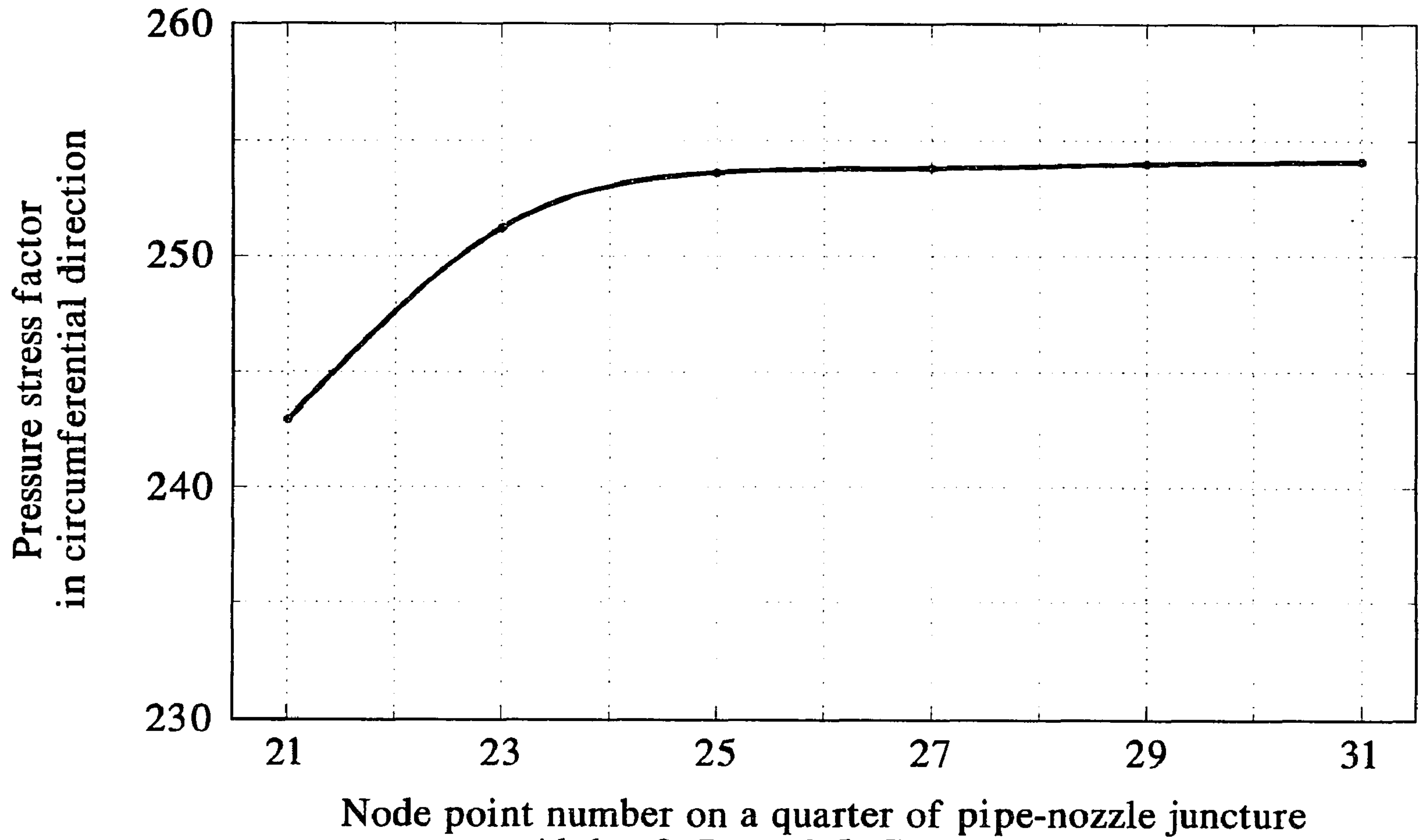

Alpha=8, Beta=0.5, Gamma=50

Figure B-14 Asymptotic study at point A_i of nozzle

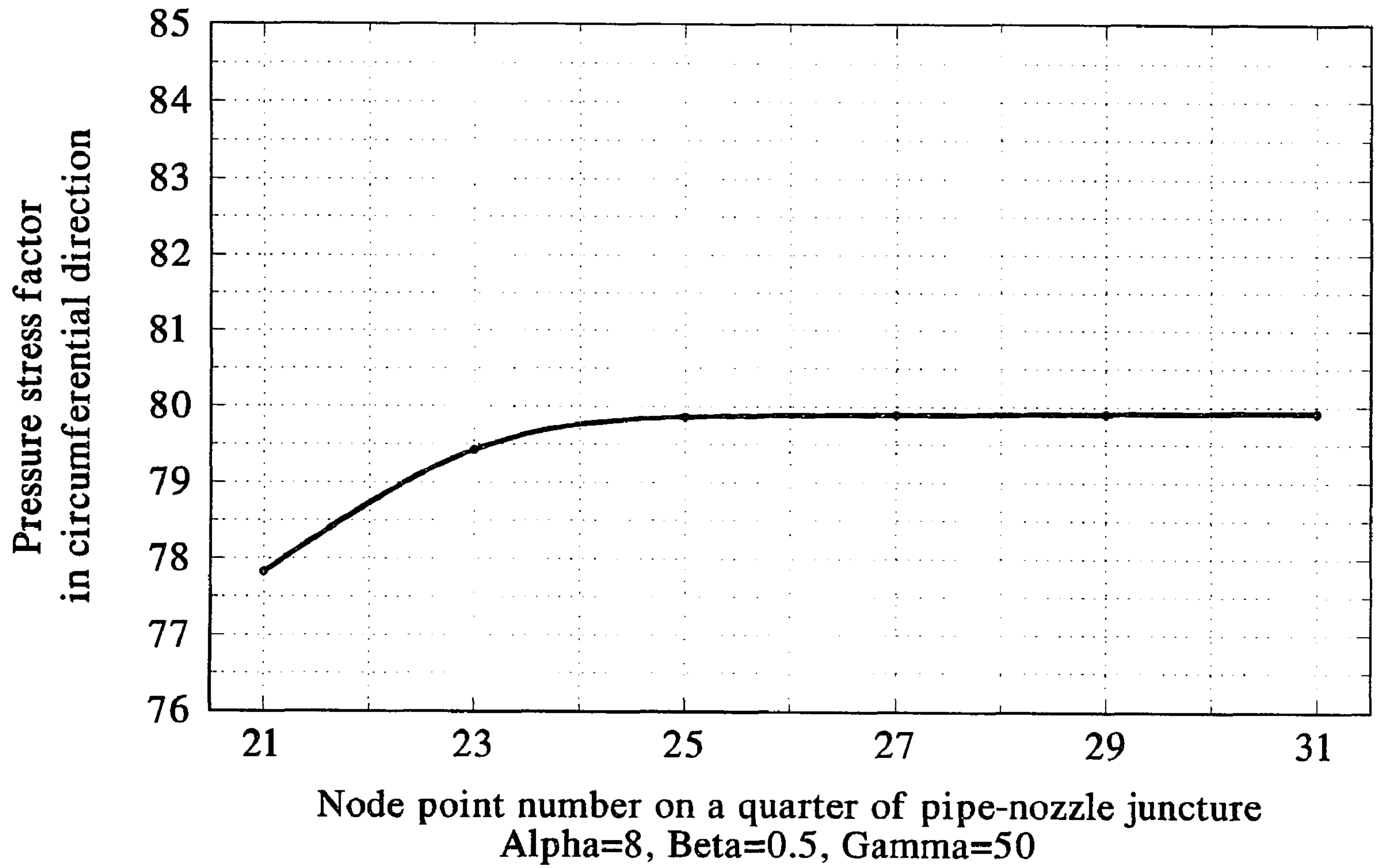

Figure B-15 Asymptotic study at point C_o of nozzle

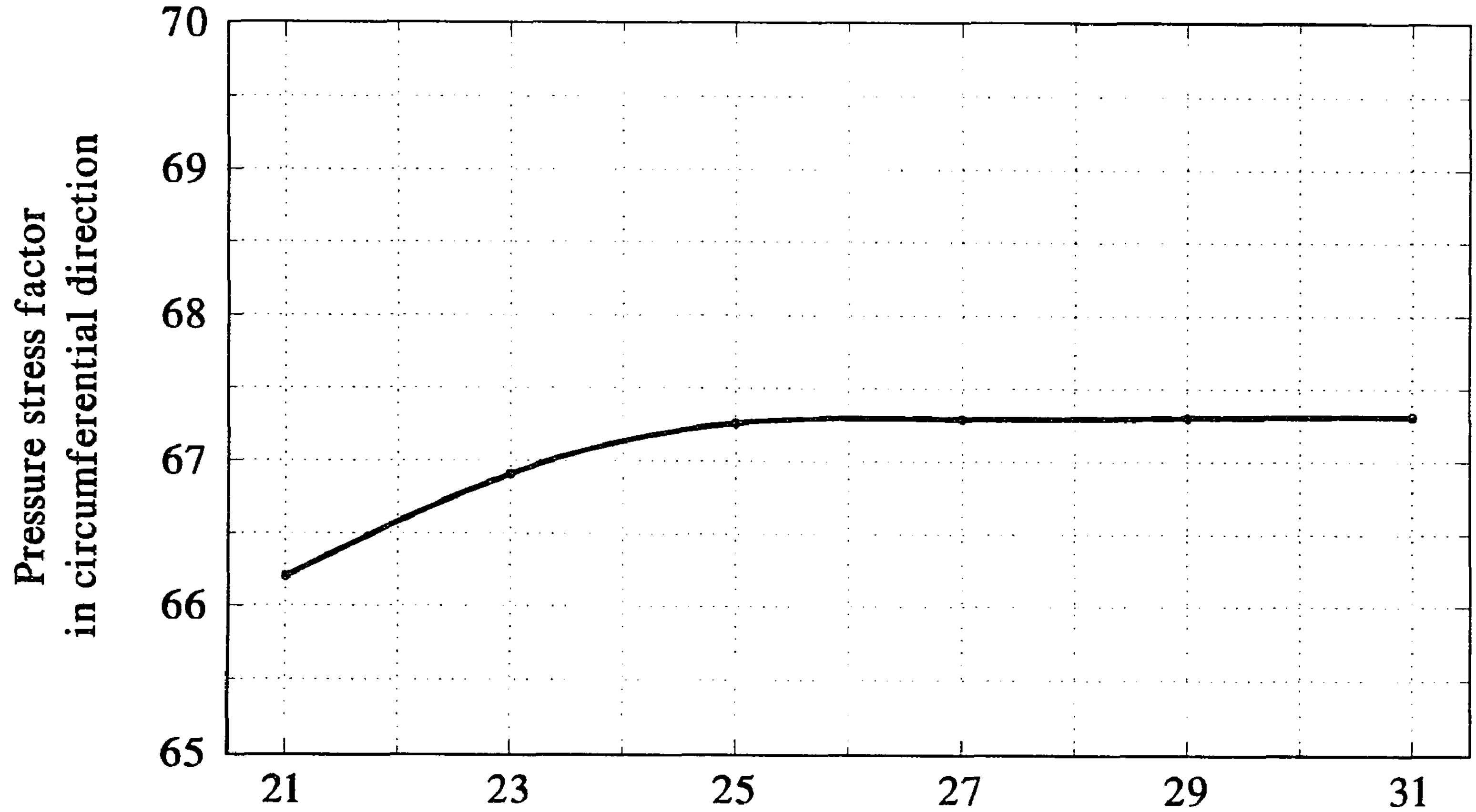

Node point number on a quarter of pipe-nozzle juncture
Alpha=8, Beta=0.5, Gamma=50

Figure B-16 Asymptotic study at point C_i of nozzle

APPENDIX C

$ALPHA_p$ AND $ALPHA_n$ ASYMPTOTIC STUDY

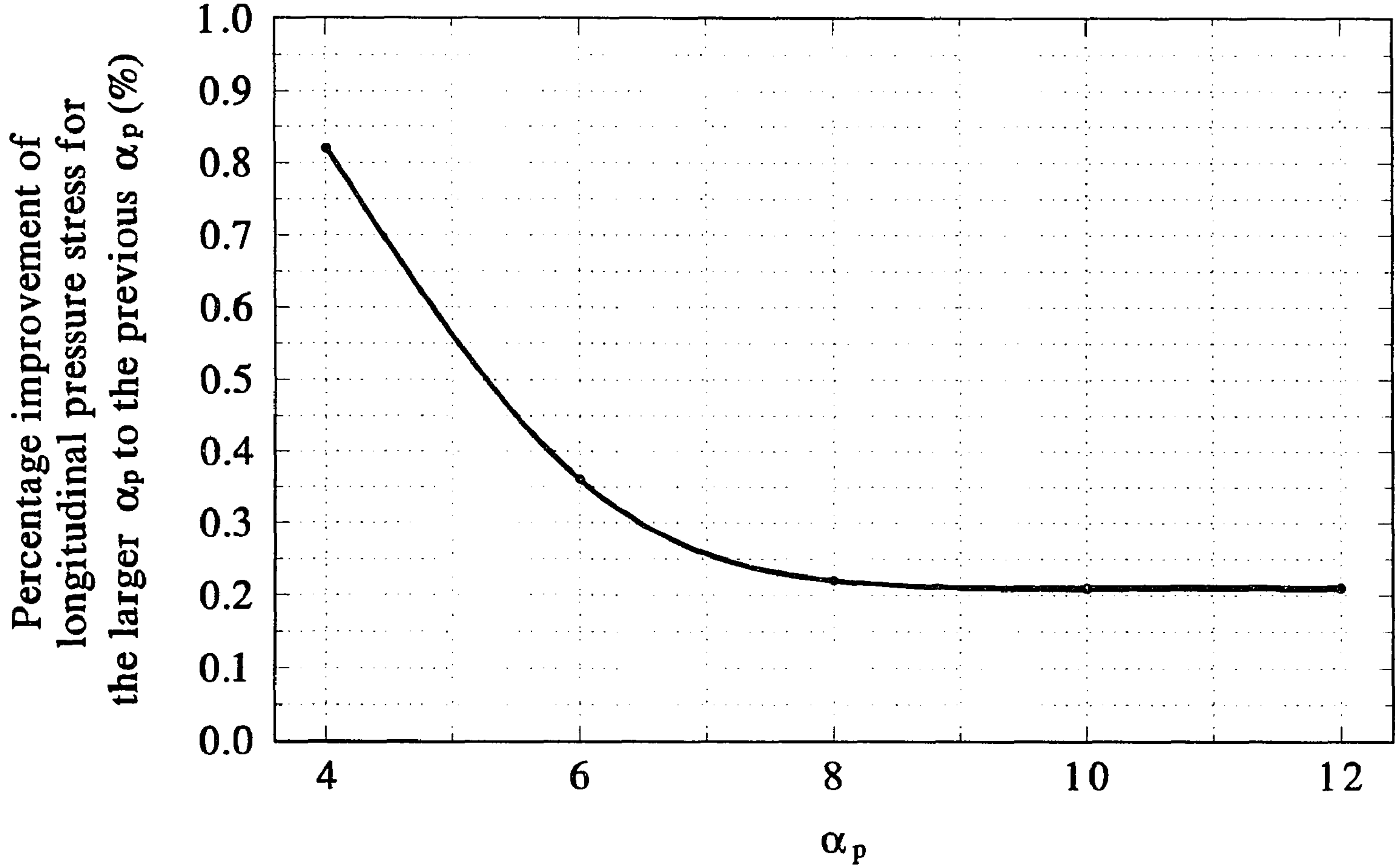

beta=0.5, gamma=75, 25 nodes on a quarter

Figure C-1 Asymptotic study on α_p at A_o of pipe

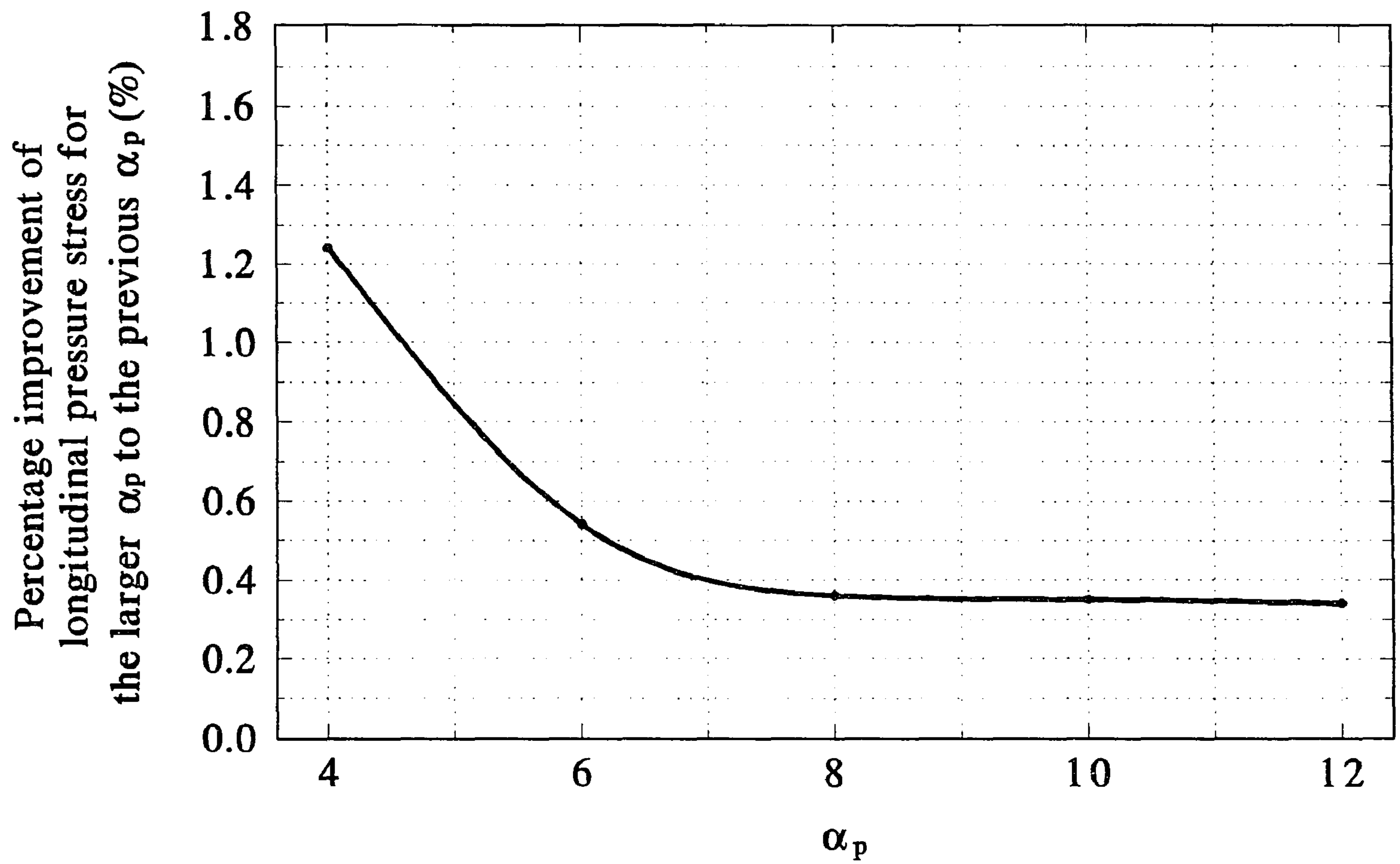

beta=0.5, gamma=75, 25 nodes on a quarter

Figure C-2 Asymptotic study on α_p at A_i of pipe

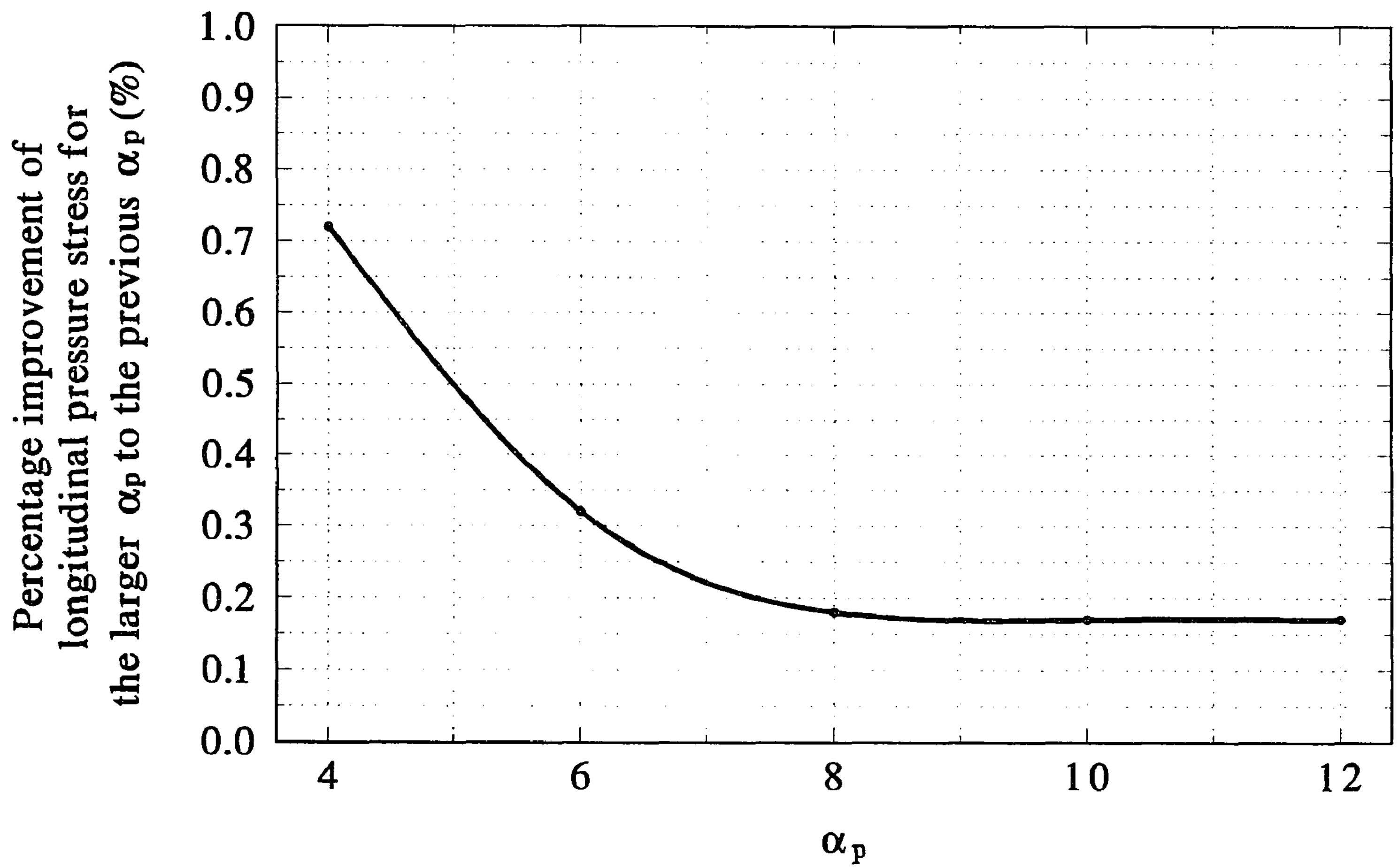

beta=0.5, gamma=75, 25 nodes on a quarter

Figure C-3 Asymptotic study on α_p at C_o of pipe

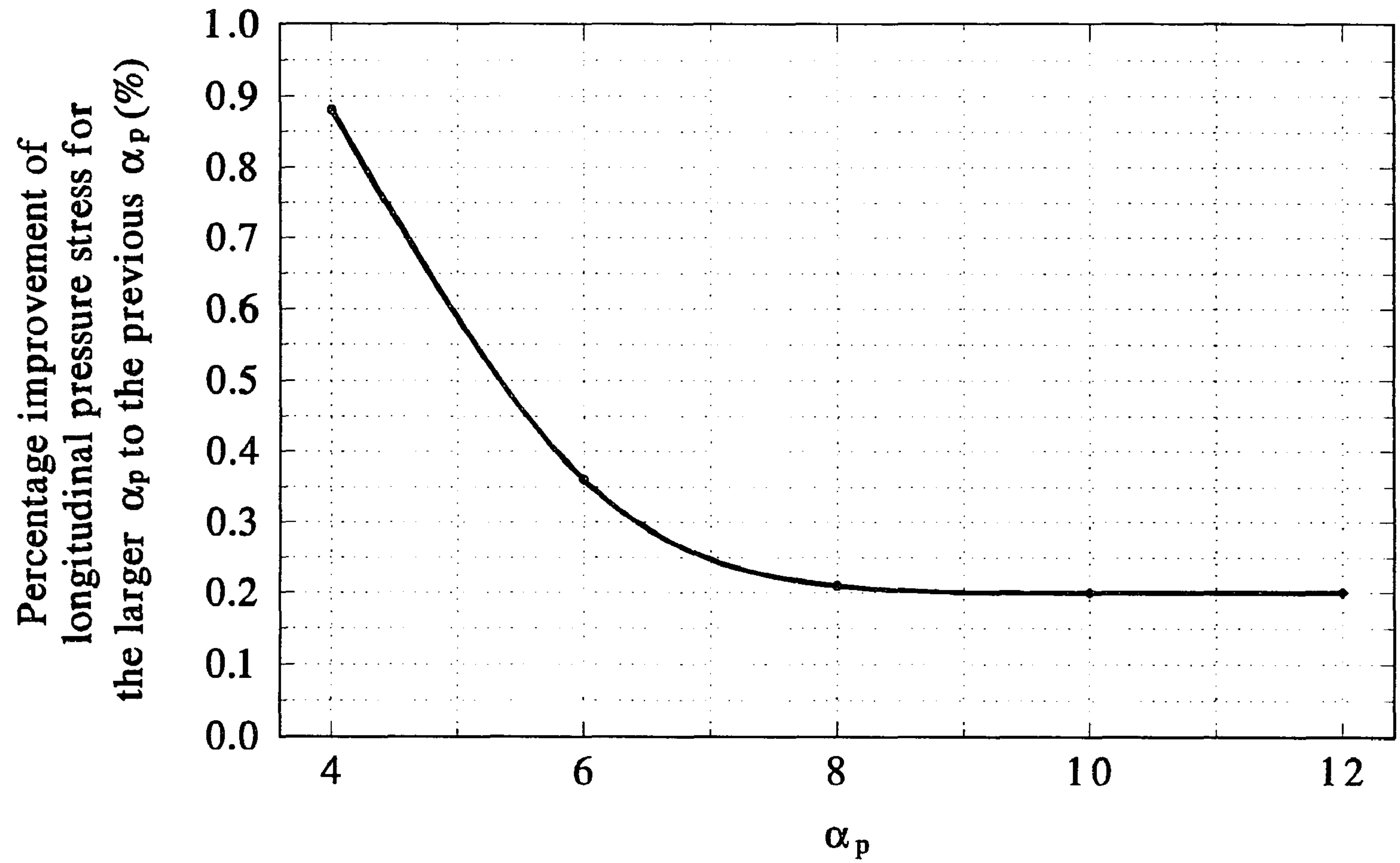

beta=0.5, gamma=75, 25 nodes on a quarter

Figure C-4 Asymptotic study on α_p at C_i of pipe

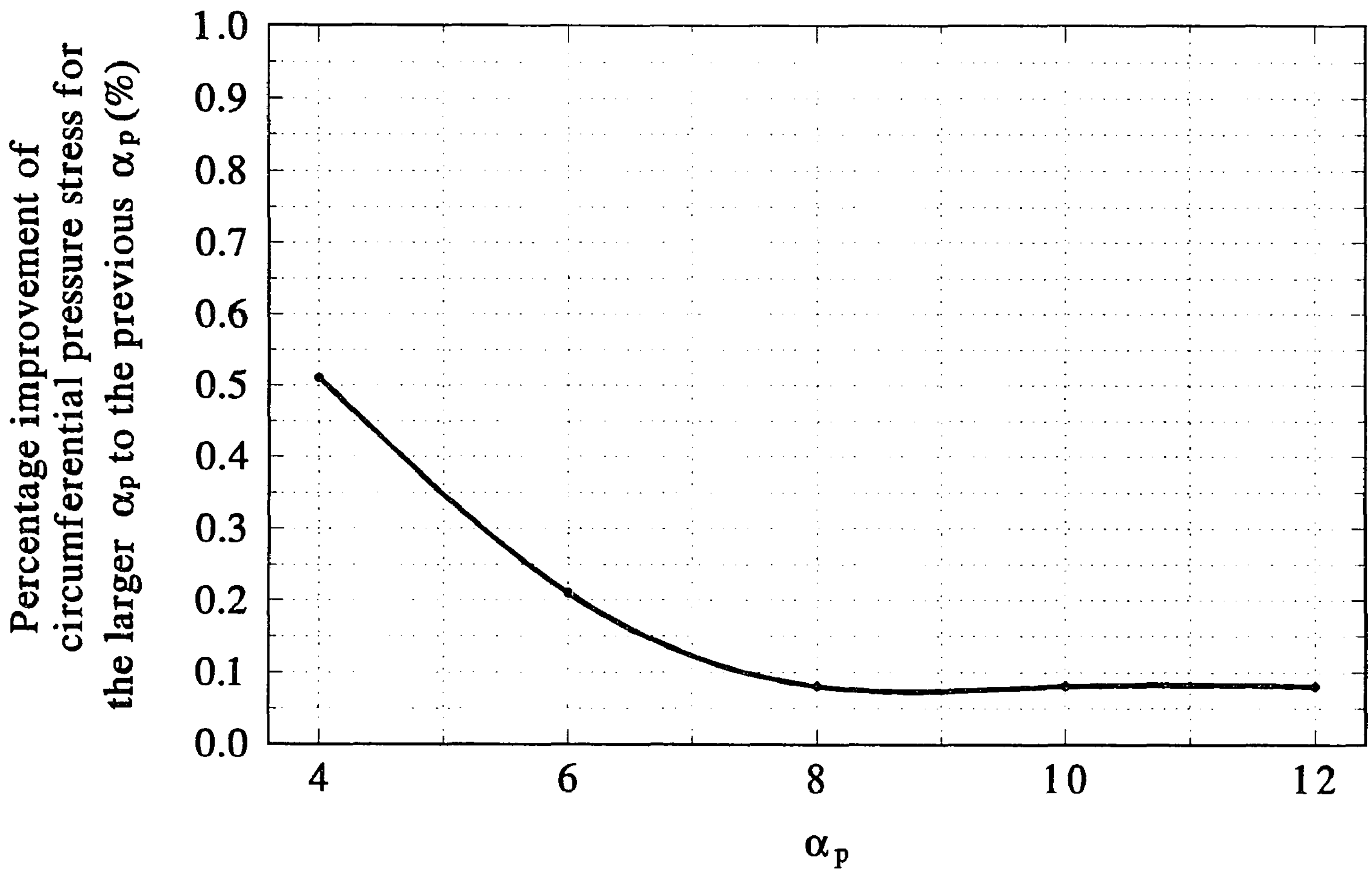

beta=0.5, gamma=75, 25 nodes on a quarter

Figure C-5 Asymptotic study on α_p at A_o of pipe

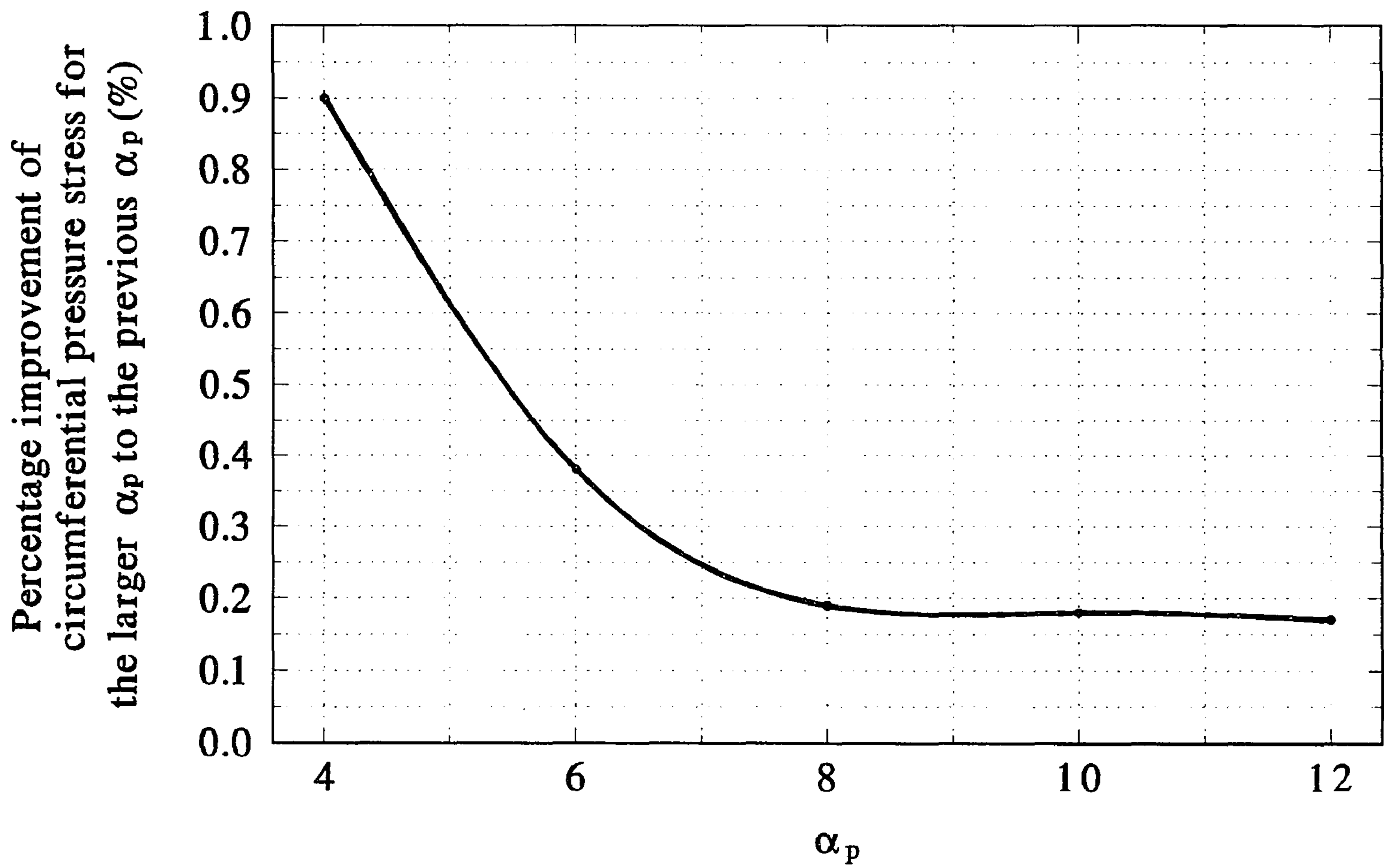

beta=0.5, gamma=75, 25 nodes on a quarter

Figure C-6 Asymptotic study on α_p at A_i of pipe

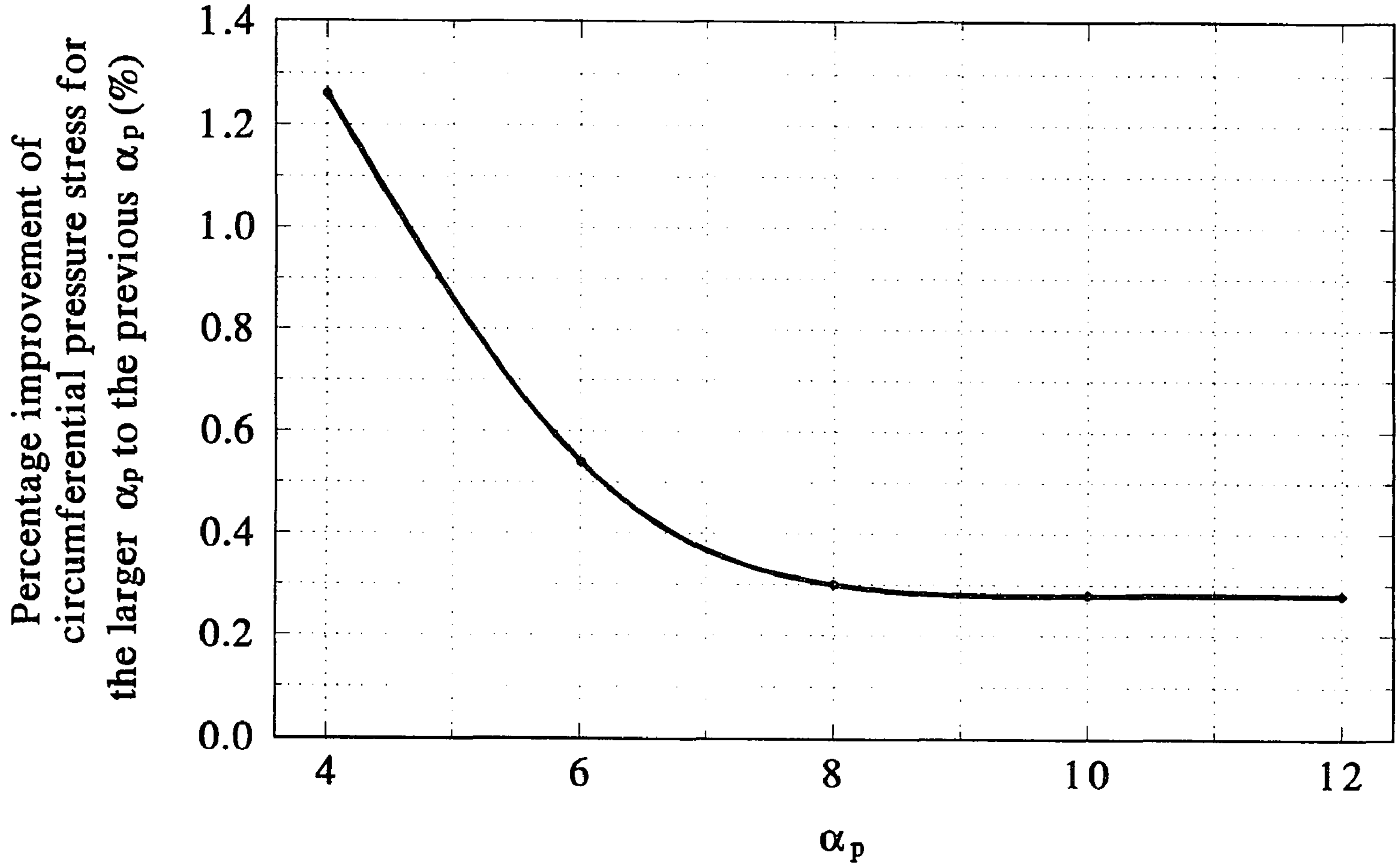

beta=0.5, gamma=75, 25 nodes on a quarter

Figure C-7 Asymptotic study on α_p at C_o of pipe

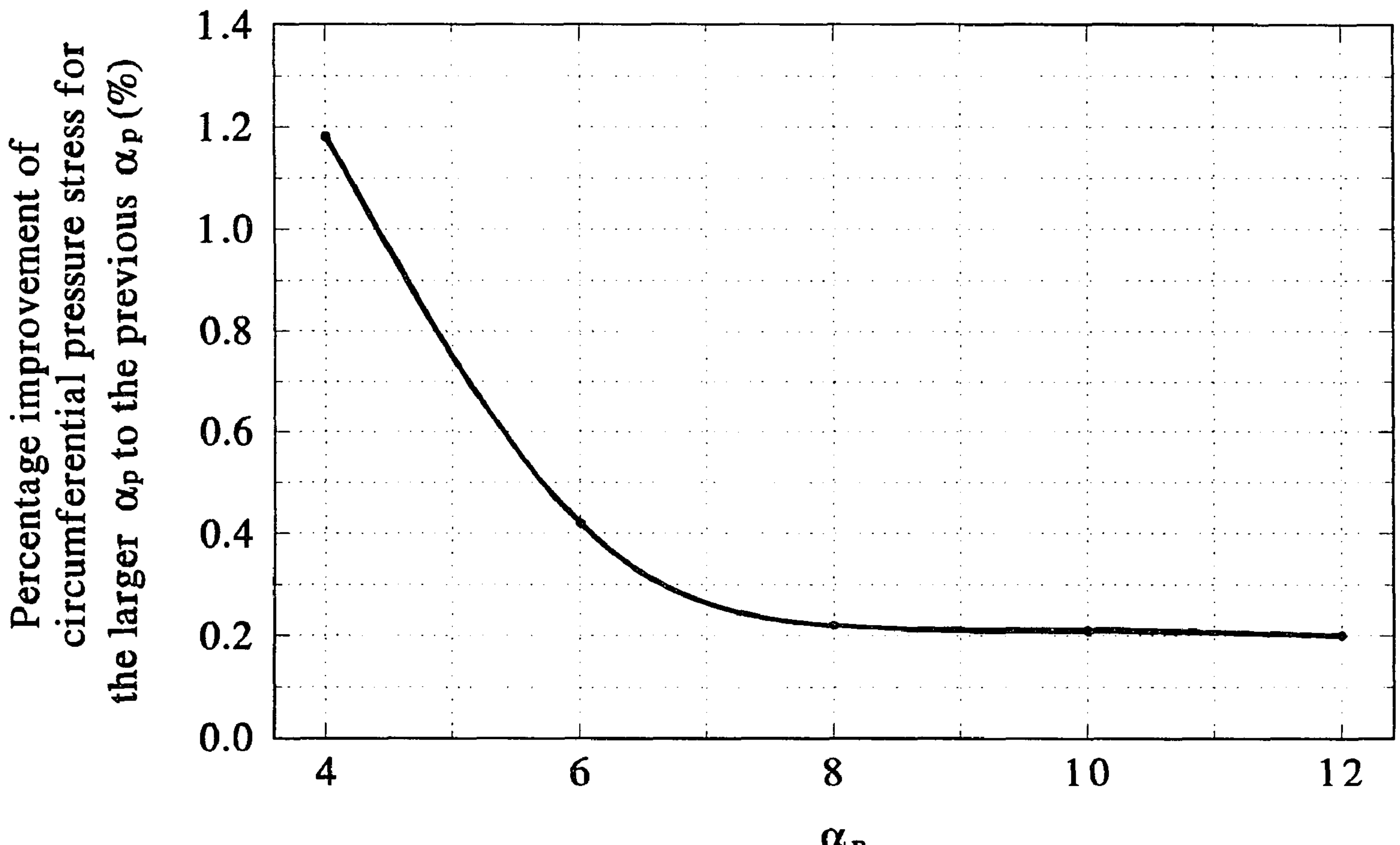

beta=0.5, gamma=75, 25 nodes on a quarter

Figure C-8 Asymptotic study on α_p at C_i of pipe

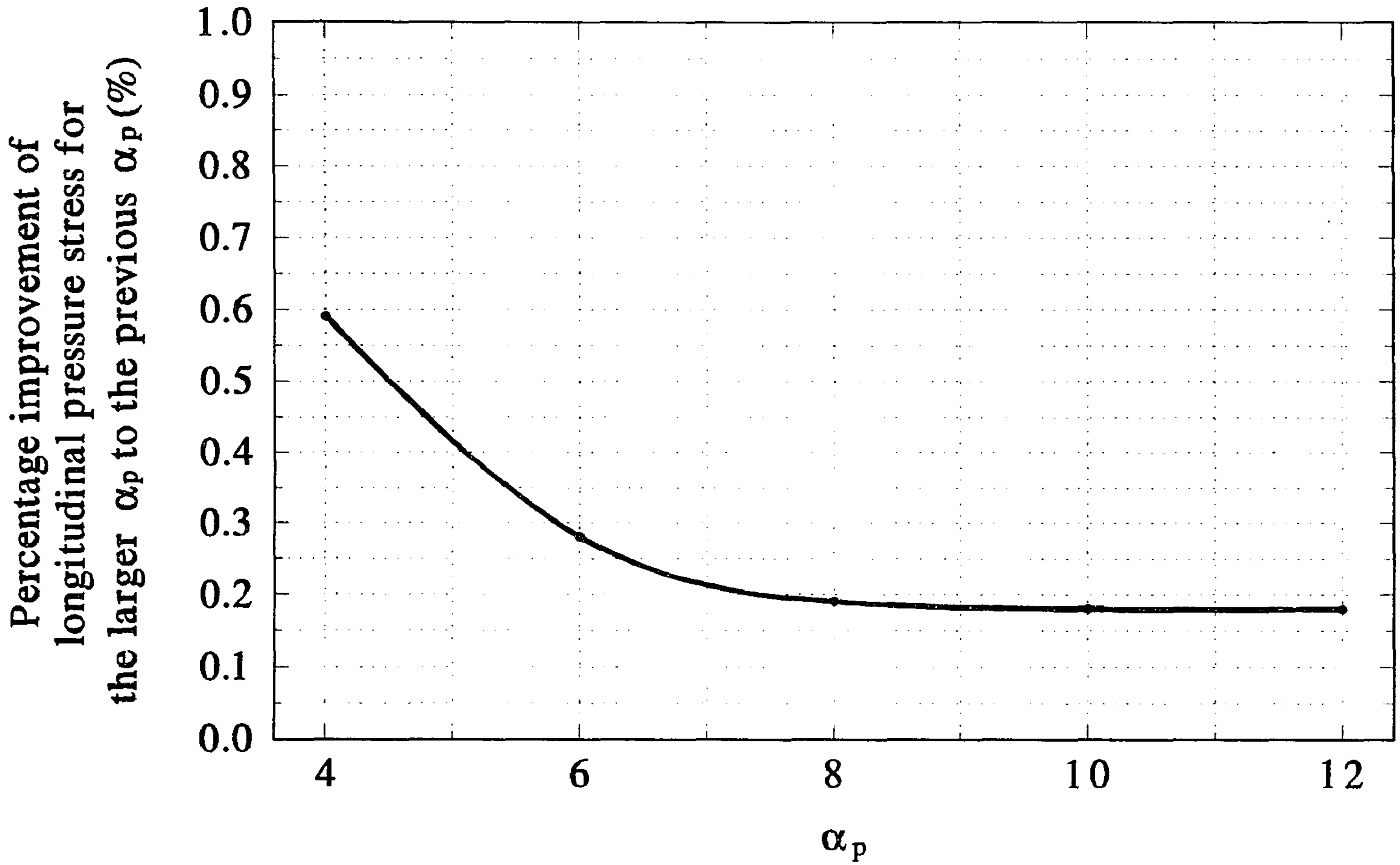

beta=0.5, gamma=75, 25 nodes on a quarter

Figure C-9 Asymptotic study on α_p at A_o of nozzle

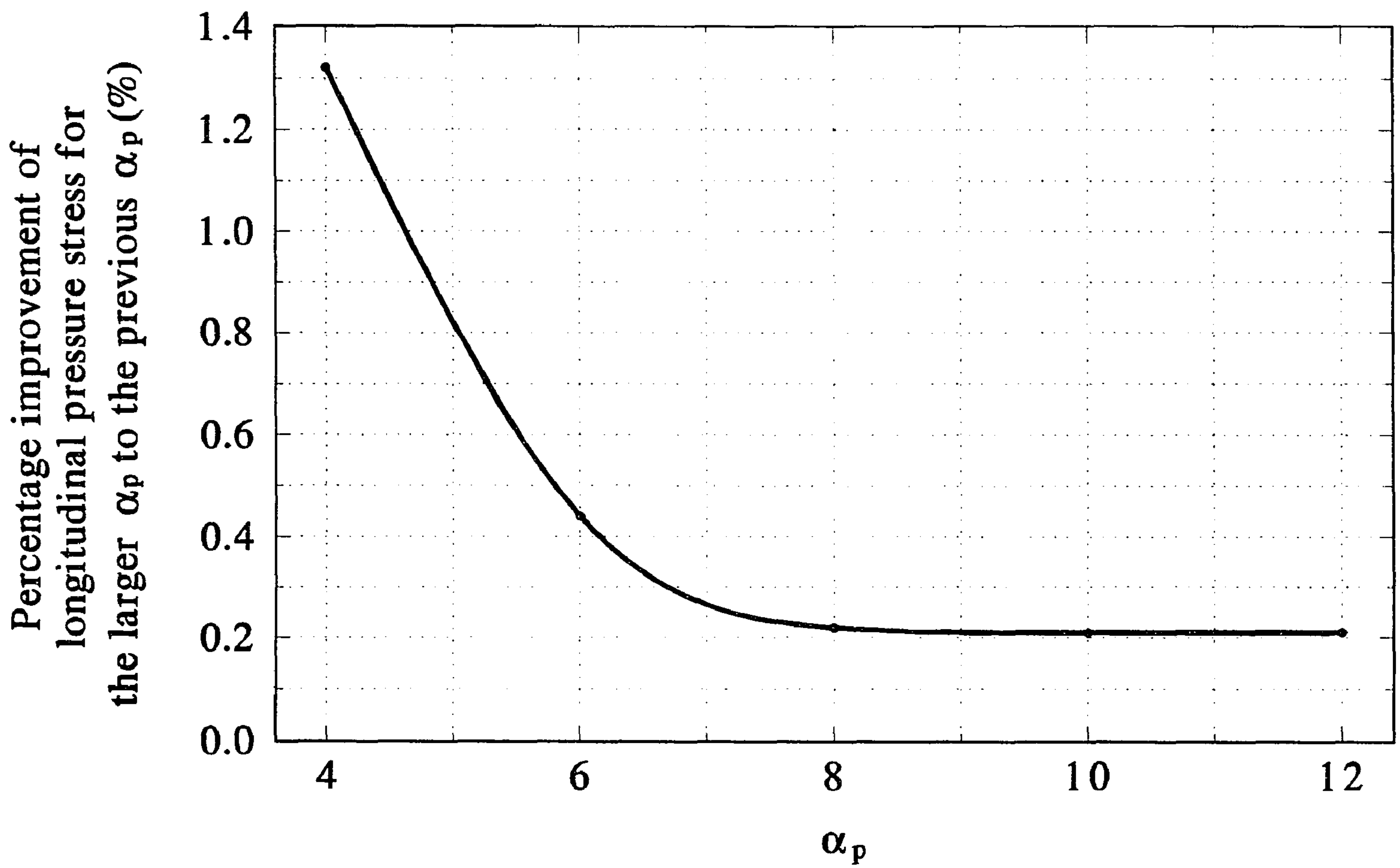

beta=0.5, gamma=75, 25 nodes on a quarter

Figure C-10 Asymptotic study on α_p at A_i of nozzle

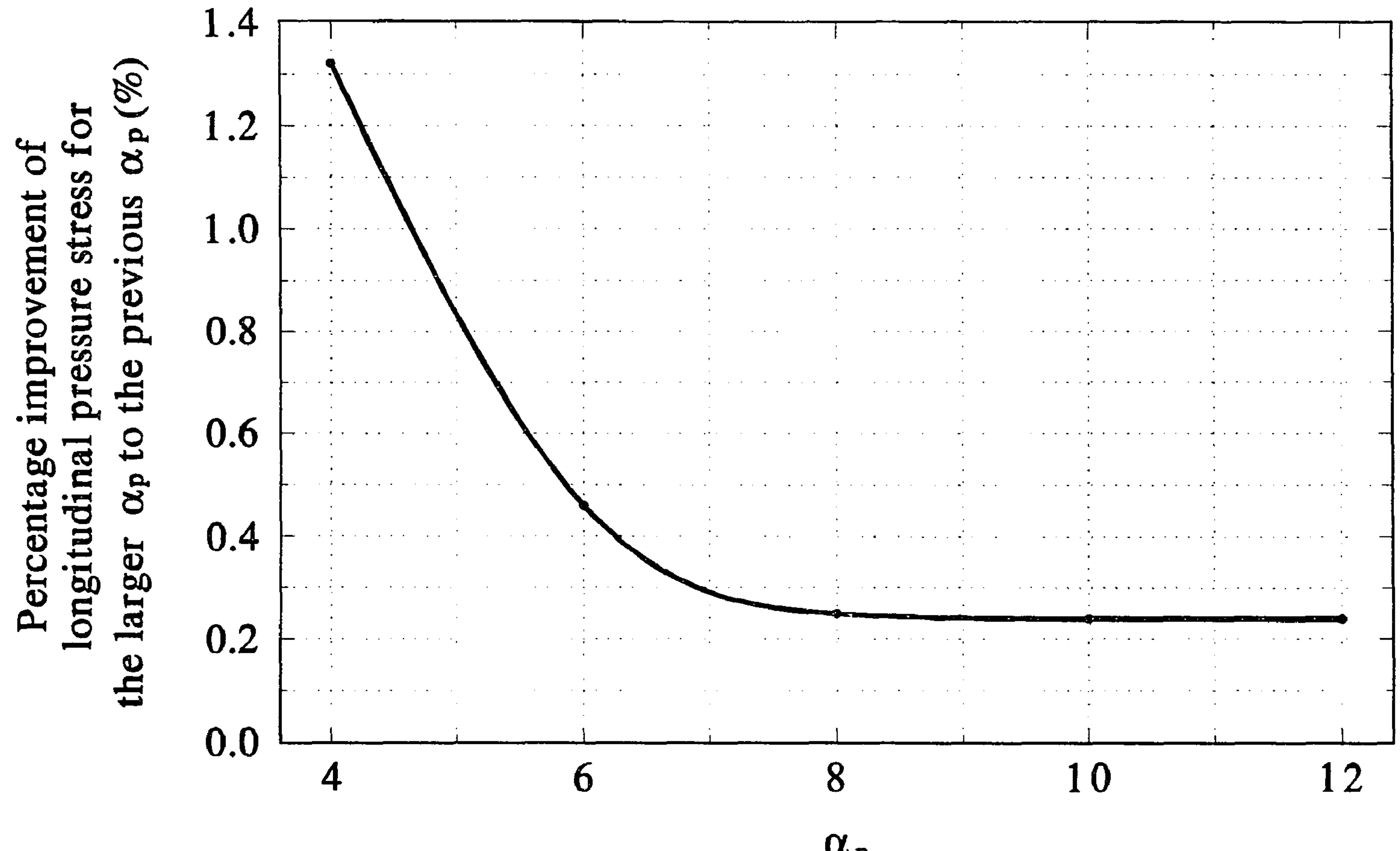

beta=0.5, gamma=75, 25 nodes on a quarter

Figure C-11 Asymptotic study on α_p at C_o of nozzle

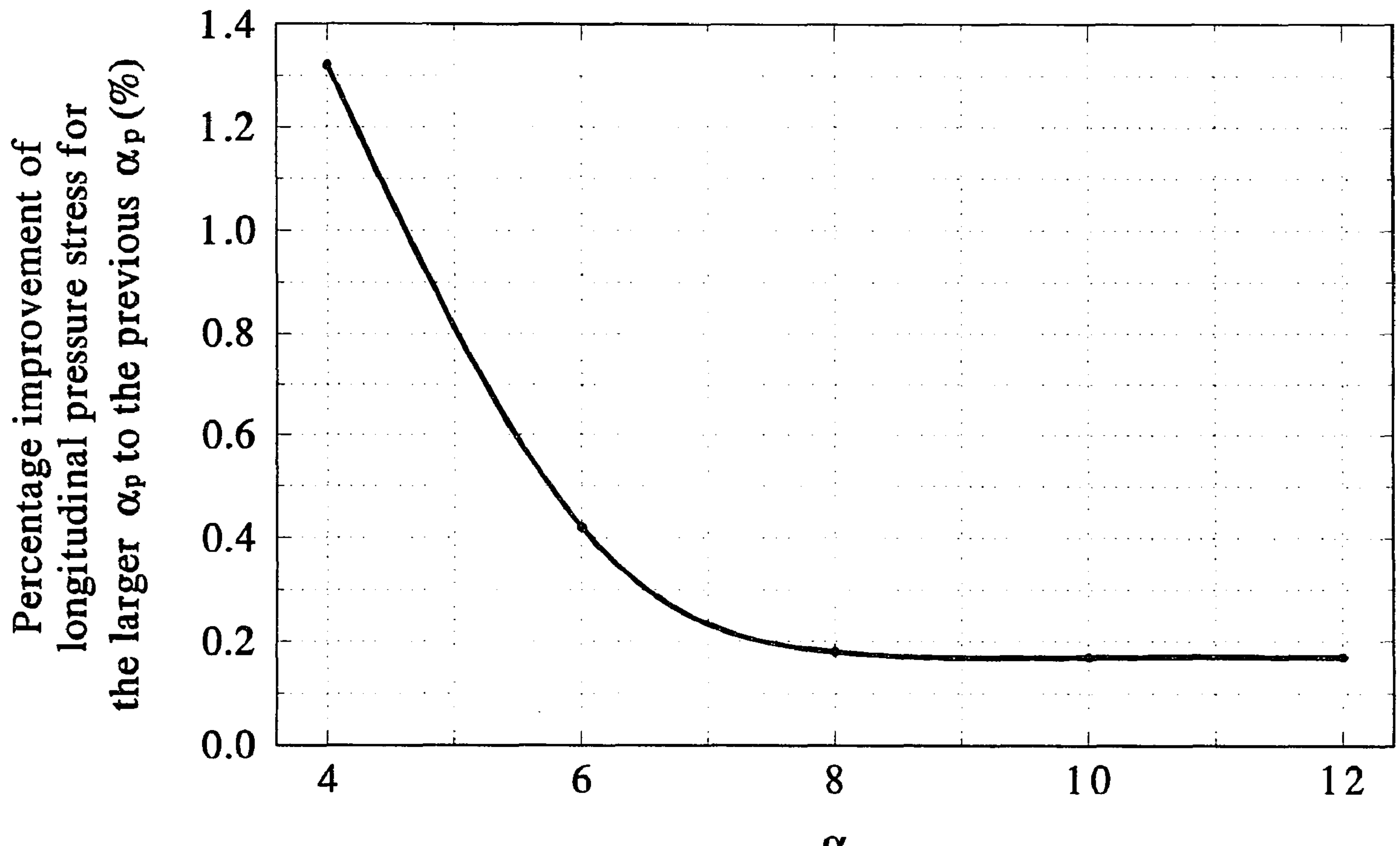

beta=0.5, gamma=75, 25 nodes on a quarter

Figure C-12 Asymptotic study on α_p at C_i of nozzle

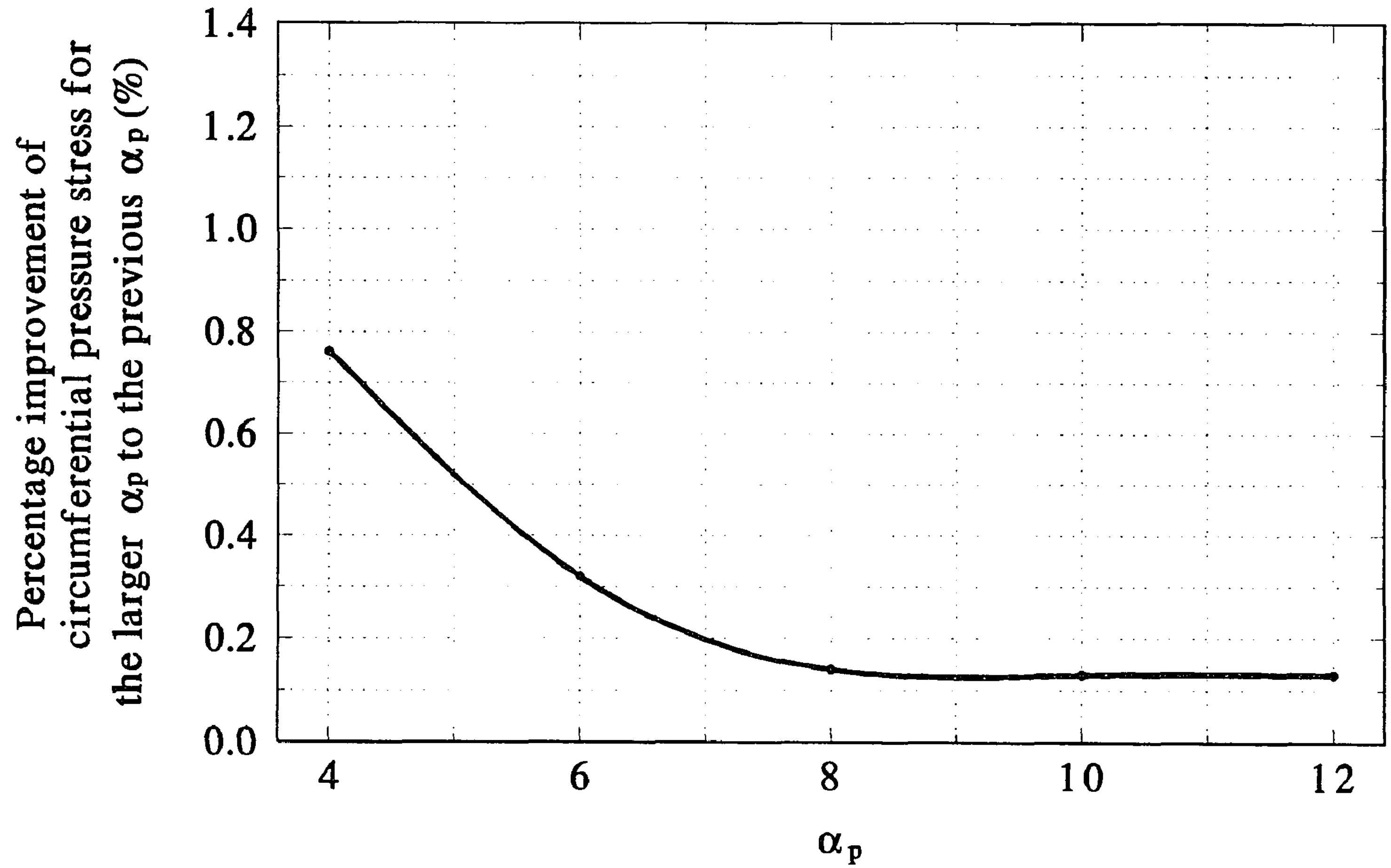

beta=0.5, gamma=75, 25 nodes on a quarter

Figure C-13 Asymptotic study on α_p at A_o of nozzle

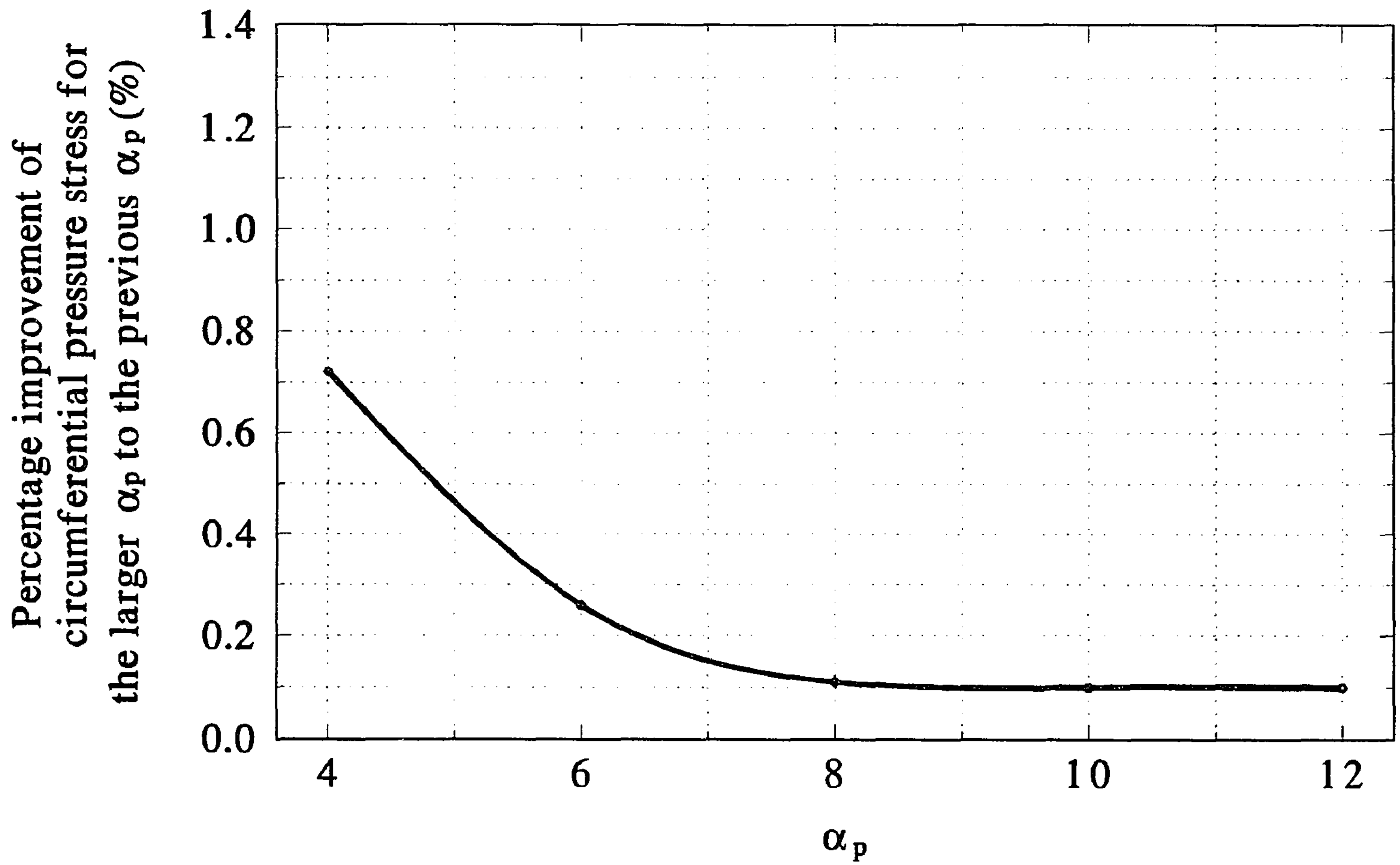

beta=0.5, gamma=75, 25 nodes on a quarter

Figure C-14 Asymptotic study on α_p at A_i of nozzle

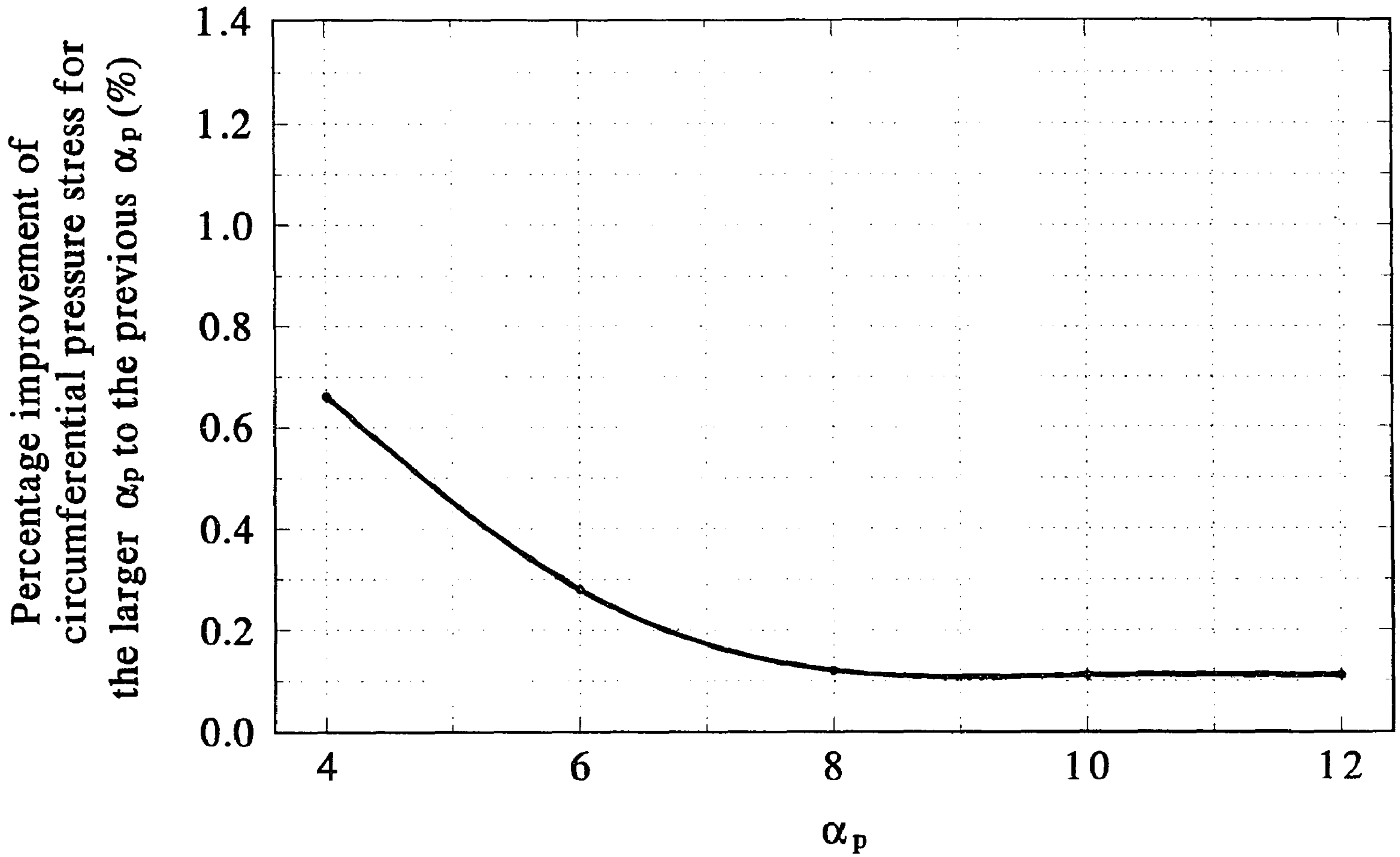

beta=0.5, gamma=75, 25 nodes on a quarter

Figure C-15 Asymptotic study on α_p at C_o of nozzle

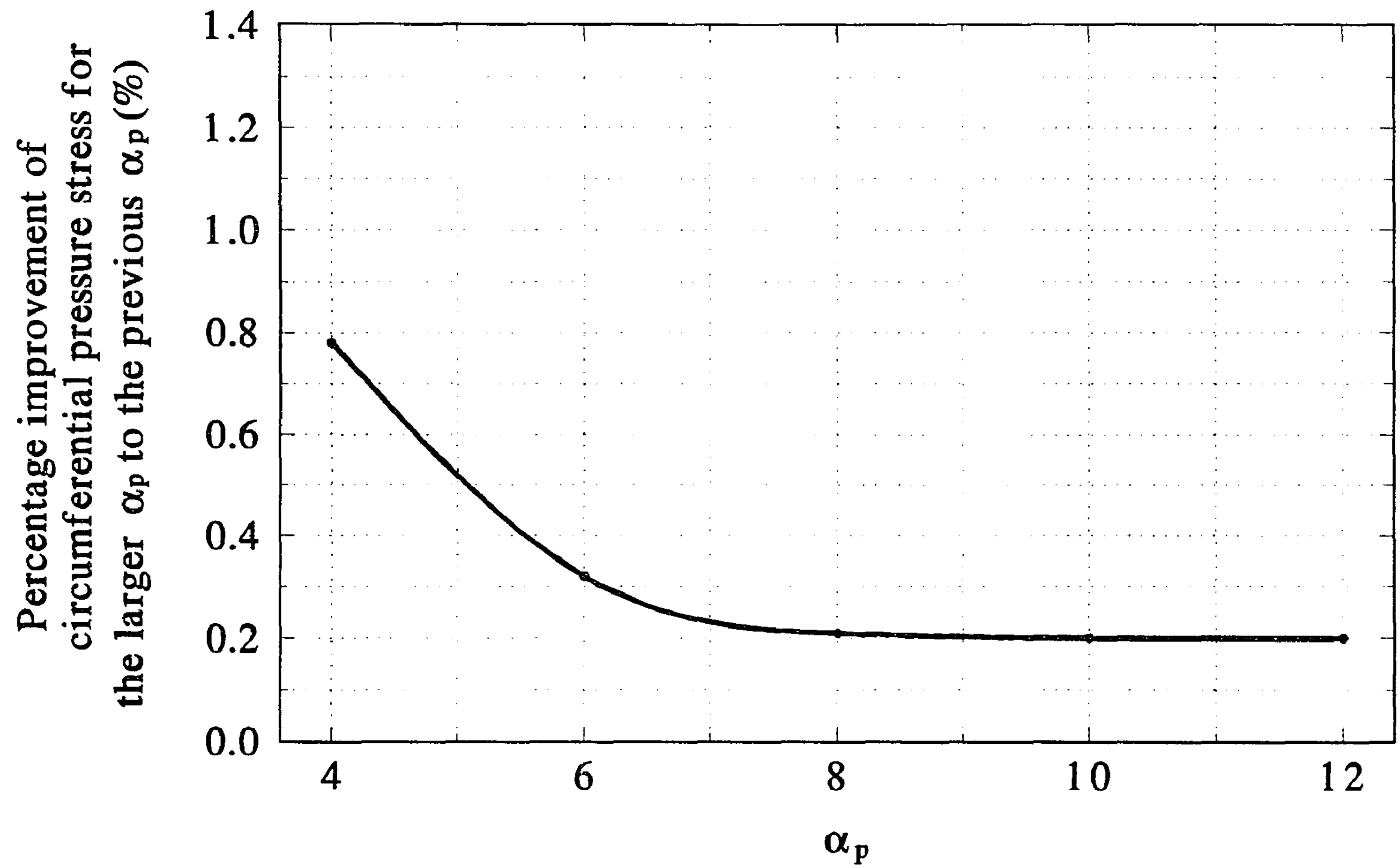

beta=0.5, gamma=75, 25 nodes on a quarter

Figure C-16 Asymptotic study on α_p at C_i of nozzle

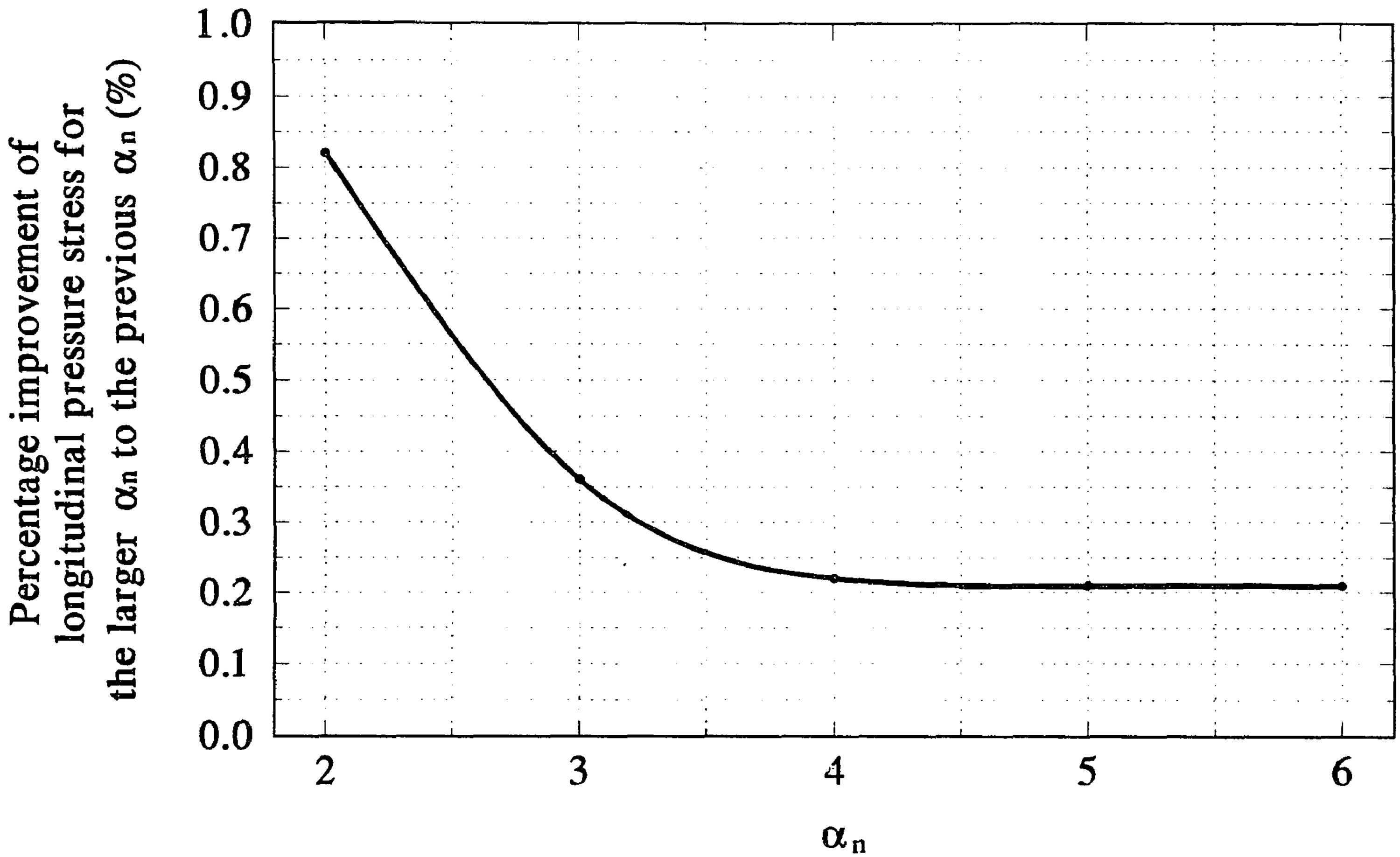

beta=0.5, gamma=75, 25 nodes on a quarter

Figure C-17 Asymptotic study on α_n at A_o of pipe

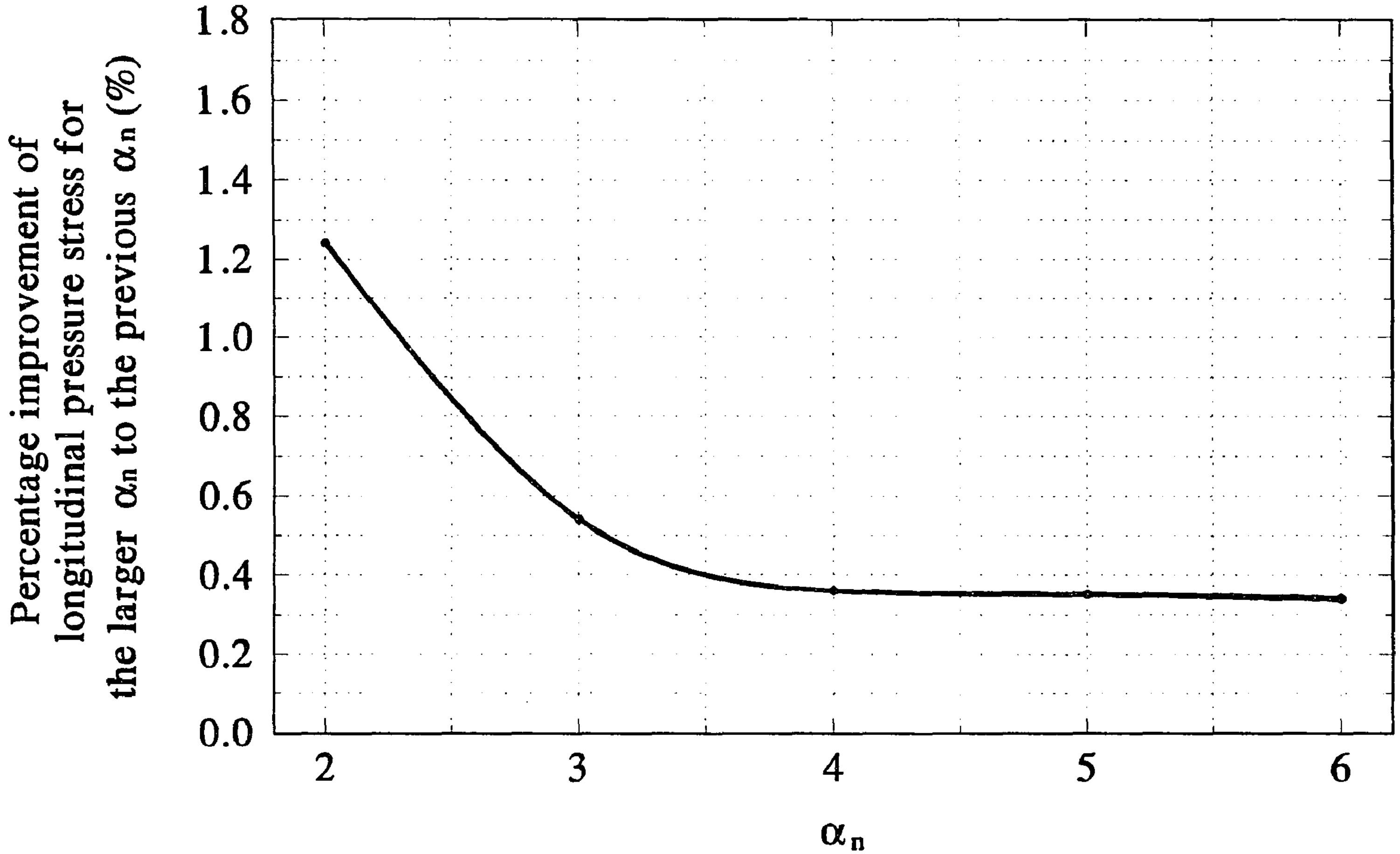

beta=0.5, gamma=75, 25 nodes on a quarter

Figure C-18 Asymptotic study on α_n at A_i of pipe

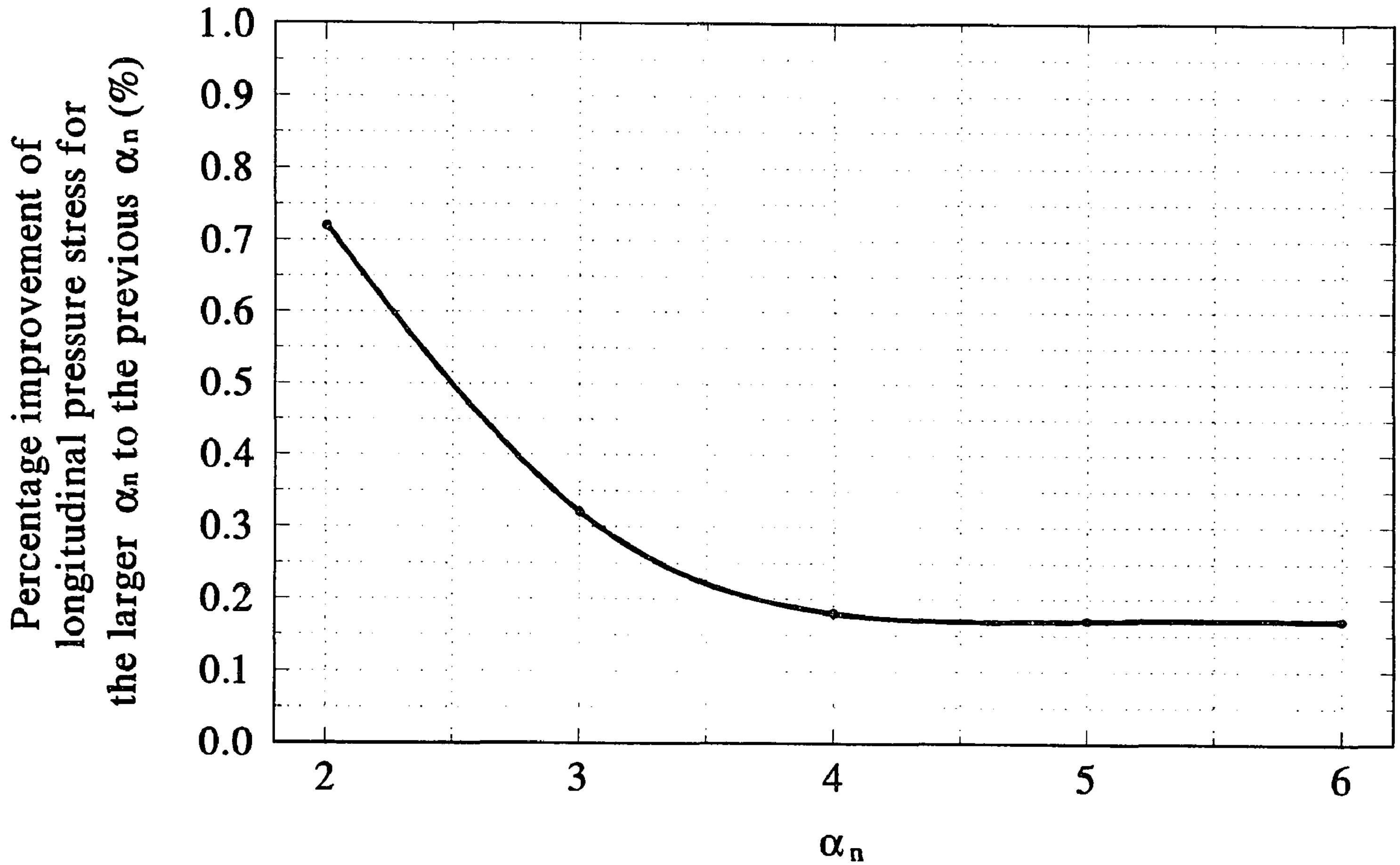

beta=0.5, gamma=75, 25 nodes on a quarter

Figure C-19 Asymptotic study on α_n at C_o of pipe

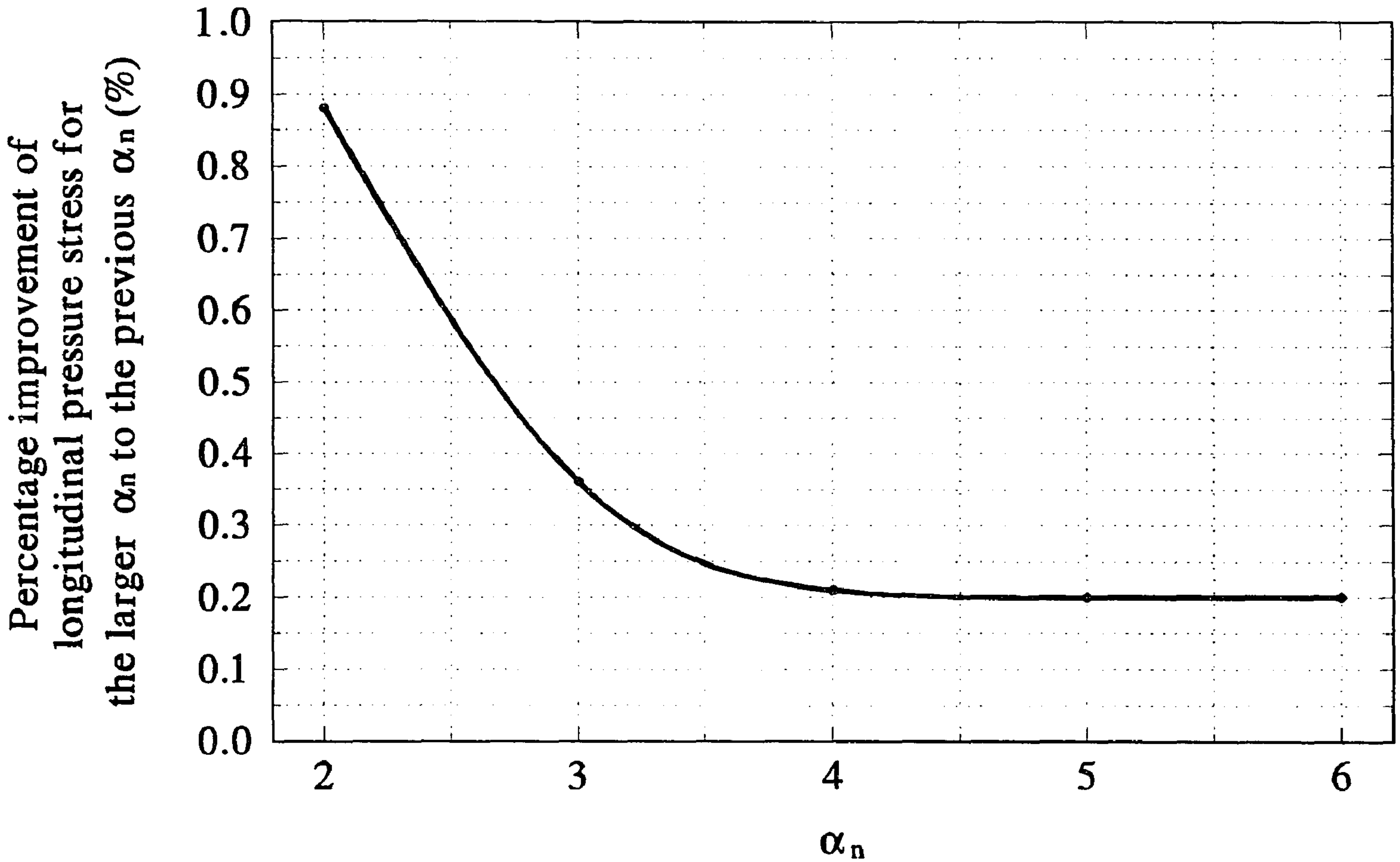

beta=0.5, gamma=75, 25 nodes on a quarter

Figure C-20 Asymptotic study on α_n at C_i of pipe

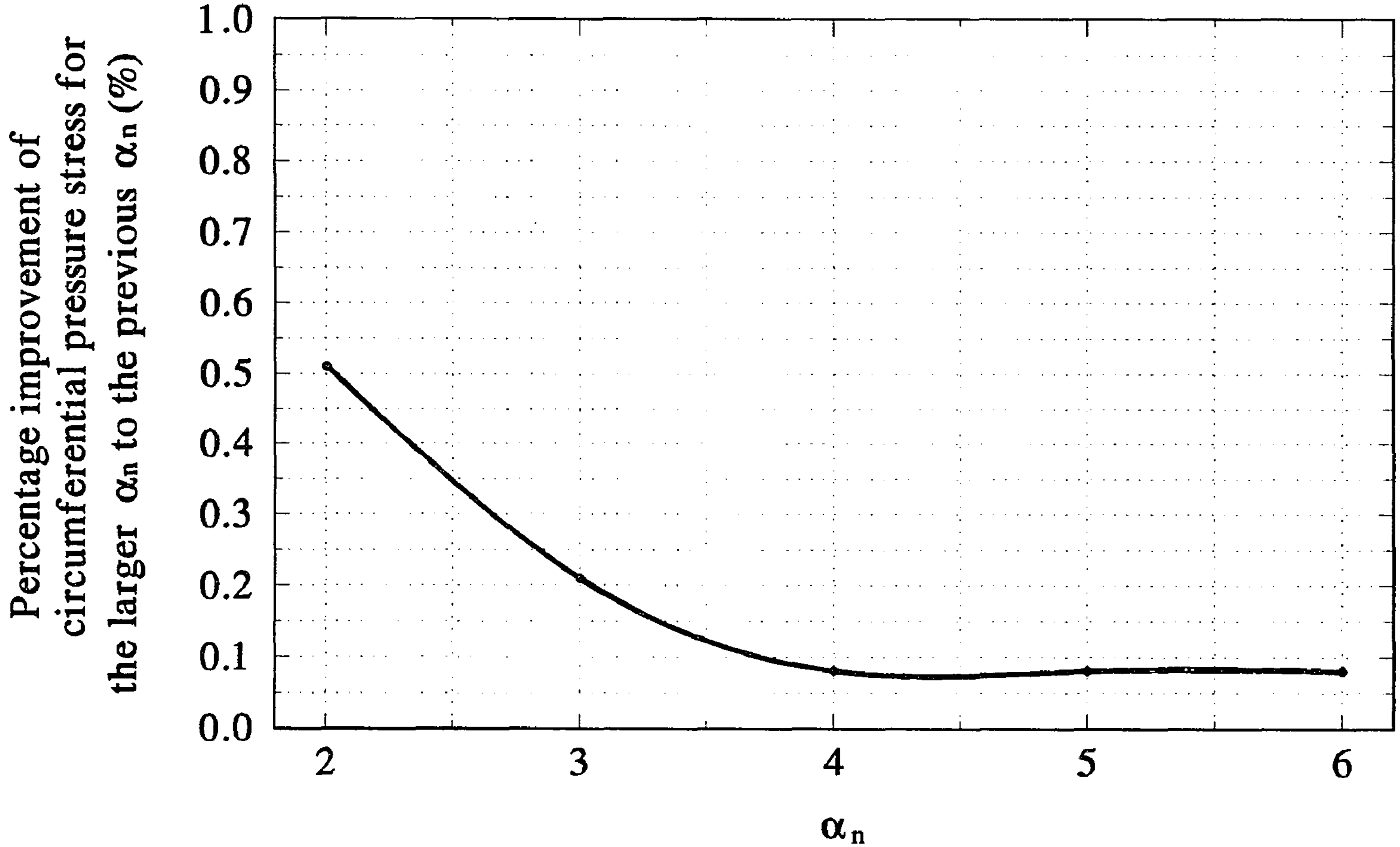

beta=0.5, gamma=75, 25 nodes on a quarter

Figure C-21 Asymptotic study on α_n at A_o of pipe

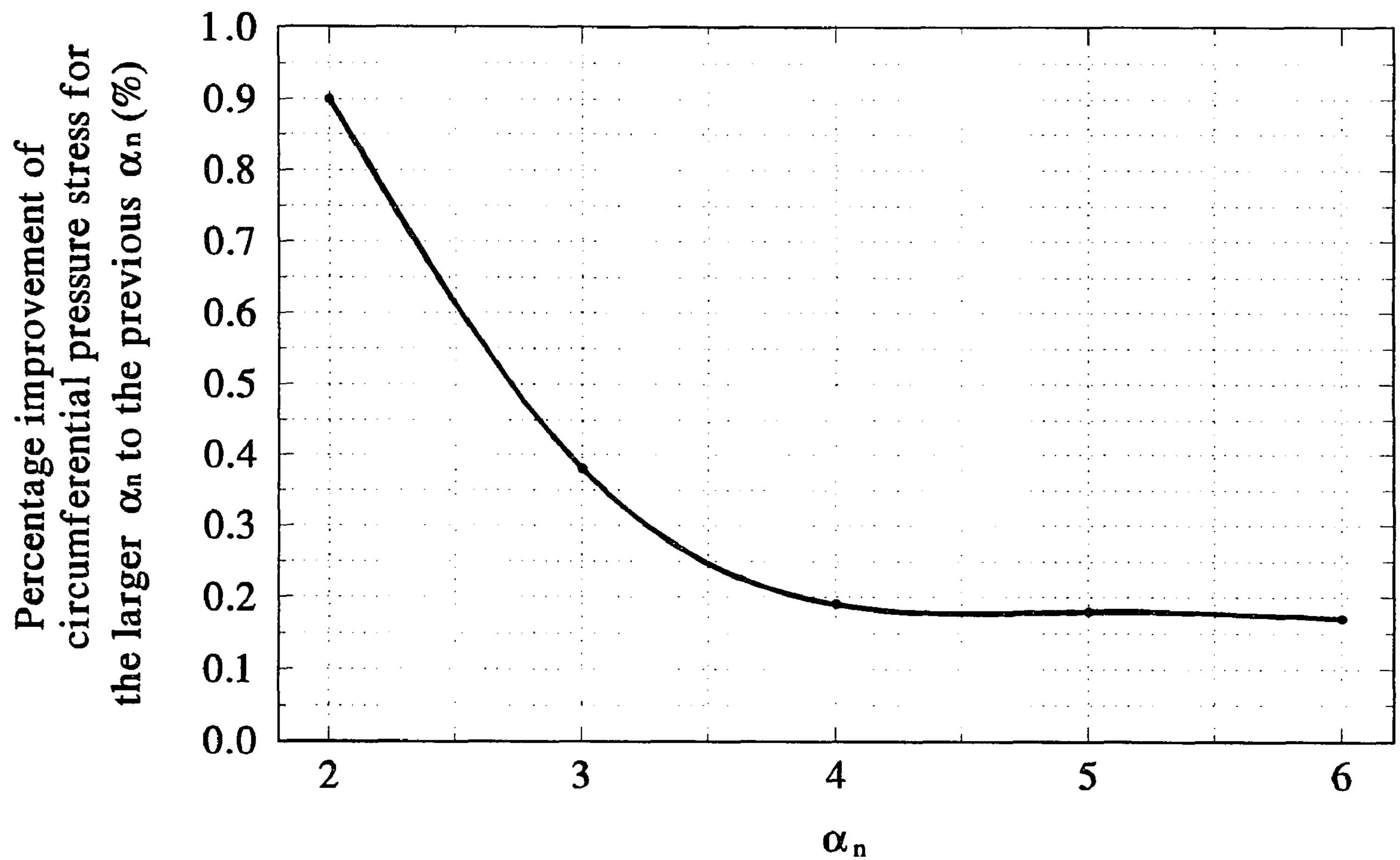

beta=0.5, gamma=75, 25 nodes on a quarter

Figure C-22 Asymptotic study on α_n at A_i of pipe

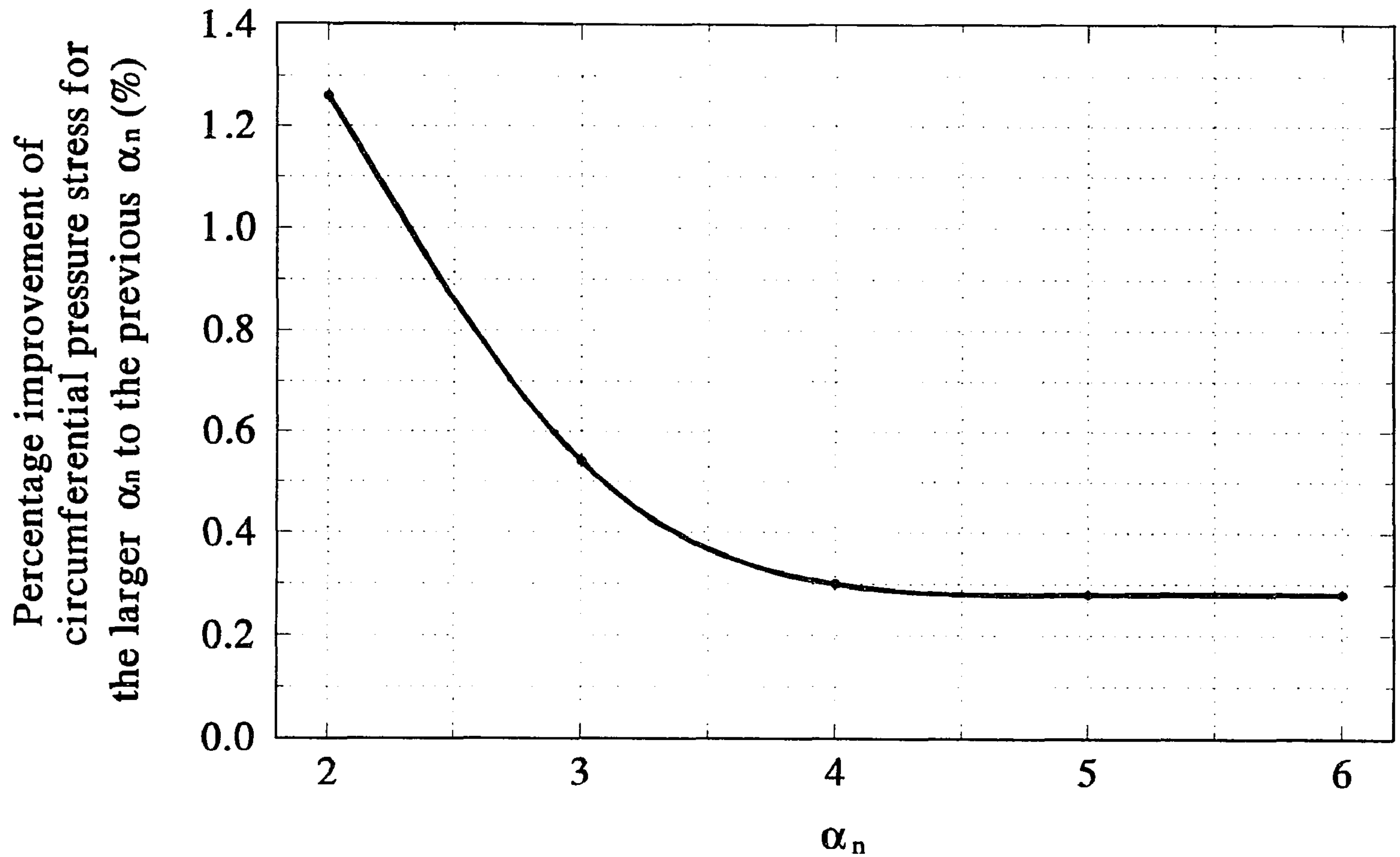

beta=0.5, gamma=75, 25 nodes on a quarter

Figure C-23 Asymptotic study on α_n at C_o of pipe

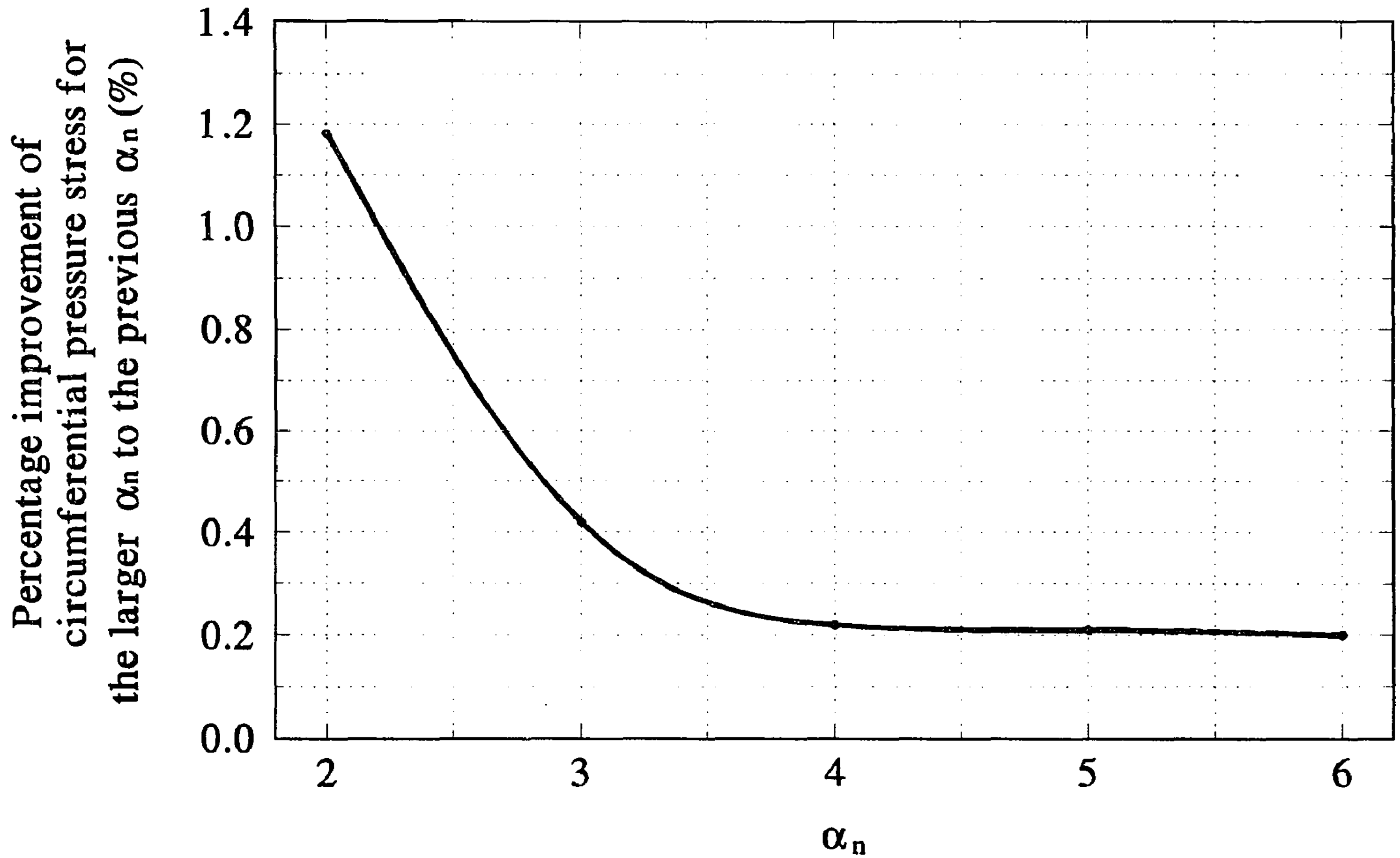

beta=0.5, gamma=75, 25 nodes on a quarter

Figure C-24 Asymptotic study on α_n at C_i of pipe

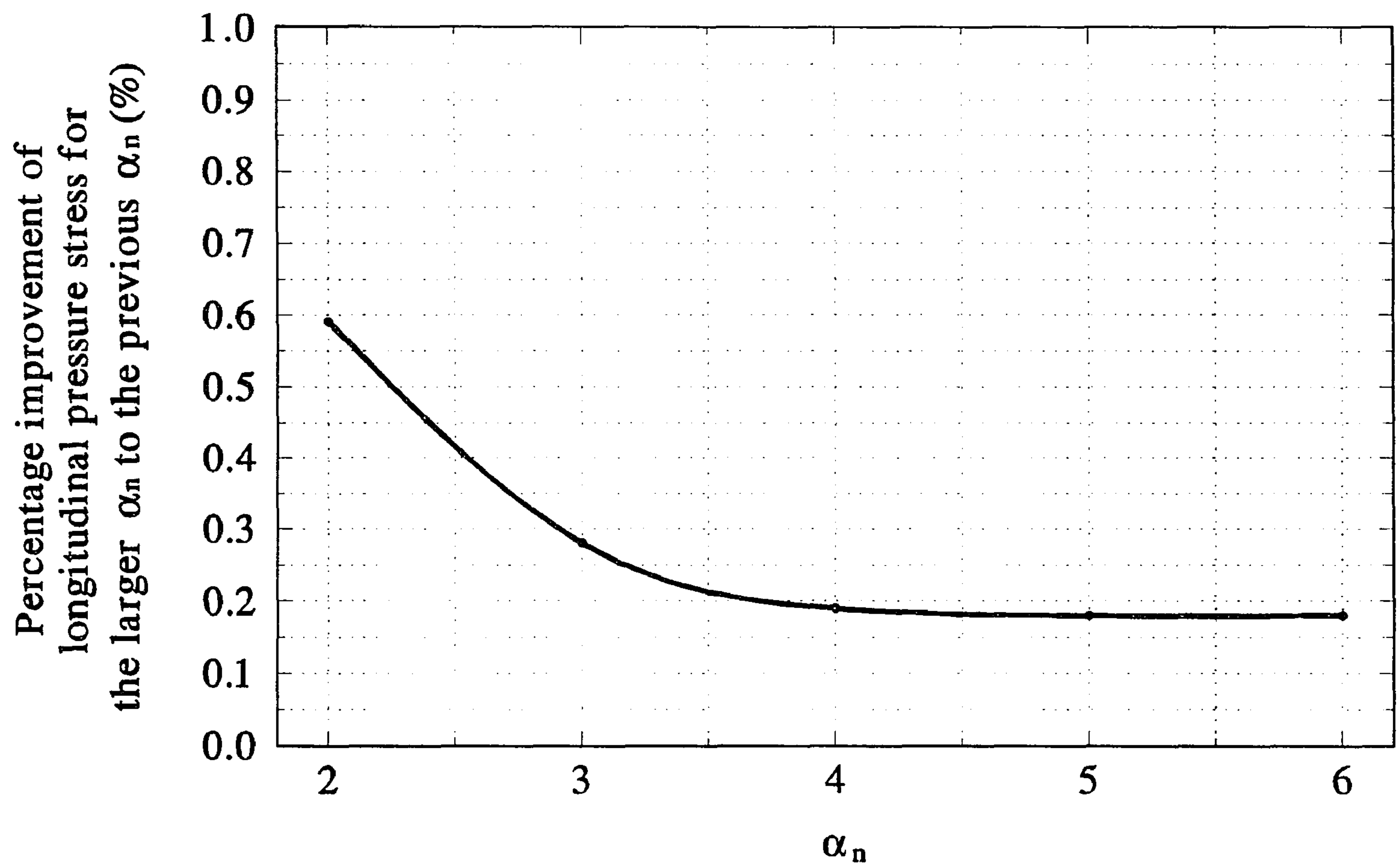

beta=0.5, gamma=75, 25 nodes on a quarter

Figure C-25 Asymptotic study on α_n at A_o of nozzle

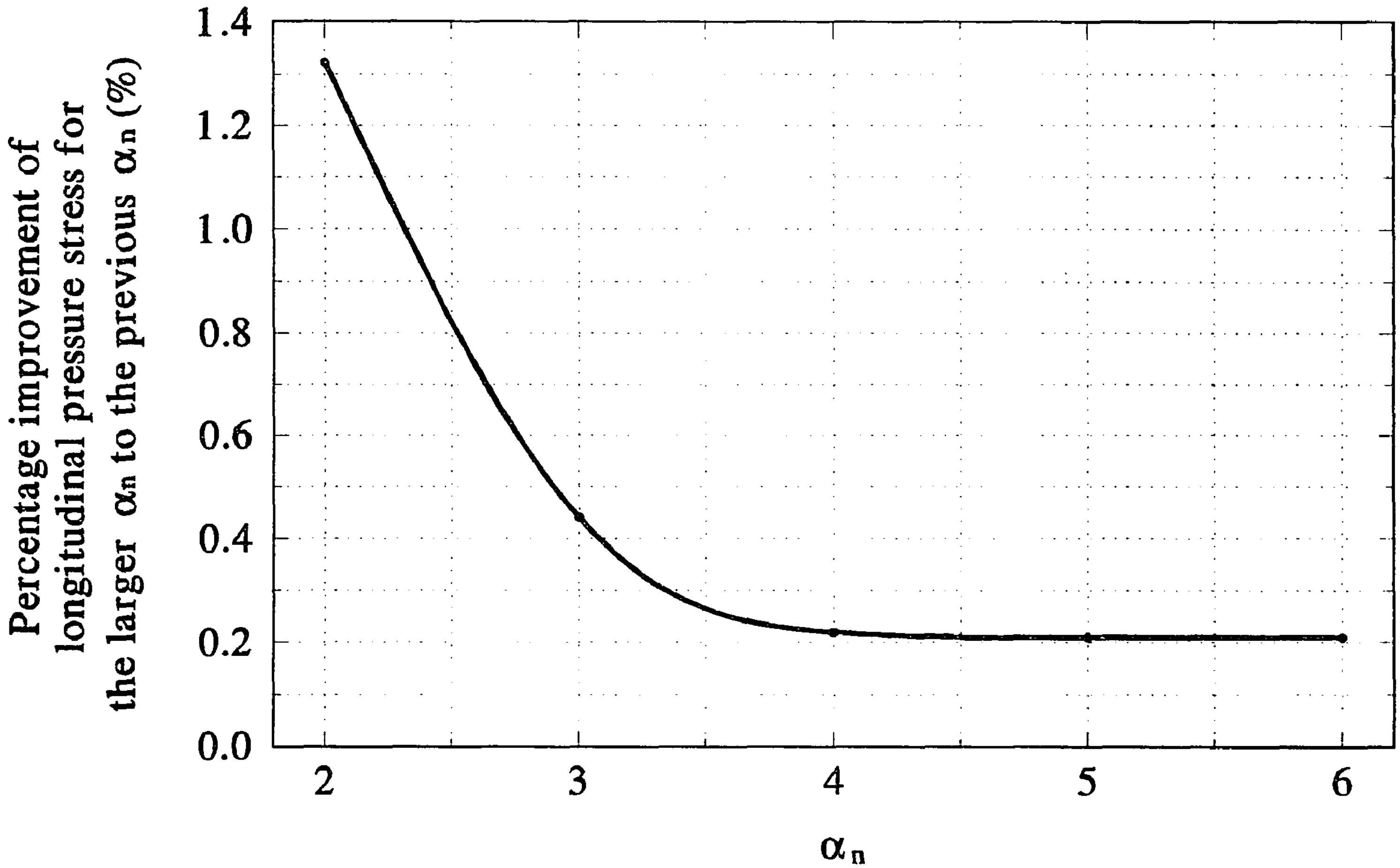

beta=0.5, gamma=75, 25 nodes on a quarter

Figure C-26 Asymptotic study on α_n at A_i of nozzle

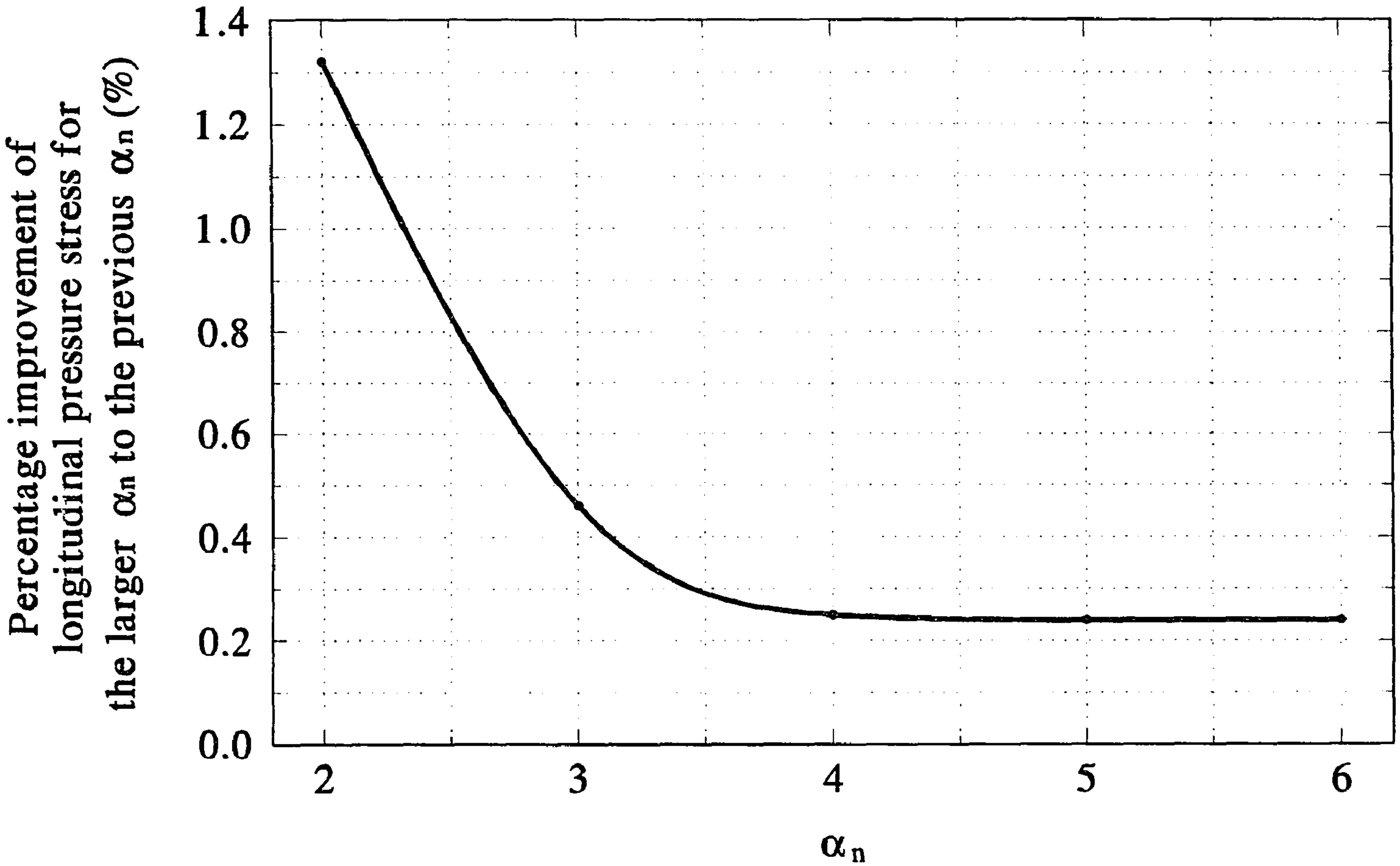

beta=0.5, gamma=75, 25 nodes on a quarter

Figure C-27 Asymptotic study on α_n at C_o of nozzle

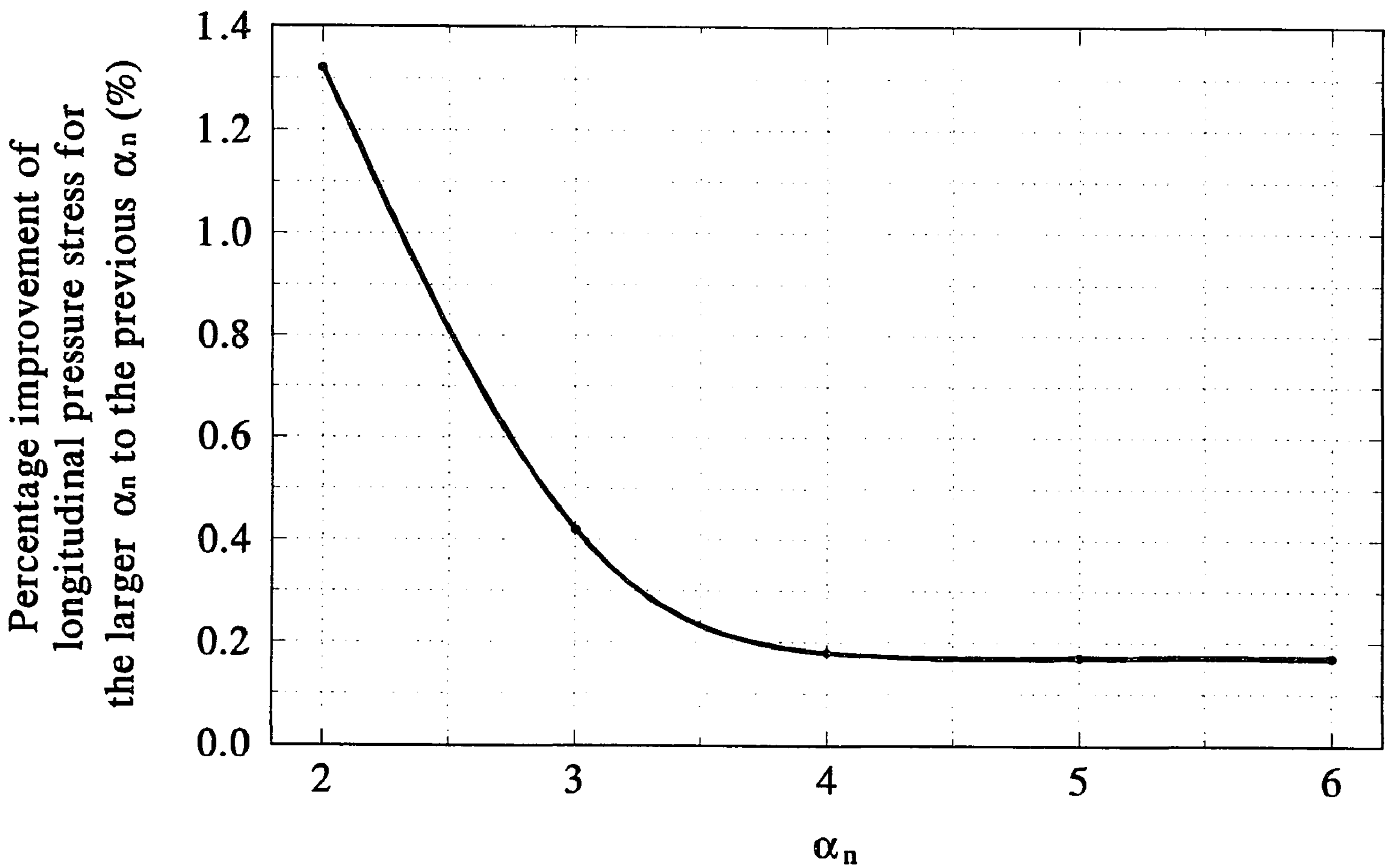

beta=0.5, gamma=75, 25 nodes on a quarter

Figure C-28 Asymptotic study on α_n at C_i of nozzle

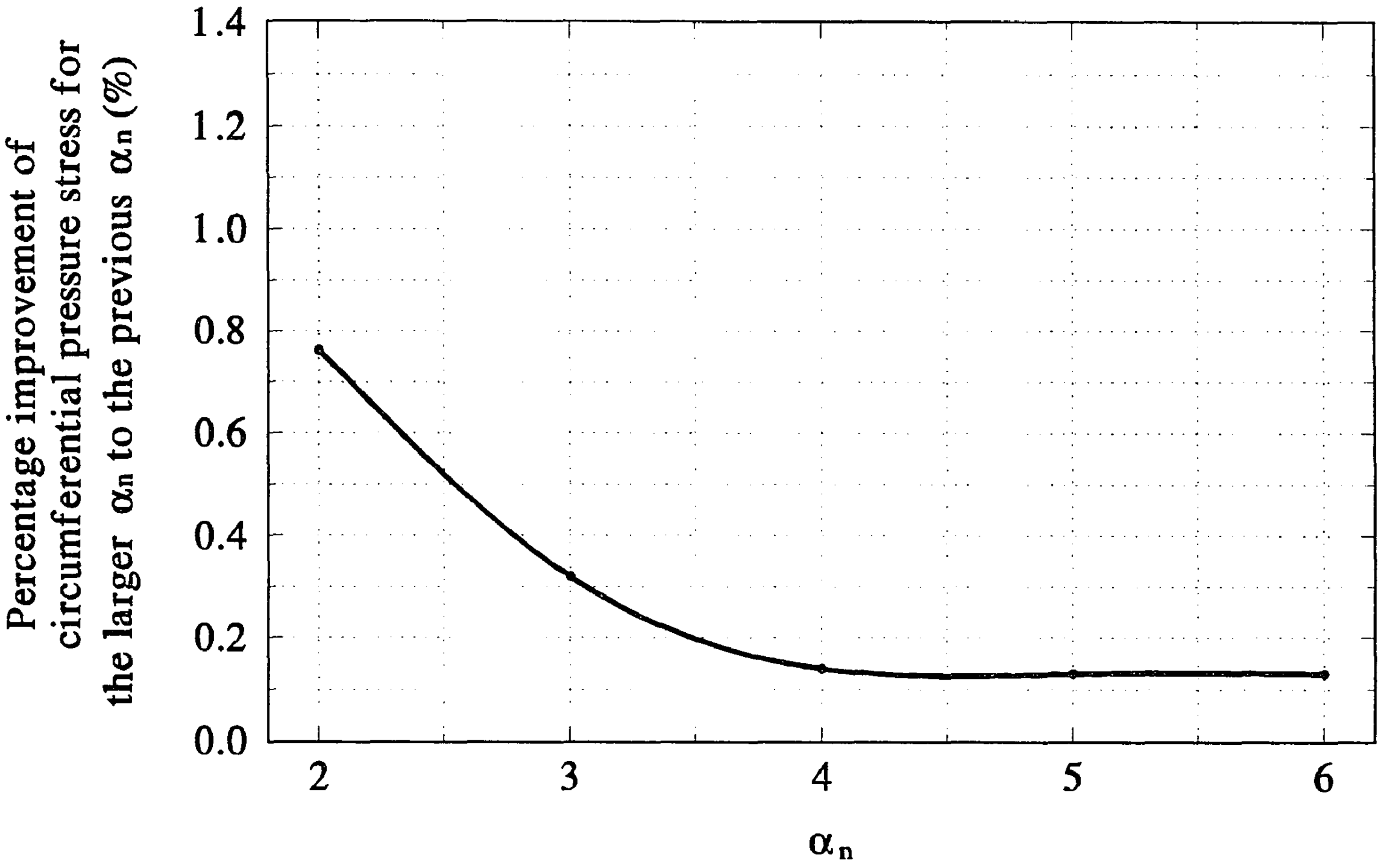

beta=0.5, gamma=75, 25 nodes on a quarter

Figure C-29 Asymptotic study on α_n at A_o of nozzle

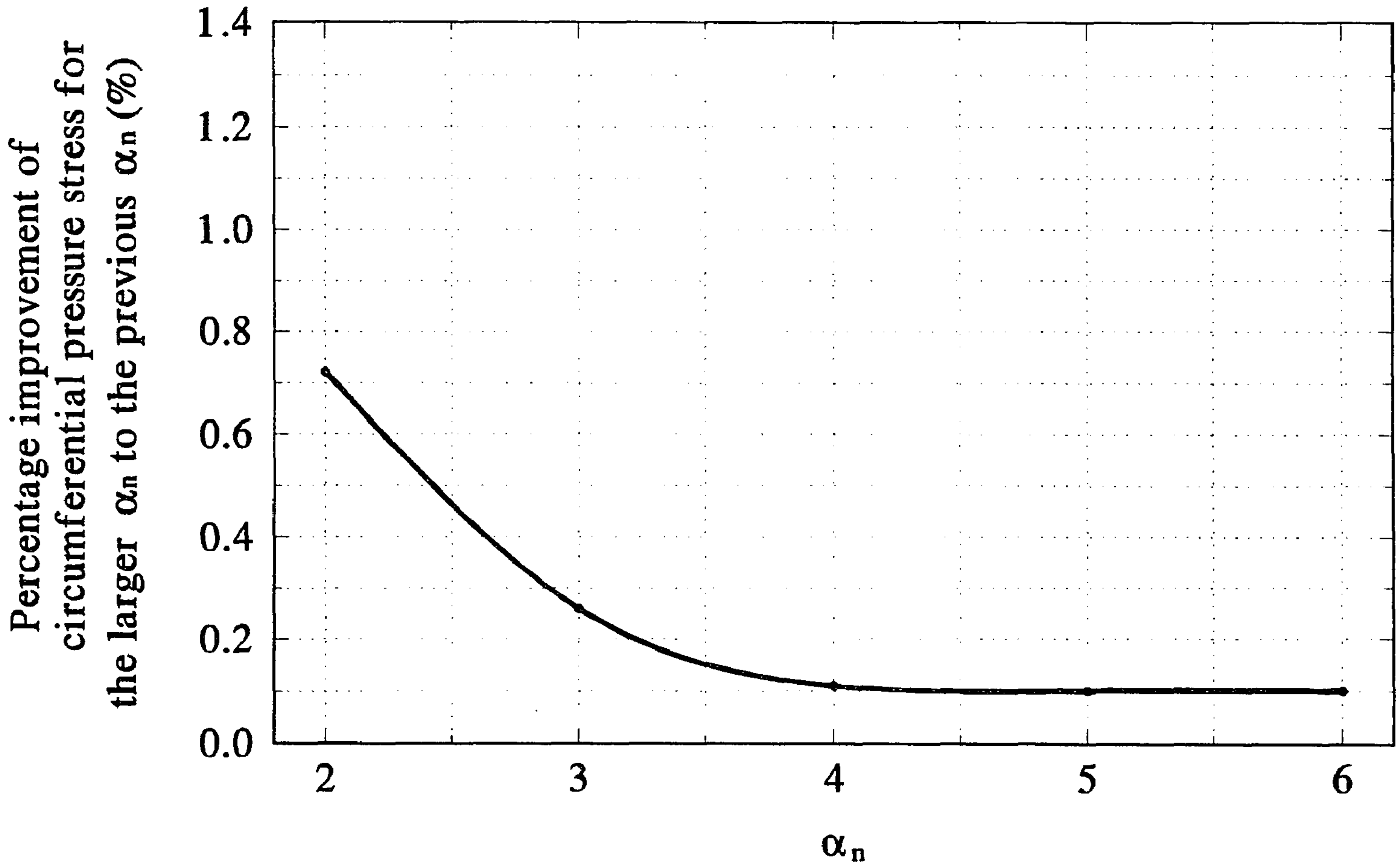

beta=0.5, gamma=75, 25 nodes on a quarter

Figure C-30 Asymptotic study on α_n at A_i of nozzle

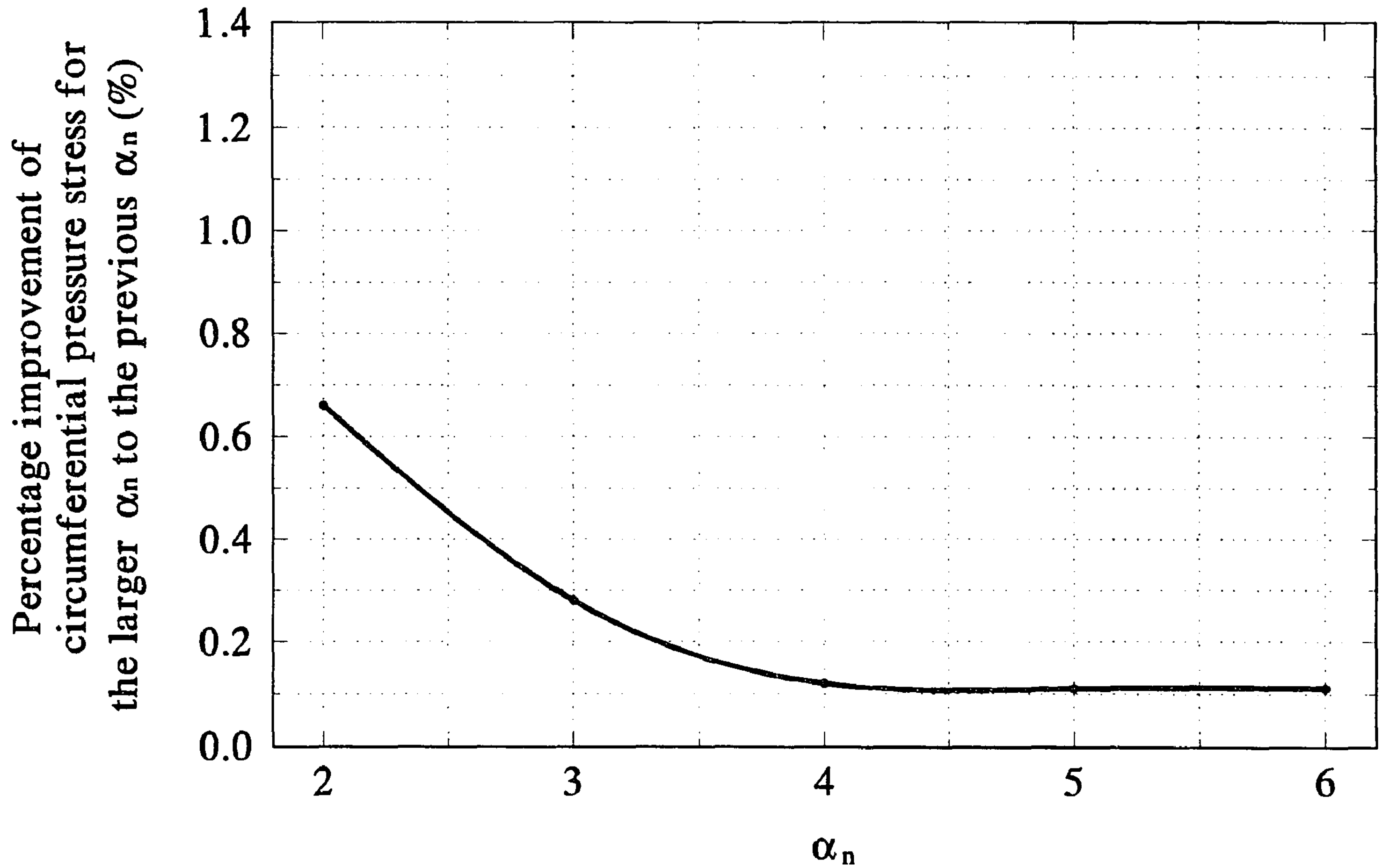

beta=0.5, gamma=75, 25 nodes on a quarter

Figure C-31 Asymptotic study on α_n at C_o of nozzle

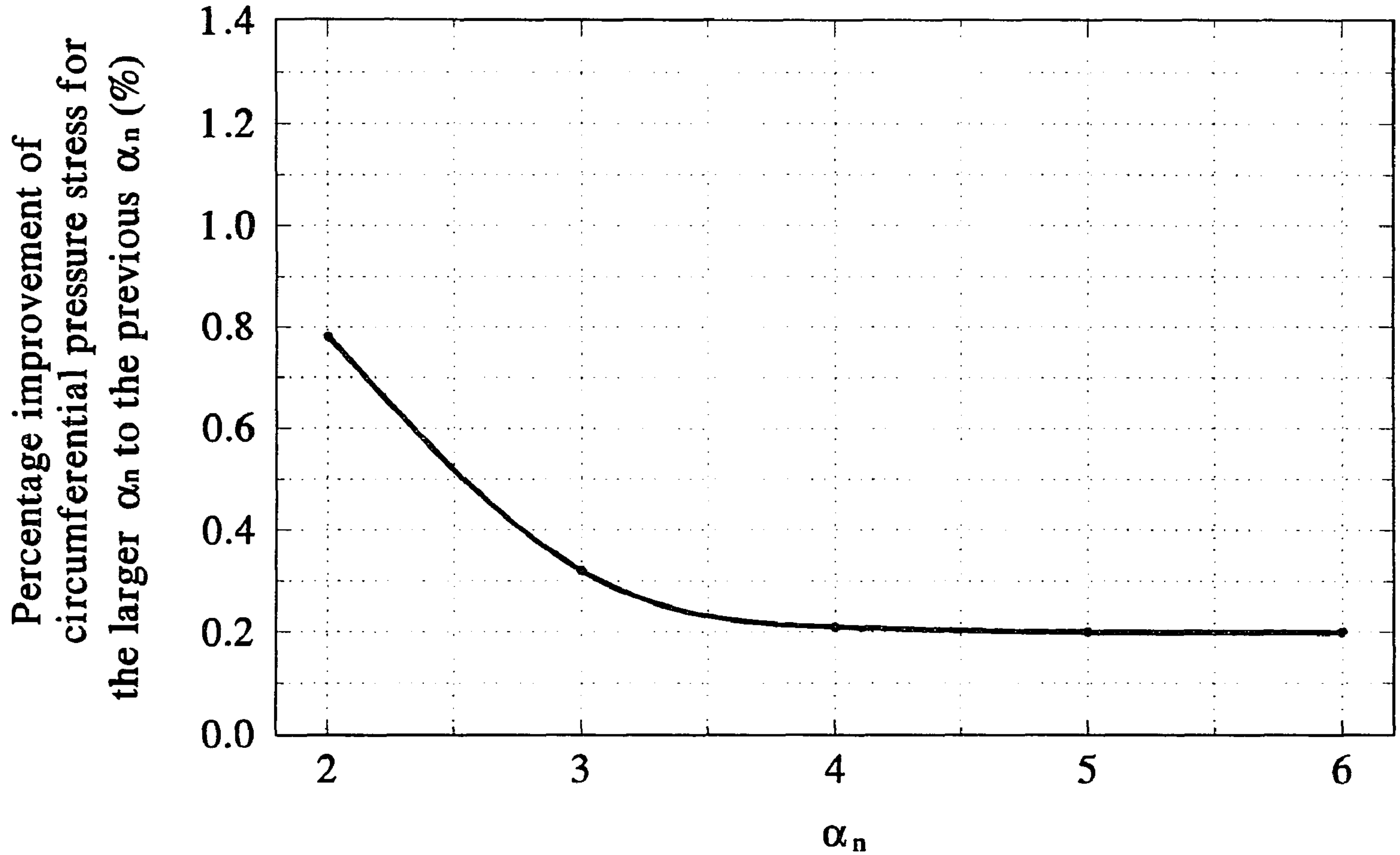

beta=0.5, gamma=75, 25 nodes on a quarter

Figure C-32 Asymptotic study on α_n at C_i of nozzle

APPENDIX D

NOMALIZATION STUDY

Normalization Studies

Model 1

$\alpha = 8$, $\beta = 0.4$, $\gamma = 75$

Case # 1 R=10 in, r= 4 in, L_p=80 in, L_n=16 in,

T= 0.13333 in, t = 0.05333 in.

Case # 2 R=20 in, r= 8 in, L_p=160 in, L_n=32 in,

T= 0.26667 in, t = 0.10667 in.

Table D-1 Material properties of case # 1 and case # 2

Material properties:

E=Young's Modules	3.00E +07 psi
μ=Poisson's ratio	0.3
p=Internal Pressure	100 psi
Pipe Material	316 SS
Nozzle Material	316 SS

Table D-2 Geometric parameters and dimension of case # 1 and case # 2

Case # 1:

α_p=Pipe length / Pipe mean radius	8
α_n=Nozzle length / Nozzle mean radius	4
β=Nozzle radius / Pipe mean radius	0.4
γ=Pipe radius / Pipe thickness	75
Lp=Pipe length	80 in
R=Pipe mean radius	10 in
Ln=Nozzle length	16 in
r=Nozzle mean radius	4 in
T=Pipe thickness	0.13333 in
t=Nozzle thickness	0.05333 in

Case # 2:

α_p=Pipe length / Pipe mean radius	8
α_n=Nozzle length / Nozzle mean radius	4
β=Nozzle radius / Pipe mean radius	0.4
γ=Pipe radius / Pipe thickness	75
Lp=Pipe length	160 in
R=Pipe mean radius	20 in
Ln=Nozzle length	32 in
r=Nozzle mean radius	8 in
T=Pipe thickness	0.26667 in
t=Nozzle thickness	0.10667 in

Table D-3 Stress and stress factor comparison table at node A of case # 1 and case # 2

Stress Factor = Stress / Internal Pressure = σ / p

(1) Outside surface of pipe at node A

Model No.	case # 1	case # 2
Longitudinal Stress, psi	52,590	52,590
Stress Factor	525.90	525.90
Circumferential Stress, psi	87,640	87,640
Stress Factor	876.40	876.40

(2) Inside surface of pipe at node A

Model No.	case # 1	case # 2
Longitudinal Stress, psi	-39,020	-39,020
Stress Factor	-390.20	-390.20
Circumferential Stress, psi	61,270	61,270
Stress Factor	612.70	612.70

(3) Outside surface of nozzle at node A

Model No.	case # 1	case # 2
Longitudinal Stress, psi	62,390	62,390
Stress Factor	623.90	623.90
Circumferential Stress, psi	91,210	91,210
Stress Factor	912.10	912.10

(4) Inside surface of nozzle at node A

Model No.	case # 1	case # 2
Longitudinal Stress, psi	-46,030	-46,030
Stress Factor	-460.30	-460.30
Circumferential Stress, psi	59,970	59,970
Stress Factor	599.70	599.70

Table D-4 Stress and stress factor comparison table at node C of case # 1 and case # 2

Stress Factor = Stress / Internal Pressure = σ / p

(5) Outside surface of pipe at node C

Model No.	case # 1	case # 2
Longitudinal Stress, psi	-11,860	-11,860
Stress Factor	-118.60	-118.60
Circumferential Stress, psi	-13,400	-13,400
Stress Factor	-134.00	-134.00

(6) Inside surface of pipe at node C

Model No.	case # 1	case # 2
Longitudinal Stress, psi	7,954	7,954
Stress Factor	79.54	79.54
Circumferential Stress, psi	-8,274	-8,274
Stress Factor	-82.74	-82.74

(7) Outside surface of nozzle at node C

Model No.	case # 1	case # 2
Longitudinal Stress, psi	-25,440	-25,440
Stress Factor	-254.40	-254.40
Circumferential Stress, psi	-17,050	-17,050
Stress Factor	-170.50	-170.50

(8) Inside surface of nozzle at node C

Model No.	case # 1	case # 2
Longitudinal Stress, psi	20,210	20,210
Stress Factor	202.10	202.10
Circumferential Stress, psi	-5,334	-5,334
Stress Factor	-53.34	-53.34

Normalization Studies

Model 2

$\alpha = 8, \ \beta = 0.5, \ \gamma = 50$

Case # 3 R=20 in, r= 10 in, L_p=160 in, L_n=40 in,

T= 0.4 in, t = 0.2 in.

Case # 4 R=30 in, r= 15 in, L_p=240 in, L_n=60 in,

T= 0.6 in, t = 0.3 in.

Table D-5 Material properties of case # 3 and case # 4

Material properties:

E=Young's Modules	3.00E +07 psi
μ=Poisson's ratio	0.3
p=Internal Pressure	100 psi
Pipe Material	316 SS
Nozzle Material	316 SS

Table D-6 Geometric parameters and dimension of case # 3 and case # 4

Case # 3:

α_p=Pipe length / Pipe mean radius	8
α_n=Nozzle length / Nozzle mean radius	4
β=Nozzle radius / Pipe mean radius	0.5
γ=Pipe radius / Pipe thickness	50
L_p=Pipe length	160 in
R=Pipe mean radius	20 in
L_n=Nozzle length	40 in
r=Nozzle mean radius	10 in
T=Pipe thickness	0..4 in
t=Nozzle thickness	0..2 in

Case # 4:

α_p=Pipe length / Pipe mean radius	8
α_n=Nozzle length / Nozzle mean radius	4
β=Nozzle radius / Pipe mean radius	0.5
γ=Pipe radius / Pipe thickness	50
L_p=Pipe length	240 in
R=Pipe mean radius	30 in
L_n=Nozzle length	60 in
r=Nozzle mean radius	15 in
T=Pipe thickness	0.6 in
t=Nozzle thickness	0.3 in

Table D-7 Stress and stress factor comparison table at node A of case # 3 and case # 4

Stress Factor = Stress / Internal Pressure = σ / p

(1) Outside surface of pipe at node A

Model No.	case # 3	case # 4
Longitudinal Stress, psi	37,900	37,900
Stress Factor	379.00	379.00
Circumferential Stress, psi	47,910	47,910
Stress Factor	479.10	479.10

(2) Inside surface of pipe at node A

Model No.	case # 3	case # 4
Longitudinal Stress, psi	-29,640	-29,640
Stress Factor	-296.40	-296.40
Circumferential Stress, psi	26,930	26,930
Stress Factor	269.30	269.30

(3) Outside surface of nozzle at node A

Model No.	case # 3	case # 4
Longitudinal Stress, psi	43,250	43,250
Stress Factor	432.50	432.50
Circumferential Stress, psi	49,060	49,060
Stress Factor	490.60	490.60

(4) Inside surface of nozzle at node A

Model No.	case # 3	case # 4
Longitudinal Stress, psi	-35,530	-35,530
Stress Factor	-355.30	-355.30
Circumferential Stress, psi	25,340	25,340
Stress Factor	253.40	253.40

Table D-8 Stress and stress factor comparison table at node C of case # 3 and case # 4

Stress Factor = Stress / Internal Pressure = σ / p

(5) Outside surface of pipe at node C

Model No.	case # 3	case # 4
Longitudinal Stress, psi	-4,676	-4,676
Stress Factor	-46.76	-46.76
Circumferential Stress, psi	-7,286	-7,286
Stress Factor	-72.86	-72.86

(6) Inside surface of pipe at node C

Model No.	case # 3	case # 4
Longitudinal Stress, psi	2,467	2,467
Stress Factor	24.67	24.67
Circumferential Stress, psi	-6,846	-6,846
Stress Factor	-68.46	-68.46

(7) Outside surface of nozzle at node C

Model No.	case # 3	case # 4
Longitudinal Stress, psi	-9,178	-9,178
Stress Factor	-91.78	-91.78
Circumferential Stress, psi	-7,982	-7,982
Stress Factor	-79.82	-79.82

(8) Inside surface of nozzle at node C

Model No.	case # 3	case # 4
Longitudinal Stress, psi	5,295	5,295
Stress Factor	52.95	52.95
Circumferential Stress, psi	-6,724	-6,724
Stress Factor	-67.24	-67.24

Normalization Studies

Model 3

$\alpha = 8, \ \beta = 0.5, \ \gamma = 50$

R=20 in, r= 10 in, L_p=160 in, L_n=40 in,T= 0.4 in, t = 0.2 in

Case # 5 Internal Pressure = 100 psi

Case # 6 Internal pressure = 125 psi

Table D-9 Material properties of case # 5 and case # 6

Material properties:

E=Young's Modules	3.00E +07 psi
μ=Poisson's ratio	0.3
p=Internal Pressure	100 psi
Pipe Material	316 SS
Nozzle Material	316 SS

Table D-10 Geometric parameters and dimension of case # 5 and case # 6

α_p=Pipe length / Pipe mean radius	8
α_n=Nozzle length / Nozzle mean radius	4
β=Nozzle radius / Pipe mean radius	0.5
γ=Pipe radius / Pipe thickness	50
Lp=Pipe length	160 in
R=Pipe mean radius	20 in
Ln=Nozzle length	40 in
r=Nozzle mean radius	10 in
T=Pipe thickness	0..4 in
t=Nozzle thickness	0..2 in

Case #5 Internal pressure = 100 psi

Case #6 Internal pressure = 125 psi

Table D-11 Stress and stress factor comparison table at node A of case # 5 and case # 6

Stress Factor = Stress / Internal Pressure = σ / p

(1) Outside surface of pipe at node A

Model No.	case # 5	case # 6
Longitudinal Stress, psi	37,900	47,375
Stress Factor	379.00	379.00
Circumferential Stress, psi	47,910	59,888
Stress Factor	479.10	479.10

(2) Inside surface of pipe at node A

Model No.	case # 5	case # 6
Longitudinal Stress, psi	-29,640	-37,050
Stress Factor	-296.40	-296.40
Circumferential Stress, psi	26,930	33,663
Stress Factor	269.30	269.30

(3) Outside surface of nozzle at node A

Model No.	case # 5	case # 6
Longitudinal Stress, psi	43,250	54,063
Stress Factor	432.50	432.50
Circumferential Stress, psi	49,060	61,325
Stress Factor	490.60	490.60

(4) Inside surface of nozzle at node A

Model No.	case # 5	case # 6
Longitudinal Stress, psi	-35,530	-44,413
Stress Factor	-355.30	-355.30
Circumferential Stress, psi	25,340	31,675
Stress Factor	253.40	253.40

Table D-12 Stress and stress factor comparison table at node C of case # 5 and case # 6

Stress Factor = Stress / Internal Pressure = σ / p

(5) Outside surface of pipe at node C

Model No.	case # 5	case # 6
Longitudinal Stress, psi	-4,676	-5,845
Stress Factor	-46.76	-46.76
Circumferential Stress, psi	-7,286	-9,108
Stress Factor	-72.86	-72.86

(6) Inside surface of pipe at node C

Model No.	case # 5	case # 6
Longitudinal Stress, psi	2,467	3,084
Stress Factor	24.67	24.67
Circumferential Stress, psi	-6,846	-8,558
Stress Factor	-68.46	-68.46

(7) Outside surface of nozzle at node C

Model No.	case # 5	case # 6
Longitudinal Stress, psi	-9,178	-11,473
Stress Factor	-91.78	-91.78
Circumferential Stress, psi	-7,982	-9,978
Stress Factor	-79.82	-79.82

(8) Inside surface of nozzle at node C

Model No.	case # 5	case # 6
Longitudinal Stress, psi	5,295	6,619
Stress Factor	52.95	52.95
Circumferential Stress, psi	-6,724	-8,405
Stress Factor	-67.24	-67.24

REFERENCE

1. Biron, A. Review of Lower-Bound Limit Analysis for Pressure Vessel Intersections. *ASME Journal of Pressure Vessel Technology* 1977. 413-419

2. Biron, A. and Courchesne, A. On Limit Analysis of Cylinder-Cylinder Intersections Subjected to Internal Pressure. *Nuclear Engineering and Design* 1976. **36,** 68-80

3. Brown, S. J. Jr. A Finite Plate Method to Solve Cylinder-to-Cylinder Structures Subjected to Internal Pressure. *ASME Journal of Pressure Vessel Technology* 1977. 404-412

4. Cloud, R. L. and Rodabaugh, E. C. Approximate Analysis of the Plastic Limit Pressures of Nozzles in Cylindrical Shells. *ASME Journal of Pressure Vessel Technology* 1968. 171-176

5. Cranch, E. T. An Experimental Investigation of Stresses in the Neighborhood of Attachments to a Cylindrical Shell. *Welding Research Council Bulletin 60* May 1960.

6. Dickey, J.R., and Krishnamurthy, N. Finite Element Parameter Study of Stresses in the Vicinity of Normally Intersecting Shells. *Finite Element Method in Civil Engineering* eds., J.O. McCutcheon, M.S. Mirza, and A.A. Mufti, Montreal,, Canada, 1972. 1199-1226

7. Ellyin, F. Experimental Investigation of Limit Loads of Nozzles in Cylindrical Vessels. *Welding Research Council Bulletin No. 219* Sept. 1976.

8. Fidler, R. A Photoelastic Analysis of Oblique Cylinder Intersection Subjected to Internal Pressure. *Welding Research Council Bulletin, No. 153* 1970. 81-85

9. Goodall, I. W. On The Design of Intersections in Pressure Vessel. *Ph. D. Thesis University of Cambridge* 1967.

10. Goodell, R. A. An Analytical and Experimental Investigation of a Nozzle-to-Cylindrical Shell Junction. *Pressure Vessels and Piping - Analysis and Computers, ASME* New York, 1974. 141-157

11. Kishida, M., Sasaki, K. and Kawano, M. Three-Dimensional Axisymmetric Elastic Stresses in Intersections of Hollow Sphere and Cylinders (Torsion, Tension and Internal pressure). *ASME Journal of Pressure Vessel Technology* 1989 **111,** 218-223

12. Lin, J., Sun, B. C. and Koplik, B. Local Stress Factors of Piping-Nozzle Due to Radial Load, Circumferential and Longitudinal Moments. *ASME, PVP, Design Analysis, Robust Methods, and Stress Classification* 1993. **265,** 307-318

13. Lind, N. C. An Elastic-Sell Analysis of the Stress Concentration of a Pressurized Tee Branch-Pipe Connection. *PVPD* 1969. 269-275

14. Lu, G., Sun, B. C. and Koplik, B. Local Stress Factors of Piping-Nozzle When Nozzle Thickness is proportionally Thinner. *ASME, PVP Pressure Vessels, Pumps, Valves, Pipe Supports and Components*, 1994, **282,** 115-123

15. Mehringer, F. J., and Cooper, W. E. Experimental Determinations of Stresses in the Vicinity of Pipe Appendages to a Cylindrical Shell. *Proceedings of the Society of Experimental Stress Analysis* 1957. **14,** 159

16. Melworm, R. F., and Berman, I. Welded Attachments to Tubes-Experimentation Analysis and Design. *Welding Journal Research Supplement* 1966. **45,** 454

17. Moffat, D. G. and Mistry, J. Interaction of External Moment Loads With Internal Pressure on an Equal Diameter Branch Pipe Intersection. *ASME Journal of Pressure Vessel Technology* 1986. **108,** 443-452

18. Redekop, D. and Schroeder, J. Approximate Prediction of Hoop Stresses at Major Sections of Tee Intersections of Cylindrical Shells Subjected to Internal Pressure. *ASME Journal of Pressure Vessel Technology* 1979. **101,** 186-193

19. Robinson, M. Lower-Bound Limit Pressures for the Cylinder-Cylinder Intersection: A Parametric Survey. *ASME Journal of Pressure Vessel Technology* 1978. **100,** 65-73

20. Robinson, M. and Gill, S. S. A Lower Bound to the Limit Pressure of a Flush Oblique Cylindrical Branch in a Spherical Pressure Vessel. *I.J.M.S.* 1972. **14,** 579-601

21. Sadd, M. H. and Avent, R. R. Stress Analysis and Stress Index Development for a Trunnion Pipe Support. *ASME Journal of Pressure Vessel Technology* 1982. **104,** 73-78

22. Schroeder, J., Gartenburg, J. and Srinivasaiah, K. R. Theoretical and Experimental Results for In-Plane and Out-of-Plane Limit Couples Applied to the Branch and Their Interaction with Pressures. *PVPD* 1973. 305-330.

23. Schroeder, J. and Rangarajan, P. Upper Bounds to Limit Pressures of Branch-Pipe Tee Connections. *PVPD* 1969. 277-291

24. Schroeder, J., Srinivasaiah, R., and Graham, P. Analysis of Test Data on Branch Connection Exposed to Internal Pressure and / or External Couples. *Welding Research Council Bulletin No. 200* Nov. 1974.

25. Simitses, George J. and Chen, Ziqi Buckling of Delaminated, Long, Cylindrical Panels Under Pressure. *Computers & Structures* 1988. **28,** 173-184

26. Srinivasaiah, Kothapalli R. and Schroeder, John Lower Bounds to Limit Pressures of a Tee-Intersection of Cylindrical Shells Based on a Three-Dimensional Stress Field. *Nuclear Engineering and Design* 1977. **41,** 265-280

27. Sun, H.C. and Sun, B. C. On Local Stresses and Spring Constants of Pipe-Nozzle Connection.. *Ph. D. Dissertation, New Jersey Institute of Technology* 1991.

28. Sun, H. C., Sun, B. C. and Herman, H. Finite Element Analysis of Piping-Nozzle Connections, Part I Spring Constants. *PVP ASME, PVPD Conference* Nashville, Tenn., June 1990. **194,**

29. Sun, H. C., Sun, B. C. and Herman, H. Finite Element Analysis of Piping-Nozzle Connections, Part II - Localized Stresses. *PVP ASME, PVPD Conference* Nashville, Tenn., June 1990. **194,**

30. Sun, H. C., Sun, B. C. and Herman, H. Local Stresses of Piping-Nozzle due to Shear Forces and Torsional Moment by Finite Element Method. *ASME, PVPD Conference* San Diego, CA., June 1991.

31. Sundara, Raja Iyengar K. T. and Yoganaada, C. V. Comparison of Elasticity and Shell Theory Solutions for Long Circular Cylindrical Shells. *AIAA Journal* 1966. **4,** 2090-2095

32. Tabone, C. J. and Mallett, R. H. Pressure-Plus-Moment Limit-Load Analysis for a Cylindrical Shell Nozzle. *ASME Journal of Pressure Vessel Technology* 1987. **109,** 297-301

33. Thiel, C. C., Eringen, A. C. and Naghdi, A. K. State of Stress in a Circular Cylindrical Shell with a Hole. *Welding Research Council Bulletin 102* January 1965.

34. Timoshenko, S.. and Woinowsky-Krieger, S. *Theory of Plates and Shells*, 2nd Edition. McGraw-Hill Book Company, Inc. 1959.

35. Truitt, J. B. and Raju, P. P. Tree-Dimensional Versus Axisymmetric Finite-Element Analysis of a Cylindrical Vessel Inlet Nozzle Subject to Internal Pressure A Comparative Study. *ASME Journal of Pressure Vessel Technology* 1978. **100,** 134-141

36. Updike, D. P. Approximate Elastic Stresses In a Tee Branch Pipe Connection Under Pressure. *ASME Journal of Pressure Vessel Technology* 1981. **103,** 104-115

37. Updike, D. P. and Kalnins, A. Approximate Analysis of Intersecting Equal Diameter Cylindrical Shells Under Internal Pressure. *ASME Journal of Pressure Vessel Technology* 1979. **101,** 194-199

38. Wichman, K.R., Hopper, A.G. and Mershon, J.L. Local Stresses in Spherical and Cylindrical Shells due to External Loadings. *Welding Research Council Bulletin, No. 107* 1965.